Biochemical and structural studies on the molecular interaction between P53 transcriptional activation domain and anti-apoptotic protein BCL-XL

Xu, Huibin

2008

Xu, H. B. (2008). Biochemical and structural studies on the molecular interaction between P53 transcriptional activation domain and anti-apoptotic protein BCL-XL. Doctoral thesis, Nanyang Technological University, Singapore.

https://hdl.handle.net/10356/18852

https://doi.org/10.32657/10356/18852

BIOCHEMICAL AND STRUCTURAL STUDIES ON THE MOLECULAR INTERACTION BETWEEN p53 TRANSCRIPTIONAL ACTIVATION DOMAIN AND ANTI-APOPTOTIC PROTEIN BCL-X_L

XU HUIBIN

SCHOOL OF BIOLOGICAL SCIENCES

A thesis submitted to the Nanyang Technological University
in fulfillment of the requirement for the degree of
Doctor of Philosophy

2008

ACKNOWLEDGEMENTS

I would like to thank all the people who have helped me during my Ph.D study. This work would not have been possible without their support and encouragement.

I would express my deep and sincere gratitude to my supervisor, A/P Yoon Ho Sup, School of Biological Sciences, Nanyang Technological University, for all his constant support and guidance during my research. His wide knowledge and hard working attitude have been of great value for me.

I would thank Dr. Christian and Ms Eliza for their effort in peptide synthesize for the project. I would also like to thank Professors. Thanabalu Thirumaran, Julien Lescar, Rupert Wilmouth, Li Jingming, Tang Kai, Tan Nguan Soon, Andrew, Susana, Jinming Torres, Lin Chun Ling, Valerie, Gong Xiandi for their patient guidance and kind help in my research.

I would like to express my thanks to my lab mates Kang Congbao, Feng Lin, Ye Wenhui, Liang Yu, Goutam, and Reema. Thanks to Dr. Ye Hong and Jeff for the help. Thanks to Joel, Dr. Vivek, Dr. Bowha, and Ravi. Thanks to all the staffs and graduate students in our school.

I would like to present this thesis to my parents, for their continuous support and love.

CONTENT

List of figures

List of Tables

Summary

p53 has been extensively studied since its discovery more than 25 years ago. This is due to its critical role in the regulation of apoptosis and control of cancer formation. p53 is believed to be the most important tumor suppressor protein and abnormality of p53 causes cancers and many other diseases. Functional studies revealed that p53 is an important transcriptional activator. It initiates transcription of many pro-apoptosis genes, which activate multiple apoptotic pathways and finally induce cell death. Besides its transcription-dependent apoptosis activity, the apoptotic activity of p53 out of the nuclei was also observed and draws attention.

p53 interacts with the anti-apoptotic proteins, Bcl-2/X_L, and induces mitochondria-mediated apoptosis. The transcription activity of p53 is not involved in this pathway, suggesting transcription-independent mechanism of p53. The p53/Bcl-2 and p53/Bcl-X_L interactions were then investigated by different groups. The DNA binding domain of p53 was believed to be the binding site in the p53/Bcl-X_L interaction. However, there is no detail structure information of the complex so far.

In this study, we identified a novel binding site on p53 N-terminal domain (NTD) for Bcl-X_L. The p53NTD/Bcl-X_L complex was observed and obtained in a co-expression system in *E.coli*. NMR study also confirmed this physical interaction *in vitro*. We also showed their interaction in mammalian cells using

FRET assay. A preliminary binding interface on Bcl-X_L was suggested according to the ^{1}H-^{15}N 2D HSQC NMR titration experiments.

To further understand the p53/Bcl-X_L binding, we truncated the proline rich domain from p53NTD and tested the interaction of p53 transcriptional activation domain (TAD) with Bcl-X_L. GST pull-down assay showed that p53TAD alone is enough to bind Bcl-X_L, which is also confirmed by NMR experiments. With previously published backbone assignment of p53TAD, the involved residues on p53TAD were identified based on the NMR titration experiment. The amino acids from S15 to N29 were affected by the interaction, indicating that this region was the binding site for Bcl-X_L. The binding study using peptide SN15 derived from S15 to N29 also suggested that this region from p53TAD interacts with Bcl-X_L.

A series of experiments were then done on SN15 peptide binding to Bcl-X_L. The binding interface on Bcl-X_L for SN15 was consists of BH1, BH2 and BH3 domains, which forms a hydrophobic pocket for "ligand" binding. This binding pocket on Bcl-X_L is similar with its interaction with BH3 peptide from pro-apoptotic proteins Bak and Bad. The competition binding experiments showed that BH3 peptide can abolish Bcl-X_L/SN15 interaction, confirming that SN15 and Bak/Bad BH3 domain peptide share the similar binding site on Bcl-X_L. The SN15 peptide also binds MDM2, which is the most important step of MDM2-dependent p53 negative regulation pathway. However, the phosphorylation of T18 residue of SN15, which abrogates the MDM2/SN15 binding, does not abolish the Bcl-X_L/SN15 binding, suggesting the difference in

detailed binding pattern between Bcl-X_L/SN15 and MDM2/SN15. Mutagenesis experiments showed that the W23A and K24A mutants of the peptide lost their ability to bind Bcl-X_L, suggesting that residue W23 and K24 of SN15 are critical for the binding.

To further understand the Bcl-X_L/SN15 complex, structure studies on SN15 and the complex was performed. NMR structures indicate that free SN15 peptide contains an unstable α-helix, which is stabilized and extended by forming complex with Bcl-X_L. Based on the NMR chemical shift change data and structure of the Bcl-X_L and SN15 in complex state, a model of Bcl-X_L/SN15 complex structure was generated by computer-based molecular docking. In the complex structure model, SN15 adopts a α-helix to bind to the hydrophobic pocket of Bcl-X_L, which is similar to Bcl-X_L/Bak and Bcl-X_L/Bax interactions.

Due to its central role in tumor suppressor system, understanding the mechanisms of p53-dependent activity is always an interesting topic. Studies in this thesis identified that SN15 from p53TAD was another binding site on p53 to bind Bcl-X_L, which enhances our understanding of the p53/Bcl-X_L interaction. NMR structure studies showed that SN15 undergoes conformational change upon binding to Bcl-X_L. A complex model of Bcl-X_L with SN15 was also presented to help understanding the complex formation. However, more biological studies are needed to be done to clarify the relationship of the transcription-independent apoptotic function with the ability of p53TAD to bind with Bcl-X_L. The contribution of different domains of p53 to the Bcl-X_L binding is also subject to be identified.

Abbreviations

AIF.....Apoptosis inducing factor

Amp.....Ampicillin

ANT.....Adenine nucleotide translocator

ATP.....Adenosine triphosphate

Apaf1.....Apoptotic protease-activating factor 1

Bad.....Bcl-X_L/Bcl-2 associated death promoter

Bcl-2.....B-cell lymphoma/leukaemia 2

BH.....Bcl-2 Homology

BSA.....Bovine serum albumin

CARD.....Caspase recruitment domain

CASPASE.....Cysteine Aspartate Specific Protease

CD.....Circular dichroism

COSY.....Correlation Spectroscopy

CO-IP.....Co-immunoprecipitation

DBD.....DNA Binding Domain

dd H_2O.....destilled and de-ioned H_2O

DISC.....The Death Inducing Signaling Complex

DIABLO.....Direct IAP(inhibition of apoptosis)-binding protein with low pI

DED.....Death effector domain

DMSO.....Dimethyl sulfoxide

DMEM.....Dulbecco's Modified Eagle Medium

DTT.....Dithiothreitol

EtBr.....Ethidium bromide

ER.....Endoplasmic reticulum

FADD.....Fas-associated Death Domain

FCS.....fetal calf serum

FPLC.....Fast Performance Liquid Chromatography

GST.....Glutathione-S-transferase

HPLC.....High performance liquid chromatography

HSP.....Heat shock protein

HSQC.....Heteronuclear single quantum correlation spectroscopy

IM.....Inner membrane

IGF-1.....Insulin-like growth factor 1

IPTG.....Isoporpyl-Thio-B-D-galactopyranoside

Kana.....Kanamycin

LB.....Luria-Bertani

NF-AT.....Nuclear factor of activated T cells

MOMP.....Mitochondrial outer membrane permeabilization

NMR.....Nuclear magnetic resonance

NOEs.....Nuclear Overhauser Effect Spectroscopy

OM.....Outer membrane

PCR.....Polymerase chain reaction

PMSF.....Phenylmethylsulfonyl fluoride

PT.....permeability transition

PVDF.....Polyvinylidene difluoride

RMSD.....Root-mean-square deviation

ROESY.....Rotating-frame Overhauser Effect Spectroscopy

RT-PCR.....Reverse transcription-polymerase chain reaction

SDS-PAGE.....Sodium dodecyl sulfate-polyacrylamide gel electrophoresis

TAE.....Tris-acetate-EDTA

TB.....Terrific broth

TBS.....Tris-buffered saline

TM.....Trans membrane

TNF.....Tumor necrosis factor

TOCSY.....Total Correlation Spectroscopy

TRAIL.....TNF related apoptosis-inducing ligand

VDAC.....Voltage-dependent anion channel

1. Introduction

1.1. Apoptosis

Cells duplicate and die everyday in multicellular organisms, which are critical for their regular development and homeostasis. A balance of cell death and survival is also essential to maintain their correct function and normal morphology (Hengartner, 2000; Vaux and Strasser, 1996). Cell death has been observed in scientific laboratories by researches many years ago. In some cases, cells die from acute tissue injury, spilling out their contents and damaging their neighbor cells. This process is called cell necrosis. In other cases, cells suicide through a special physiological process, executed by proteins encoded and synthesized by the host itself. These cells share many particular morphological features, which are very different from necrosis cells. This physiological and endogenous cell death is called program cell death or apoptosis (Wyllie et al., 1980). The discovery of apoptosis includes efforts from many scientists. The name of "apoptosis" was initially introduced in 1972 by a group who observed apoptosis in different cell types and tissues and was accepted by the research society (Kerr et al., 1972).

Apoptosis is one of the essential physiological processes in all multicellular organisms. It maintains a proper cell number of organisms, keeps their healthy size and correct function, and protects them from the threat of rogue cells (Vaux and Strasser, 1996). Besides human beings, stuies of apoptosis were performed

extensively in three principal organisms, including nematode, fruit fly, and mouse (Meier et al., 2000). It is now clear that apoptosis process is heavily conserved in all metazoan cells. Nematode *C. elegans* is the first system used by scientists as a model organism to study the apoptosis intensively. The genes involved in the apoptosis and its regulation in *C. elegans* were identified (Ellis and Horvitz, 1986; Ellis et al., 1991; Horvitz, 1999; Liu and Hengartner, 1999). Another model organism, fruit fly *Drosophila melanogaster,* is a system with medium complexity between mammals and nematode. It provides more information of apoptosis pathways than simple nematode system. It contains components and pathways similar but with less complexity as mammals, allowing easier identification of the specific functions (Abrams, 1999; Hay et al., 2004; Muqit and Feany, 2002). In mammalian cells, some homologies of these apoptosis related genes were also discovered and some details of apoptosis pathways were then revealed accordingly (Colussi and Kumar, 1999; Hawkins and Vaux, 1997; Jacobson et al., 1997; Ranger et al., 2001).

With critical functions and precise process, cell apoptosis disorder unsurprisingly results in different kinds of diseases. Loss of apoptotic responses to death signals contributes to cancer development and resistance to anti-cancer treatment. It induces autoimmune diseases as well. Abnormally enhanced cell apoptosis contributes to degenerative and immune deficient diseases (Hipfner and Cohen, 2004; MacFarlane and Williams, 2004). Among these abnormal apoptosis induced diseases, cancer is the most concerned one. And apoptosis is

regarded as the target in most cancer treatment (Kasibhatla and Tseng, 2003; Thompson, 1995; Yue et al., 1999).

1.1.1. The extrinsic apoptosis pathway

Most of the morphological changes occurred in apoptosis process are executed by cysteine protease family proteins which are called caspases (Budihardjo et al., 1999; Degterev et al., 2003; Thornberry and Lazebnik, 1998). The apoptotic pathways are specific procedures to activate these proteases. It has been revealed that there are two major apoptotic pathways in mammalian cells, including extrinsic pathway and intrinsic pathway. Both of them are very important for the activation and regulation of apoptosis (Wajant, 2002; Zimmermann et al., 2001).

The extrinsic pathway is also named as death-receptor pathway. In this pathway, some specific protein ligands out of cells, which are called death signals, bind to cell surface transmembrane death receptors and activate the subsequent signal pathways to initiate the caspases-dependent apoptosis (Ashkenazi and Dixit, 1998; Debatin and Krammer, 2004; Fumarola and Guidotti, 2004).

In the extrinsic pathway, the death receptors on the cell surface work as a bridge cross the cell membrane to receive the extracellular death signals and to activate the intracellular apoptosis pathway. Death receptors belong to the tumor necrosis factor (TNF) receptor superfamily. All death receptors share a conserved cysteine-rich extracellular domain and an intracellular death domain

which executes a protein-protein interaction function to activate intracellular signal pathways (Debatin and Krammer, 2004).

So far, six death receptors have been identified: CD95, TNFR1, DR3, TRAIL and DR6. Among these, CD95 has been studied most intensively (Gruss and Dower, 1995; Nagata, 1997). In CD95 mediated apoptosis pathway, CD95 ligand binds to CD95 and induces its clustering (Ashkenazi and Dixit, 1998; Huang et al., 1996). The protein complex then recruits multiple procaspase-8 molecules via an adaptor protein named Fas-associated Death Domain (FADD) (Boldin et al., 1996; Boldin et al., 1995; Chinnaiyan et al., 1995). Oligomerization of procaspase-8 undergoes self-cleavage, resulting in caspase-8 activation (Muzio et al., 1998). Active caspase-8 then activates downstream effectors like caspase 3 to execute protein degradation and finally apoptosis (Figure 1-1).

1.1.2. The intrinsic apoptosis pathway and mitochondria

The intrinsic apoptosis pathway is also called mitochondria-mediated pathway. Mitochondria is originally known as energy provider of cells, producing adenosine triphosphate (ATP) via an oxidative phosphorylation pathway, and cytochrome c. Besides its role as powerhouse of cell, mitochondria received increasing interests for its important role in cell death during the past years (Degli Esposti, 2004; Desagher and Martinou, 2000; Green and Reed, 1998; Wang, 2001).

Mitochondria comprises an inner membrane (IM), an out membrane (OM) and the intermembrane space in between. The IM contains various molecules, including ATP synthase, electron transport chain and adenine nucleotide translocator (ANT) which enable the respiratory chain to create an electrochemical gradient. The OM contains a voltage-dependent anion channel (VDAC). The intermembrane space contains several important death factors, such as cytochrome c, certain pro-caspases, adenylate kinase 2, Endo G, Smac and apoptosis-inducing factor (AIF).

Mitochondria-mediated apoptosis pathway seems to be the main form of apoptosis in vertebrate cells (Desagher and Martinou, 2000). Different from extracellular death signals induced apoptosis pathway, mitochondria-mediated intrinsic apoptosis pathway is initialized by a series of intrinsic signals caused by DNA damage, chemotherapeutic agents, UV radiation, stress molecules and growth factor withdrawal. In mitochondria mediated apoptosis, the most critical event is mitochondrial outer membrane permeabilization (MOMP). As a bridge between death signals and executors, MOMP activates apoptosis through three different mechanisms: i) release of molecules involved in the activation of caspases from the mitochondrial intermembrane space to cytoplasm; ii) release of molecules involved in caspases-independent cell death and iii) the loss of mitochondrial functions essential for cell survival.

So far, the mechanisms of MOMP during apoptosis are still controversial. But in general, two different mechanisms have been described with evidences, which are permeability transition (PT) pore dependent and independent

mechanisms. The PT pore is comprised of the matrix protein cyclophilin D, the inner mitochondrial membrane protein adenine nucleotide translocator (ANT), and the outer mitochondrial membrane protein voltage dependent anion channel (VDAC) (Crompton et al., 1998). Recent report also showed that ANT may not be indispensable in the forming of PT pore (J. E. Kokoszka et al., Nature 427, 461, 2004).

In the PT pore dependent mechanism, the opening of PT pore causes the dissipation of the proton gradient created by electron transport, causing the uncoupling of oxidative phosphorylation. It also triggers water to enter the mitochondrial matrix, resulting in swelling of the intermembrane space and rupturing of the outer membrane, causing the release of apoptogenic proteins from mitochondria to cytosol.

The second mechanism of MOMP is PT pore independent and is regulated by Bcl-2 family proteins. Bcl-2 family proteins are believed to activate MOMP directly on the outer mitochondrial membrane. There are two groups of Bcl-2 family proteins with opposite function on MOMP, which are anti-apoptotic and pro-apoptotic Bcl-2 family proteins. Anti-apoptotic Bcl-2 family members function to block MOMP whereas pro-apoptotic members promote it. Anti-apoptotic group members, including Bcl-2 and Bcl-X_L, are characterized by four conserved Bcl-2 homology (BH) domains (BH1, BH2, BH3, and BH4). Pro-apoptotic group is further divided into two subfamilies according to sharing of the BH domains. Multidomain proteins, such as Bax and Bad, share BH1, BH2, and BH3 domains and seem to be promotor of MOMP. The other

subfamily is called BH3-only proteins which lack BH1, BH2, and BH4 domains. These BH3-only proteins, such as Bid and Bik, can either activate Bax and Bak or interfere with the anti-apoptotic family members.

It gains lots of efforts from scientists to understand how Bcl-2 family proteins control the MOMP process. The mechanism detail still remains controversial, but several hypotheses have been described. One of them is that Bcl-2 family proteins form channels on the mitochondrial membrane that allow protein transport. This hypothesis is supported by the fact that Bcl-X_L shares structural similarity with the pore-forming subunit of diphtheria toxin. It has been suggested that Bcl-2 proteins might occur conformational change to insert into the outer mitochondrial membrane, then to form channels or even large holes to allow proteins transport. As experimental evidences of this suggestion, some paper reported that Bcl-2 and Bcl-X_L can insert into synthetic lipid bilayers, oligomerize, and form channels with discrete conductances (Minn et al., 1997; Schendel et al., 1998; Schendel et al., 1997). But there is still no evidence shows that these channels are big enough to allow proteins to pass through.

Another hypothesis is that Bcl-2 family members form channels with assistant of other proteins. Bcl-2 family proteins interact with a lot of other proteins. It is suggested that Bcl-2 family members recruit some other proteins and form complexes to insert into the outer mitochondrial membrane and form channels. Voltage-dependent anion channel (VDAC) is the most noticed candidate of partner to assist Bcl-2 family members to form channels. Several Bcl-2 family

members can interact with VDAC and regulate its channel activity. But the VDAC channel also has too small pore size to allow proteins to pass through.

Third hypothesis is Bcl-2 members inducing disruption of the out mitochondrial membrane. It is possible that Bcl-2 family proteins change the homeostasis of the mitochondria, cause the organelle to swell and result in physical disruption of the outer mitochondrial membrane. Proteins can be transport by diffuse through the lipid bilayer in this mechanism. However, there are no direct evidences reported to support this hypothesis currently.

After MOMP occurs, several death factors release from intermembrane space of mitochondria to cytosol where they activate the following apoptotic pathways. These death factor proteins include cytochrome c, apoptosis-inducing factor (AIF), Smac/DIABLO, and several pro-caspases such as procaspase-2, -3, and -9. Among these proteins, cytochrome c is the only protein to be essential for the apoptosis so far. Released cytochrome c induces multimerization of apoptosis protease-activation factor (Apaf)-1 to activate pro-caspases-9 and -3, resulting in following apoptosis procedures (Figure 1-1).

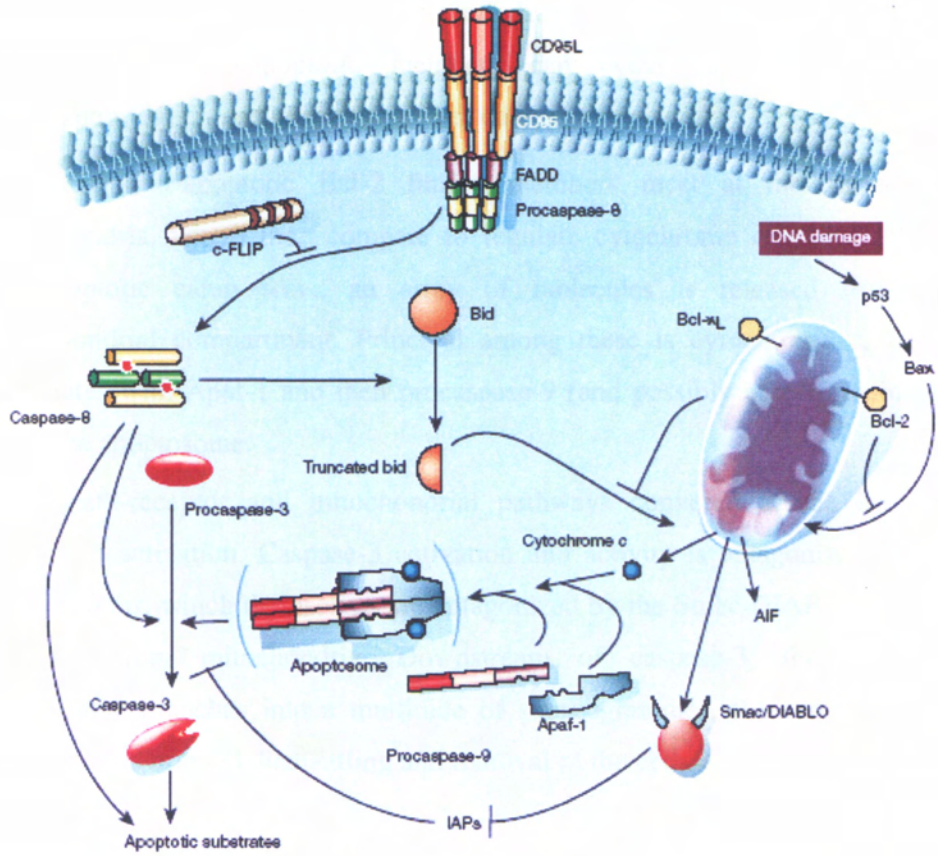

Copied from Hangartner, M.O. (2000). "The biochemistry of apoptosis." Nature **407**(6805): 770-6.

Figure 1-1 The apoptosis pathways.

The extrinsic pathway (left pathway in the figure) is triggered by members of the death-receptor superfamily. Binding of CD95 ligand to CD95 induces receptor clustering and formation of a death-inducing signaling complex. This complex recruits, via the adaptor molecule FADD (Fas-associated death domain protein), multiple procaspase-8 molecules, resulting in caspase-8 activation through induced proximity.

The intrinsic pathway (right) is used extensively in response to extracellular cues and internal insults such as DNA damage. These diverse response pathways converge on mitochondria, often through the activation of a pro-apoptotic member of the Bcl-2 family. Pro-apoptotic signals redirect these

proteins to the mitochondria, where the fight for the cell's fate will take place. Activation of pro-apoptotic members can occur through proteolysis, dephosphorylation and probably several other mechanisms.

Pro- and anti-apoptotic Bcl-2 family members meet at the surface of mitochondria, where they compete to regulate cytochrome c release. If the pro-apoptotic camp wins, an array of molecules is released from the mitochondrial compartment. Principal among these is cytochrome c, which associates with Apaf-1 and then procaspase-9 (and possibly other proteins) to form the apoptosome.

The death-receptor and mitochondrial pathways converge at the level of caspase-3 activation. Caspase-3 activation and activity is antagonized by the IAP proteins, which themselves are antagonized by the Smac/DIABLO protein released from mitochondria. Downstream of caspase-3, the apoptotic programme branches into a multitude of subprogrammes, the sum of which results in the ordered dismantling and removal of the cell.

1.2. Bcl-2 family proteins

Bcl-2 family proteins are center regulators of apoptosis, especially in mitochondria-mediated apoptosis pathway (Kuwana and Newmeyer, 2003). The first discovered member of Bcl-2 family proteins was B-cell lymphoma/leukemia 2 (Bcl-2), which was identified originally at the breakpoint of a t(14; 18) translocation in a lymphocytic leukemia cell line in 1984 (Tsujimoto et al., 1984). After that, numerous homologous of the Bcl-2 have been identified in vertebrates. So far there are more than 20 Bcl-2 family members in mammalian cells (Adams and Cory, 1998; Cory and Adams, 2002; Gross et al., 1999). All these members share at least one of the four Bcl-2 homology (BH) domains, which are BH1, BH2, BH3 and BH4.

Bcl-2 family members can be divided into two sub-families: anti-apoptotic subfamily (Bcl-2, Bcl-X_L and Bcl-w) and pro-apoptotic subfamily. Pro-apoptotic subfamily contains Bax subfamily (Bax and Bad) and BH3-only subfamily (Bid and Bim) (Cory et al., 2003). The anti-apoptotic subfamily promotes cell survival, where as the pro-apoptotic and BH3-only subfamilies promote apoptosis (Figure 1-2). The ratio between anti- and pro-apoptotic Bcl-2 family members determines the susceptibility of cells to a death signal (Oltvai et al., 1993).

Although the detail mechanisms still need to be discovered, the main function of Bcl-2 family members has been known to directly control the mitochondrial membrane permeability and thereby regulate the release of apoptogenic factors from mitochondria and subsequent apoptosis (Martinou and Green, 2001). Anti- and pro-apoptotic members of Bcl-2 family have opposite functions and regulate each other. Anti-apoptotic proteins in the Bcl-2 family preserve mitochondrial respiration and maintain mitochondrial membrane integrity (Decaudin et al., 1997). With Bcl-2 expression, the depolarization of mitochondrial transmembrane potential is not observed in apoptosis (Zamzami et al., 1995). Isolated mitochondria enriched with Bcl-2 are resistant to the opening of permeability transition (PT) pores (Zamzami et al., 1996). Another important anti-apoptotic member Bcl-X_L was reported to inhibit mitochondrial swelling during apoptosis (Vander Heiden et al., 1997).

Pro-apoptotic members can induce MOMP to release the inner apoptotic factors. Bax, one of the most important pro-apoptotic Bcl-2 family proteins was

reported to induce cytochrome c release and apoptosis (Pastorino et al., 1998; Rosse et al., 1998).

Pro- and anti-apoptotic family members of Bcl-2 can form homodimers and heterodimers. The ability to interact with opposite functional family members enables them to regulate functions of each other, suggesting the neutralizing competition between anti- and pro-apoptotic members (Oltvai et al., 1993). Three-dimensional structures of anti-apoptotic Bcl-X_L and the Bcl-X_L/Bak complex solidly support the heterodimer formation and provide the detailed explanation (Muchmore et al., 1996; Sattler et al., 1997). According to the 3D structures, α-helices in BH1, BH2 and BH3 domain of Bcl-X_L create a hydrophobic pocket that BH3 domain of Pro-apoptotic proteins can bind.

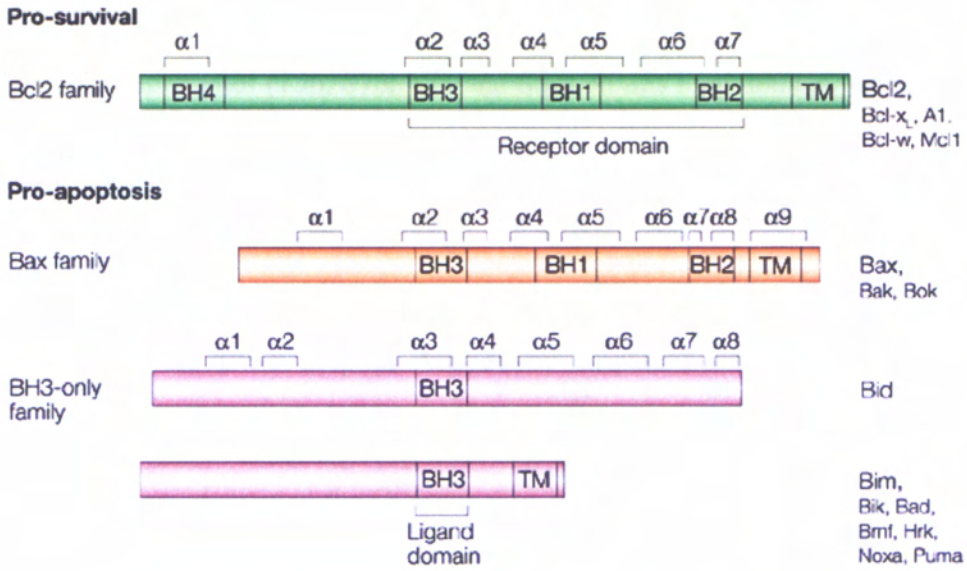

Copied from Cory, S. and Adams, J. M. (2002). "The Bcl-2 family: regulators of the cellular life-or-death switch." Nature Review Cancer **2**(9): 647-56.

Figure 1-2 Bcl-2 family proteins.

Bcl-2 family contains two subfamilies. Pro-survival subfamily promotes cell survival, whereas pro-apoptosis subfamily induces apoptosis. Pro-apoptosis subfamily also contains Bax subfamily and BH3-only subfamily. BH1 to BH4 are Bcl-2 homology domains in Bcl-2 family. α1 to α9 are α-helices in the Bcl-2 family proteins structure. TM is transmembrane domain.

1.2.1. Bcl-2

Bcl-2 (B-cell lymphoma/leukemia 2) is the founding member of Bcl-2 family proteins, which was identified at the chromosomal breakpoint of a t(14;18) translocation in a lymphocytic leukemia cell line (Bakhshi et al., 1985; Cleary and Sklar, 1985; Tsujimoto et al., 1985; Tsujimoto and Croce, 1986). Bcl-2 consists of 239 amino acids, containing all the four BH domains: BH1 (residues 136-155), BH2 (187-202), BH3 (93-107) and BH4 (10-30). It also contains a

long flexible loop between BH3 and BH4 domains. There are several phosphorylation sites (T56, S70, T74 and S87) on this loop domain, which are identified to be targets for the regulators to associate with (Huang and Cidlowski, 2002; Ojala et al., 2000). Phosphorylation of S70 abrogates the anti-apoptotic function of Bcl-2 (Dramsi et al., 2002). Furthermore, proteolytic cleavage of the Bcl-2 loop at Asp 34 by caspase-3 converts it from an anti-apoptotic protein to a pro-apoptotic protein (Cheng et al., 1997). A transmembrane domain at the C-terminal of Bcl-2 facilitates Bcl-2 localization to membranes of some organelles, such as mitochondria, endoplasmic reticulum (ER) and nuclear (Nguyen et al., 1993).

After its discovery, Bcl-2 has been established to be a proto-oncogene that promotes proliferation by inhibiting apoptosis (Adams and Cory, 1998; Chao and Korsmeyer, 1998). Expression of Bcl-2 blocks cell death (Tsujimoto, 1989; Vaux et al., 1988). Transgenic mice bearing a Bcl-2-Ig minigene initially displayed a polyclonal follicular lymophoproliferation that selectively expanded a small resting IgM/IgD B-cell population (McDonnell et al., 1989; McDonnell et al., 1990). Bcl-2 is also found to maintain the integrity of mitochondrial membrane (Zamzami et al., 1995; Zamzami et al., 1996). Apart from its anti-apoptotic function, Bcl-2 seems to also play an important role in differentiation and maturation. It can induce differentiation of neural cell line (Zhang et al., 1996).

Several hypotheses have been proposed to explain the anti-apoptotic function of Bcl-2. Bcl-2 may act as a regulator for Ca^{2+} homeostasis or an antioxidant. It

also prevent the release of the mitochondrial activators of the cytosolic caspases which mediates following apoptosis-specific intracellular proteolysis (Chao and Korsmeyer, 1998). Further more, Bcl-2 may act by modulating the collapse of the mitochondrial transmembrane potential that occurs during apoptosis (Hockenbery et al., 1990).

With its carboxyl-terminal transmembrane domain, Bcl-2 protein acts as a membrane protein and localizes to the outer mitochondrial membrane, endoplasmic reticulum membrane or nuclear membrane. Its amino-terminal is facing the cytosol when inserts into membrane (Nguyen et al., 1993). The intracellular localization of Bcl-2 is critical for its physiological functions (Germain and Shore, 2003). It is also very important that Bcl-2 is able to form homodimer, or form heterodimers with pro-apoptotic members of Bcl-2 family proteins. Bcl-2 forms heterodimer with Bax, a pro-apoptotic protein of Bcl-2 family (Oltvai et al., 1993). Several other Bcl-2 family members also have been reported to form heterodimers with Bcl-2 (Reed, 1998). This ability enables Bcl-2 to regulate the function of its pro-apoptotic members and maintain a balance between the opposite Bcl-2 family proteins (Cory et al., 2003; Reed, 1998).

The three-dimensional structure of Bcl-2 was determined by NMR in 2001 (Petros et al., 2001). Like its homolog Bcl-X_L, the NMR structure of Bcl-2 contains eight helices with a hydrophobic groove on the surface. The C-terminal transmembrane domain of Bcl-2 was also deleted to make the protein soluble. To improve Bcl-2 solubility, the loop region between BH4 and

BH3 domains was replaced by a part of Bcl-X_L loop. The NMR structure of Bcl-2 provided explanation of the Bcl-2 functions and give information of the interactions of Bcl-2 with other proteins.

1.2.2. Bcl-X_L

Bcl-X was discovered in the chicken by low stringency hybridization with a murine Bcl-2 cDNA (Boise et al., 1993). Alternative splicing of Bcl-X results in two distinct mRNAs. The larger mRNA encodes Bcl-X_L protein containing 233 amino acids and the small one encodes Bcl-X_S protein containing 170 amino acids. Bcl-X_S lacks a 66 amino acids region of Bcl-X_L from residue 126 to 188. Functional studies on both Bcl-X_L and Bcl-Xs revealed that they have opposite apoptotic activities. Bcl-X_L inhibits cell death while Bcl-X_S promote cell death.

As one of the most important homologs of Bcl-2, Bcl-X_L displays 43% amino acid identity with Bcl-2. Bcl-X_L has all four BH domains and a carboxyl-terminal transmembrane domain. Like Bcl-2 protein, there is a nonstructural loop between BH3 and BH4 in Bcl-X_L as well.

Bcl-X_L belongs to anti-apoptotic subfamily of Bcl-2 family. It has similar anti-apoptotic functions and is a key anti-apoptotic regulator in apoptosis pathways. Compared with Bcl-2, Bcl-X_L is five to six folds more abundant in the adult kidney, brain, and thymus. It is also found to be highly expressed in the embryonic liver (Gonzalez-Garcia et al., 1994).

Bcl-X knock-out mice provide a good system to study the Bcl-X_L function. Bcl-$X^{-/-}$ mice die around embryonic day 13. Extensive apoptotic cell death was evident in postmitotic immature neurons of the developing brain, spinal cord, and dorsal root ganglia. Hematopoietic cells in the liver were also apoptotic. Analyses of Bcl-X double-knockout chimeric mice showed that the maturation of Bcl-X deficient lymphocytes was diminished. The life-span of immature lymphocytes, but not mature lymphocytes, was shortened. Bcl-X functions to support the viability of immature cells during the development of the nervous and hematopoietic systems (Motoyama et al., 1995). Further more, Bax deficient in Bcl-$X_L^{-/-}$ mice promotes neuron survival extensively, suggesting Bax and Bcl-X_L interaction regulates apoptosis of immature neurons (Shindler et al., 1997).

The three-dimensional structure of Bcl-X_L was determined by both X-ray crystallography and NMR spectroscopy in 1996 (Muchmore et al., 1996). It is the first published three-dimensional structure of the Bcl-2 family members. The structure of the protein consists of eight α-helices with loops of different length connecting them. The structure consists of two central α-helices, which are α5 and α6, flanked on one side by α3 and α4 and on the other side by α1, α2 and α7. These two central helices contain mainly hydrophobic residues, and are arranged in an antiparallel fashion. The N-terminal helix binds to α2, α5 and α6 through tight hydrophobic interactions, stabilizing the protein structure (Figure 1-3) (Muchmore et al., 1996).

Both of X-ray and NMR structures show no Bcl-X_L secondary structual signals from the residues Ser 28 to Val 80, suggesting that it is a nonstructural loop region. This long flexible loop region between α1 and α2 also exists in several other anti-apoptotic Bcl-2 family members, such as Bcl-2 and Mcl-1. Deletion of this loop region from Bcl-X_L increased its ability to inhibit apoptosis, implying that this loop may play some negative regulative role of its anti-apoptotic function (Muchmore et al., 1996). Unlike BH domains which are heavily conserved in Bcl-2 family proteins, this flexible loop region is highly variable among the proteins containing it, suggesting possible different regulatory mechanisms between them.

Structural comparison showed that the overall three-dimensional structure of Bcl-X_L displayed a similarity to the membrane insertion domains of diphtheria toxin and of the colicins (Muchmore et al., 1996). These domains also contain two hydrophobic α-helices which are long enough to span a bilayer. It was then suggested that Bcl-2 family proteins may also be able to insert into the membrane to form pores. Subsequent studies confirmed that Bcl-X_L, Bcl-2 and Bax can all insert into synthetic lipid vesicles and planar lipid bilayers to form ion-conducting channels (Minn et al., 1997; Schendel et al., 1997; Schlesinger et al., 1997). However, more evidences are still required to support the relationship between the pore-forming ability of Bcl-2 family proteins with their function of regulating the release of cytochrome c and controlling the apoptosis. Besides its soluble structure, an NMR structure of Bcl-X_L in lipid micelles was also determined, providing some information of Bcl-X_L

conformation in a membrane environment (Losonczi et al., 2000). In lipid micelles, Bcl-X_L undergoes a conformational change. α1, α6, and the initial part of the long loop were shown to be embedded in the hydrophobic core of the micelle. Bcl-X_L shows monomer when incorporated in the micelle, contradicting the previous findings that Bcl-2 family proteins form multimers in lipids. So far the detailed structure information and function of Bcl-X_L in the membrane are still not well defined.

Bcl-X_L has all of the four BH domains. From the three-dimensional structure, it is notable that the BH1, BH2 and BH3 domains are proximal to one another and define the top of an elongated hydrophobic groove on the surface of the protein. α3 and α4 form the bottom of the groove. Bcl-X_L forms heterodimers with pro-apoptotic Bax and Bad. NMR structures of Bcl-X_L/Bak and Bcl-X_L/Bad complexes showed that BH3 domains of Bax and Bak interact with Bcl-X_L on this hydrophobic groove (Petros et al., 2000; Sattler et al., 1997). This hydrophobic groove may also provide a binding site for other Bcl-X_L-binding proteins.

As we mentioned, it is an important feature of Bcl-2 family proteins to form heterodimers to regulate apoptosis functions of each other. To determine the molecular basis for the interaction between anti- and pro-apoptotic proteins of Bcl-2 family, a three-dimensional complex structure of Bcl-X_L with a BH3 peptide from Bak was solved by NMR (Figure 1-3) (Sattler et al., 1997). The interaction of BH3 peptide does not cause major conformational change of Bcl-X_L. The Bak peptide binds to the hydrophobic groove formed on the

surface of the protein by the BH1, BH2 and BH3 regions of Bcl-X_L and adopts an amphipathic α-helix. The mutant Bak peptides with alanine substitutions shows different binding affinities with Bcl-X_L, indicates the different contributions of the amino acids from peptide to the interaction. Substituting Leu 78 with alanine caused largest effect on binding. Substituting other hydrophobic residues (Ile85, Ile81, and Val74) to alanine also resulted reduced binding to Bcl-X_L. These data indicateded the importance of hydrophobic interactions in complex forming. In addition, charged side chains of the peptide (Arg76, Asp83, and Asp84) also made significant contributions to bind based on structure.

In the complex structure, the interaction between Asp83 of the Bak peptide and Arg139 of Bcl-X_L stabilizes the complex formation. Asp83 is found to be conserved in Bcl-2 family proteins. The binding affinity of peptide with Bcl-X_L decreases 120-fold when the Asp83 was changed to alanine. Moreover, Arg139 is also highly conserved and mutation of Arg139 to Gln in Bcl-X_L inhibits its anti-apoptotic activity and binding to the Bax protein (Cheng et al., 1996). Another pro-apoptotic protein, Bad, also binds to Bcl-X_L. However, the peptide of Bad binding to Bcl-X_L was found to have different residue numbers from Bak. To form a tight binding, it require five additional residues at the amino terminus and four residues at the carboxy terminus (Kelekar et al., 1997; Ottilie et al., 1997). The overall structure of the Bcl-X_L/Bad peptide complex was found to be very similar to that of the Bcl-X_L/Bak peptide complex (Petros et al., 2000). Like the Bak peptide, the Bad 25-mer binds as an amphipathic α-helix,

and similar interactions stabilize complex formation. The structures of Bcl-2 family proteins and their complexes provided insight information about the interactions between them. It also helped the understanding of the mechanism that Bcl-2 family proteins bind each other to balance the cell apoptosis and cell survival. However, the detailed mechanism of how Bcl-2 family proteins regulate apoptosis still remains unclear.

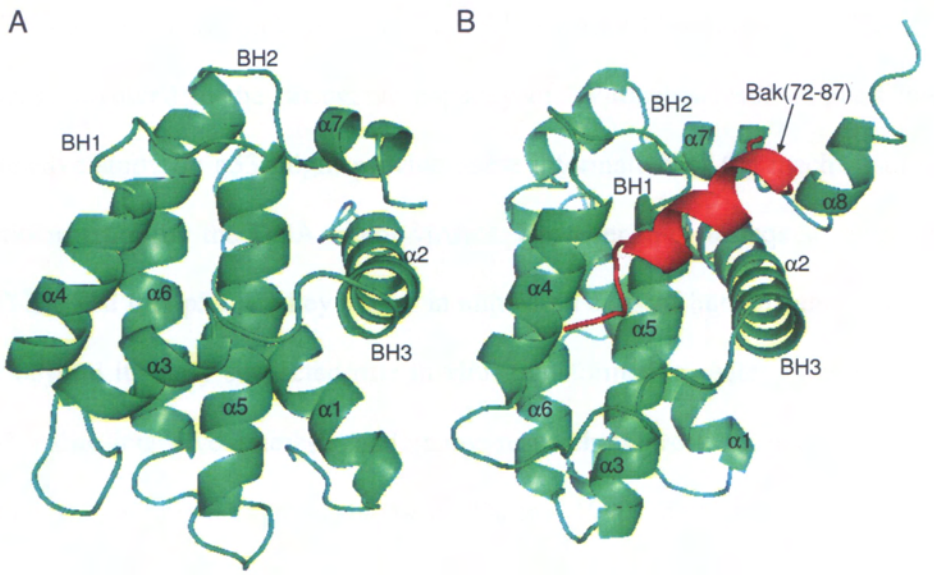

Figure 1-3 3D structures of Bcl-X_L and Bcl-X_L/Bax BH3 peptide complex.
A) Bcl-X_L contains 7 α-helices forming all four BH domains of Bcl-2 family proteins. BH1, BH3 and BH2 domains of Bcl-X_L forms a hydrophobic pocket. B) Bak BH3 domain peptide GR16, from residue 72 to 87, adopts a α-helix to bind to the hydrophobic pocket of Bcl-X_L.

1.3. p53

p53 is now known as the key tumor suppressor protein in the network of cellular stress response pathways. In 1979, when people use an oncogenic DNA virus simian virus 40 (SV40) to induce experimental neoplastic transformation and to study the biology of transformed cells, a cellular protein was found to bind tightly to a nonstructural protein of the virus SV40LT. This protein was later denoted as p53 from its molecular weight (DeLeo et al., 1979; Kress et al., 1979; Lane and Crawford, 1979; Linzer and Levine, 1979). Since SV40LT was heavily involved in the oncogenic capacity of SV40, this result implied that extensive study on p53 might provide some information of the mechanism of transformation by the DNA tumor viruses. However, the subsequent work on p53 showed that p53 is a key player in almost all sorts of human cancer, much far beyond its early suspected role in viral transformation. After its discovery, p53 gains intensive interests and many researchers work to understand its functions and regulation mechanisms. During 1990s and early part of this millennium, there are more than 20000 scientific reports on p53, indicating that it is one of the hottest areas in the life sciences (Hofseth et al., 2004).

p53 gene encodes a 393 amino acids length protein with a molecular weight of around 53 kD. It contains several well-defined domains, including an amino-terminal domain (NTD), a carboxyl-terminal domain (CTD) and a DNA-binding domain (DBD) in between. NTD contains a transcriptional activation domain (TAD) from start to amino acid 73 followed by a proline-rich

domain (PPD). A nuclear export signal also locates here. DBD consists of amino acids from residue 94 to 312 which interacts with specific DNA sequences and most of the p53 point mutations found in cancers occur within this domain. A tetramerization domain is localized at CTD which facilitate p53 to form a tetramer. CTD also contains several nuclear-localization signals and a nuclear export signals which is important for the localization and distribution of p53 in cells.

In the early years after its discovery, the p53 gene was cloned from neoplastic rodent and human cells, and found to have weak oncogenic activity when expressed in rodent cells. The misunderstanding was corrected in the late 1980s, when people realized that they cloned the p53 mutations instead of the wide-type gene. By the early 1990s, after more than 10 years of its discovery, p53 was widely recognized as a tumor suppressor gene. It is found to be mutated or lost in more than 50% of all human cancer cases, which put it in the center of the cancer research area (Hollstein et al., 1991; Levine et al., 1991). After that, besides its major tumor suppressor activity, p53 was found to have multiple functions. It was first shown to be involved in apoptosis and cell cycle regulation and then in development, differentiation, gene amplification, DNA recombination, chromosomal segregation and cellular senescence (Harris, 1996). Then, in the later part of 1990s, p53 was found to function to repair damaged DNA, including nucleotide excision repair and base excision repair (Adimoolam and Ford, 2003; Offer et al., 1999; Zhou et al., 2001). Recently, it was discovered that chronic constitutive expression of p53 accelerates aging in

mice while normal expression of p53 under its own promoter does not (Garcia-Cao et al., 2002; Tyner et al., 2002).

1.3.1. Regulation of p53

p53 is one of the most important tumor suppressor genes. It has been named as "Guardian of the Genome" and "Cellular Gatekeeper" for its well-known apoptotic activity and cell cycle arrest activity in response to a variety of cellular damage (Lane, 1992; Levine, 1997). Both of the function and regulation mechanisms of p53 are intensively studied and known to be extremely complicated. Although thousand of publications have been reported on this topic, there are still many unknown mechanisms inside.

As a potent inhibitor of cell growth, p53 is maintained at very low level in normal cells not to disrupt the normal growth and development of cells. It has a very short half-life (from 6 to 20 minutes) in several cell types. p53 knock out mouse develops normally, showing that p53 is not essential for normal cell cycle. However, deficient of p53 gene results in dramatic tumor-prone phenotype (Donehower et al., 1992). Transgenic mice with over expression of mutant alleles of p53 oncogene are also highly prone to developing spontaneous and carcinogen-induced tumors (Lavigueur et al., 1989). Therefore, it is critical for cells to regulate the p53 level, keeping it at low level when cells are in normal condition and increasing its level quickly when needed.

Regulation of p53 has been studied at different levels. Transcriptional regulation of the p53 gene plays a minor role (Raman et al., 2000; Webster and Perkins, 1999), and the regulation at protein level on p53 contributes most. DNA damage induces increased protein level of p53 by prolonging protein half-life (Kastan et al., 1991; Maltzman and Czyzyk, 1984). It is also revealed that p53 stability is mainly regulated through an ubiquitin-dependent proteolytic machinery (Maki et al., 1996). The mechanism details remain unclear until MDM2 was identified to be one of the central components in the p53 regulation mechanism (Haupt et al., 1997; Kubbutat et al., 1997; Midgley and Lane, 1997). MDM2 is a p53 target gene. It is transcriptionally activated by p53 (Barak et al., 1993). However, not like other p53 targets, MDM2 does not mediate any of the downstream function of p53, such as cell cycle arrest or apoptosis (Marston et al., 1994; Reinke and Lozano, 1997). In contrast, MDM2 binds to p53 and inhibit its functions by blocking its transcriptional activity (Haupt et al., 1996; Momand et al., 1992; Oliner et al., 1993). The MDM2/p53 complex structure was determined using the N-terminal domain of MDM2 with a SN15 peptide derived from p53 transcriptional activation domain (Figure 1-4). Thus, MDM2 and p53 established a negative feedback loop which is regarded as the most important p53 regulation mechanism to maintain p53 protein at low level in normal cells (Wu et al., 1993). Subsequent studies showed that MDM2 deficient mice displayed a very early embryonic lethality due to the apoptosis in the embryo, and this lethality is entirely rescued by simultaneous deletion of p53, which indicated the important role of MDM2 in regulation of p53 (de Rozieres et al., 2000; Jones et al., 1995; Montes de Oca Luna et al., 1995). It is

shown that MDM2 bind to p53 transcriptional activation domain to block its transcriptional activity, and promote p53 degradation through enhanced ubiquitin-proteasome mediated degradation pathway (Haupt et al., 1997; Kubbutat et al., 1997; Midgley and Lane, 1997). Though MDM2 has been established as one of the principal regulators of p53 stability, MDM2 independent degradation of p53 is also observer by other regulators, such as E6/E6AP complex, JNK and calpain (Fuchs et al., 1998; Kubbutat and Vousden, 1997; Pariat et al., 1997; Scheffner et al., 1993; Zhang et al., 1997).

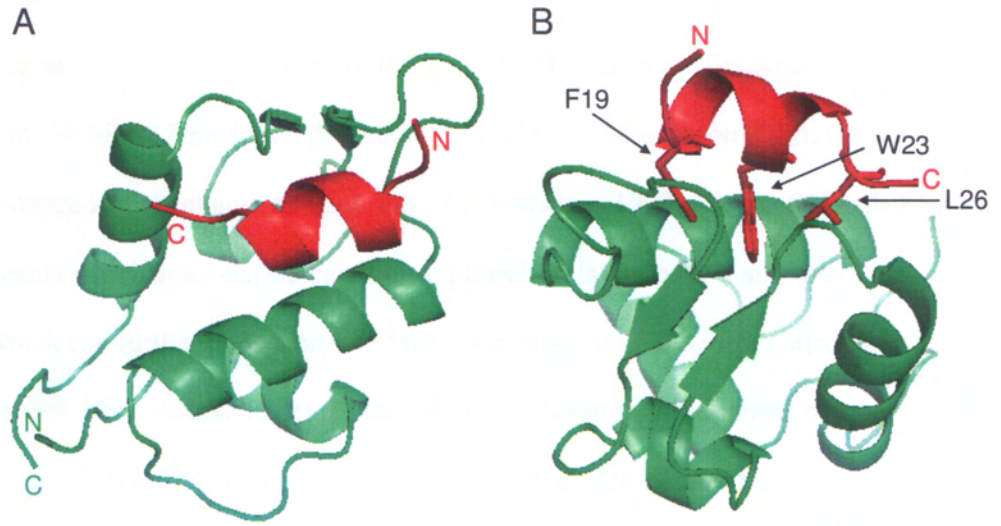

Figure 1-4 p53/MDM2 complex.

The complex structure of MDM2 N-terminal domain (green) and peptide from p53 N-terminal domain (red). A and B show different rotations of the complex structure. SN15 peptide of p53TAD from residue S15 to N29 adopts a α-helix to bind to a hydrophobic cleft. Hydrophobic residues F19, W23 and L26 are directed into the hydrophobic cleft of MDM2 as shown in figure B.

Although it is at very low level in normal cells, p53 must switch from its silence state to its "active" state to execute its tumor suppressor function upon stress signals. These stress signals, both intrinsic and extrinsic to the cell, include DNA damage, oncogene activation, hypoxia, heat-shock and so on. The precise mechanism of p53 activated by stress signals is not entirely lucid. Evidences suggested that it may involve both p53 protein level increase and post-translation of p53. An increase in p53 protein level may be achieved by inhibiting the degradation of p53 directly or indirectly, as well as enhancing the rate of translational initiation of mRNA. Post-translation of p53 includes

phosphorylation, dephosphorylation, acetylation, and so on. The most studied activation of p53 was to break the p53-MDM2 pathway. Evidences suggested that the MDM2-mediated degradation of p53 can be overcome through several independent mechanisms (Lohrum and Vousden, 1999). Some DNA damage agents which activate p53 can induce phosphorylation of p53 and many kinases which can further phosphorylated the N-terminal of p53 in vitro (Jayaraman and Prives, 1999; Meek, 1998). Evidences have shown that the interaction between p53 and MDM2 is disrupted by phosphorylation of threonine 18, which requires the prior phosphorylation of serine 15 (Sakaguchi et al., 2000; Schon et al., 2002). Dissociation of p53 from MDM2 bypassed the MDM2-dependent p53 degradation and resulted in the stabilization of p53 for further apoptotic activity. Many other mechanisms are also reported to contribute to the stabilization and activation of p53 (Ashcroft and Vousden, 1999).

1.3.2. p53 and apoptosis

The most extensively demonstrated activity of p53 is its transcription activity to bind to specific DNA sequences and activate the target gene expression (Crook et al., 1994; Pietenpol et al., 1994). Many genes have been identified to be regulated by p53 and more genes have been found to contain p53-binding sites and thus to have the potential to mediate the effects of p53 on cells (el-Deiry, 1998; Wei et al., 2006).

Most of p53 functions were mediated through its target gene expression. p53 induced proteins to mediate several p53 functions, including cell cycle arrest,

inhibition of growth factor signaling, angiogenesis, promotion of senescence, maintenance of genome, and apoptosis. Difference protein product induced by p53 will lead cell to different fate. However, the criteria that influence p53 to induce specific protein expression are still partially understood. It is only known that several general factors, such as p53 protein levels, type of stress signal, the cell type, and the cellular context and environment, will affect this decision (Sionov and Haupt, 1999). For example, in Saos2 and H1299 cells, high levels of p53 protein induce apoptosis and low levels induce cell cycle arrest (Chen et al., 1996). More intensive studies need to be done to clarify the p53-dependent cell fate determination.

Among all the functions of p53, the apoptotic activity is most critical and central to its tumor suppressor activity. p53 plays a major role in triggering apoptosis under many different physiological conditions (Symonds et al., 1994). The most direct association between the transactivation of p53 with apoptosis comes from its ability to control transcription of pro-apoptotic members of Bcl-2 family. During these proteins, pro-apoptotic Bcl-2 family protein Bax is the first identified p53 target gene product to induce p53-mediated apoptosis (Miyashita and Reed, 1995). p53 induced Bax translocates to mitochondria and releases cytochrome c, which triggers the subsequent caspases activation and apoptosis (Eskes et al., 1998; Goping et al., 1998). Other p53-induced Bcl-2 family proteins include Puma (Nakano and Vousden, 2001), Noxa (Oda et al., 2000), and Bid (Sax et al., 2002). In general, the effect of p53-induced pro-apoptotic Bcl-2 family proteins is to increase the ratio of pro- to

anti-apoptotic Bcl-2 protein, break the balance and trigger the mitochondria-mediated apoptotic pathway.

Besides the Bcl-2 family proteins, other p53 target genes involved in apoptosis activity include Fas/APO1 (Owen-Schaub et al., 1995), KLLER/DR5 (Wu et al., 1997), PAG608 (Israeli et al., 1997), PIG's (Polyak et al., 1997), p85 (Yin et al., 1998), and IGF-BP3 (Buckbinder et al., 1995). Fas/APO1 belongs to the tumor necrosis factor (TNF) receptors superfamily. The Fas/APO1 signal is transmitted through the FADD (Fas-associated death domain) adapter which recruits initiator caspases 8 and 10 resulting in the activation of the caspase cascade (Owen-Schaub et al., 1995). KLLER/DR5 is a death-domain containing pro-apoptotic member of TRAIL (TNF-related apoptosis including ligand) receptors (Ashkenazi and Dixit, 1998). Induction of KLLER/DR5 appears to be increased following exposure of wide-type p53 expressing cells to cytotoxic DNA damaging agents such as γ-radiation, doxorubicin or etoposide (Wu et al., 1997). All these p53-induced proteins together form a complicated matrix to induce apoptosis, which need intensively study to be fully understood.

1.3.3. p53 transcription-independent apoptosis

For a very long time, it is believed that the transcription activity of p53 was indispensable for its apoptotic function, and p53 triggers apoptosis pathway through its transcription target. However, more and more evidences suggested another transcription-independent apoptosis pathway of p53. The first report described transcription-independent apoptosis activity of p53 was published in

1994 (Caelles et al., 1994). Caelles et al. observed transcription-independent apoptosis in p53-deficient cells stably expressing a temperature-sensitive mutant p53 protein (p53Val135). They found that upon shift to the permissive temperature, p53Val135 transcriptionally regulated p53 targets and induce apoptosis. However, when they treated cells with drugs to block the transcription or translation, apoptosis was still induced without p53 targets expression. This observation hinted another p53-dependent pathway besides its transcription activity pathway for the first time.

This transcription-independent apoptotic activity of p53 was then confirmed to be universal by several subsequent papers using different systems. In interleukin 3 (IL-3)-dependent DA-1 lymphoma cells, interleukin-3 withdrawal triggered apoptosis without detectable p53 transcriptional activity (Gottlieb et al., 1996). Balb/c 3T3 cells treated with okadaic acid, which increased p53 phosphorylaion and transcriptional activity, also underwent apoptosis without detectable p53 target gene expression (Yan et al., 1997).

Further studies using several transcription inactivate p53 mutants also confirmed the existence of transcription-independent apoptosis pathway. A truncated form of p53 (referred as p53dl214), containing the first 214 amino acids of wide type p53, was reported to be sufficient to induce apoptosis, albeit at a slower rate than wide type p53 (Haupt et al., 1995). p53dl214 was also able to suppress the transformation of rat fibroblasts by several oncogene combinations and particularly by myc plus ras and HPV E7 plus ras, even though it lacks a major portion of the DNA-binding domain and cannot activate

p53-responsive promoters (Haupt et al., 1995). Moreover, another p53 mutant carrying mutations in residues 22 and 23 (referred as p53Gln22, Ser23) also triggered apoptosis in HeLa cells, without significant activation of relevant p53 target promoters (Chen et al., 1996; Haupt et al., 1995; Kokontis et al., 2001). Another transactivation-deficient p53 mutant, p53R273H, can function normally in apoptosis but not in transcriptional activation following DNA damage. After activated by irradiation with ionizing or UVB radiation in several transformed human cell lines, p53R273H was able to induce apoptosis, but did not increase p21/Waf-1 expression (Bissonnette et al., 1997). A C-terminal truncation, p53K351stop, was also reported to prevent colony formation in Saos-2 cells without G1/S cell cycle arrest and transactivation of a p53 reporter (Ishioka et al., 1995). Furthermore, a p53 loop-helix mutant, p53175P was identified to lose the ability of inducing apoptosis, even with increased transcriptional activity for both a synthetic p53 responsive reporter along with endogenous MDM2 and p21/Waf-1 inducing capacity (Rowan et al., 1996).

Even with accumulating evidences pointing to transcription-independent apoptosis pathway of p53, this idea of novel p53 pathway was received by the scientific community slowly and carefully with doubt for a long time. It is primarily due to the lack of any reported detail mechanism. Recently, several studies revealed the correlation of p53 transcription-independent apoptotic activity with the intrinsic mitochondria-mediated apoptotic pathway. This

improvement suggested a possible mechanism of p53 transcription-independent apoptotic activity and linked it to a well studied apoptotic pathway.

Before the mechanism was described, several papers had already shown the direct connection between p53 and mitochondria. It is reported that p53 could rapidly induce cytochrome c release from freshly isolated murine liver mitochondria (Schuler et al., 2000). In cell-free cytoplasts, activation of cytosolic p53 can induce mitochondrial cytochrome c release (Schuler and Green, 2001). In mitochondria-containing cell-free S100 extracts that model p53-dependent but transcription-independent apoptosis, p53 protein directly mediates caspase-3 activation, and immunodepletion of p53 completely blocks this activation (Ding et al., 2000). These results suggested the direct affect of p53 on mitochondria and mitochondria-mediated apoptosis.

After that, Mull and his group recently reported that a fraction of induced p53 rapidly translocates to the mitochondria upon apoptotic stimuli (Marchenko et al., 2000; Sansome et al., 2001). ML-1 cells treated with camptothecin target a fraction of wild type p53 to mitochondria at the onset of p53-dependent apoptosis but not during p53-independent apoptosis or p53-mediated cell cycle arrest. The accumulation of p53 to mitochondria occurrs rapidly (within 1 hour after p53 activation) and precedes changes in mitochondrial membrane potential, causing cytochrome c release and procaspase-3 activation. The majority of mitochondrial p53 localized to the outer membrane. A small portion of p53 was in a complex with mt hsp70 and mt hsp60, which are the major mitochondrial import motors for protein refolding and importing in the mitochondrial matrix.

This stress signal-induced mitochondrial p53 accumulation and apoptosis but not cell cycle arrest can be inhibited by overexpression of anti-apoptotic Bcl-2 or Bcl-X_L (Marchenko et al., 2000). This mitochondrial localization of endogenous p53 was also observed by immunofluorescence of whole cells when stressed by hypoxic conditions, which provided virtual evidence of the p53 mitochondrial localization (Sansome et al., 2001). *In vivo* data also illustrated p53 localization to mitochondria upon DNA damage and contribution to the apoptosis induction in mice system (Erster et al., 2004; Erster and Moll, 2004). p53 accumulated at mitochondria in radiosensitive organs but not in radioresistant organs. Further more, it is observed that the apoptotic response in the radiosensitive organs occurred in two waves. Upon γ-irradiation, p53 rapidly translocated and accumulated to mitochondria and triggered a first wave of caspase-3 activation. The transcriptional p53 response occurred later and was followed by a subsequent second wave of caspase-3 activity, which was mediated by p53 target proteins (Erster et al., 2004). This mitochondrial p53 localization was also observed and studied by other groups and laid the foundation of mitochondria-mediated transcription-independent apoptosis pathway of p53 (Arima et al., 2005; Erster and Moll, 2005; Essmann et al., 2005; Nemajerova et al., 2005; Zhao et al., 2005).

In parallel, a polymorphism of p53 at amino acid residue 72 was identified to determine the capability of p53 mitochondrial binding and its apoptogenic potential (Dumont et al., 2003). This amino acid residue 72 has two different variants, Arg72 and Pro72, in wide type p53. They have similar expression

level, localization and the transactivation ability of several endogenous p53-induced genes, like p21, MDM2, and PIG3. However, compared to Pro72, Arg72 has significantly higher efficiency to induce the cleavage of procaspase-3, MDM2 and PARP, resulting in an about threefold increased ability to induce apoptosis. This may due to the higher ability to localize to mitochondria of Arg72 than Pro72. The differences in the apoptotic potentials of Arg72 and Pro72 variants can be eliminated when their mitochondrial localization was drawn to the same level by coupling a leader sequence to both of them, confirmed that the mitochondria localization ability decided their apoptotic activation ability (Dumont et al., 2003).

Base on the evidences that p53 translocates to the mitochondria during apoptosis, a mechanistic basis for p53 transcription-independent apoptosis was proposed recently. It is reported that p53 can directly induce permeabilization of the outer mitochondrial membrane by forming complex with the anti-apoptotic protein Bcl-X_L and Bcl-2, resulting in cytochrome c release and apoptosis (Mihara et al., 2003). p53 rapidly accumulates at mitochondria of primary thymocytes undergoing γIR-induced apoptosis and mitochondrial p53 forms a specific complex with Bcl-2 and Bcl-X_L. Mitochondrial p53 binds to Bcl-2/X_L, resulting in inhibition of the anti-apoptotic activity of Bcl-2/X_L and induction of mitochondria-mediated apoptosis pathway. This report described the first p53 transcription-independent apoptosis mechanism after 10 years of its discovery.

After that, several papers reported that besides Bcl-2/X_L, other Bcl-2 family proteins can also interact with p53, such as Bak, Bax, Bad and PUMA. First, Green and colleagues showed that the pro-apoptotic protein, Bax is one of the principal cytoplasmic targets of p53 (Chipuk et al., 2004). Based on their *in vitro* assays they found that p53 and Bax together trigger the permeabilization of model liposomes which mimic the mitochondrial membrane. It is accompanied by the oligomerization of Bax induced by p53, which is a critical step in the Bax-dependent apoptosis pathway. p53 alone is not able to induce permeabilization of isolated mouse liver mitochondria without presence of Bax. $Bax^{-/-}$ mouse embryonic fibroblasts can not undergo p53 transcription-independent apoptosis. Interestingly they failed to observe stable and prolonged physical interaction between Bax and p53, therefore they suggested that p53 bind to Bax through a hit-and-run type mechanism (Chipuk et al., 2004).

Controversially, another group reported that another pro-apoptotic protein of Bcl-2 family Bak, rather than Bax, is the principal target of p53 (Leu et al., 2004). They suggested that the interaction of p53/Bak removes Bak from its association with Mcl-1, which is a mitochondrial anti-apoptotic Bcl-2 protein. Released Bak from Bak/Mcl-1 complex was shown to be activated by oligomerization and mediate subsequent mitochondrial membrane permeabilization and apoptosis (Leu et al., 2004).

PUMA is another BH3 only member of Bcl-2 protein family. Like some of the other Bcl-2 family proteins, PUMA is also a p53 target protein. Its expression is

activated by nuclear p53. It is reported recently that after PUMA expression activated by nuclear p53, PUMA removed cytoplasmic p53 from p53/Bcl-X_L complex. Released p53 can then induce mitochondrial membrane permeabilization and subsequent apoptosis (Leu et al., 2004). This study integrated the nuclear and cytoplasmic proapoptotic functions of p53 by PUMA and suggested a model of p53-dependent transcription-independent apoptosis.

Furthermore, another Bcl-2 family protein Bad is also reported to interact with p53 (Jiang et al., 2006). This interaction prevented cytoplasmic p53 from entering nucleus to activate more Bad expression. Bad is also observed to lead p53 to the mitochondria and forms a p53/Bad complex at the mitochondria. The mitochondrial p53/Bad complex promotes apoptosis via oligomerization and activation of Bad. Taken together, this study indicated that Bad plays dual roles in both p53 transcription-dependent and -independent apoptosis pathways (Jiang et al., 2006).

Even though there are still some controversies, the consensus is that p53 mediates transcription-independent mitochondrial membrane permeabilization, and the interactions between p53 and Bcl-2 family proteins are involved in this pathway. Bcl-2 family proteins are under precise regulation and anti- and pro-apoptotic protein members of Bcl-2 can inhibit each other to balance their function. Therefore it is possible that the particular activation state of the cell and the network of Bcl-2 family proteins determine which pathway p53 uses to trigger mitochondrial membrane permeability and induce apoptosis. It also depends on the different expression levels of various Bcl-2 family proteins in

different cells and tissues. It still needs more efforts to clarify the condition and contribution of different Bcl-2 family proteins involved in p53 transcription-independent apoptotic pathways.

1.4. The interaction between p53 and Bcl-X_L

As discussed above, the p53/Bcl-X_L interaction was the first identified interaction between p53 and Bcl-2 family proteins. It provided the first mechanism of transcription-independent apoptosis of p53 and opened a new avenue to understand the complexity of p53 apoptotic function. It also inspired scientists to discover more regulation relatives between p53 and Bcl-2 family proteins which make the mechanism complete and systematic.

p53 directly induce permeabilization of the outer mitochondrial membrane by forming complex with Bcl-X_L. It is also determined that the p53 DNA binding domain is involved in the interaction. A model of p53DBD/Bcl-X_L was also proposed and amino acids 239-248 were identified to be critical for the p53DBD/Bcl-X_L interaction (Mihara et al., 2003). The p53DBD/Bcl-X_L interaction was also confirmed by subsequent NMR study (Petros et al., 2004). From the NMR study, the p53-binding site on Bcl-X_L was identified to consist of the carboxyl-terminus of the first α-helix, the loop between α3 and α4, and the loop between α5 and α6 of Bcl-X_L. The hydrophobic groove on the Bcl-X_L surface, which is the binding site with BH3 peptide of Bax/Bak, is not involved in the interaction with p53DBD according to the NMR study.

Interestingly, Chipuk et al. reported that p53NTD including p53TAD and proline rich domain are necessary and sufficient to induce transcription-independent apoptosis, while the DNA binding domain is dispensable (Chipuk et al., 2003). It is also reported that p53 can be cleaved *in vivo* through a caspase-dependent pathway. Two out of the four generated fragments of p53, p53-(1-186) and p53-(22-186), which contain N-terminal domain and part of DNA binding domain, translocate to mitochondria and induce mitochondrial membrane depolarization in the absence of transcriptional activity (Sayan et al., 2006). If p53 amino-terminus alone is sufficient to induce transcription-independent apoptosis, the question will be asked that if the p53 amino-terminus also executes the p53/Bcl-2 pathway on mitochondrial and that if amino-terminus of p53 can also interact with Bcl-X_L. Considering its critical role in the transcription-independent apoptosis activity of p53, it is very interesting to study more information about the interaction between p53 with Bcl-X_L.

1.5. Objective of the study

The discovery of p53/Bcl-X_L interaction improved the understanding of the mechanism basis of the transcription-independent apoptotic activity of p53. The structure basis of the p53/Bcl-X_L interaction was studied by mutagenesis, modeling and NMR studies. However, the structure details of the p53/Bcl-X_L complex are still indistinct. There is no any complex structure of p53 with Bcl-2 family proteins available. It is still controversial that which domain of p53 is

involved in the transcription-independent apoptosis and the interactions with Bcl-2 family proteins.

Toward understanding on the transcription-independent apoptosis mechanism of the tumor suppressor protein p53, in this study we aimed to (1) clone, express, purify, and characterize the protein of p53, Bcl-X_L and others used in this thesis; (2) identify the protein-protein interaction between p53NTD and p53TAD with Bcl-X_L; (3) map the binding interface on both p53TAD and Bcl-X_L; (4) identify the interaction between SN15 peptide from p53TAD with Bcl-X_L; (5) figure out the critical amino acids from SN15 for the binding; (6) present a structure model of Bcl-X_L/SN15 to help understanding the detail of p53/Bcl-X_L interaction.

2. Materials and Methods

2.1. Materials

2.1.1. Chemicals

Ni^{2+}-NTA resin, Miniprep plasmid purification kit, PCR purification kit, gel extraction kit, and RNeasy mini kit were purchased from Qiagen (Hilden, Germany). Carbenicillin was purchased from Invitrogen (Carlsbad, CA, USA). dNTP (dTTP, dATP, dGTP and dCTP) mixtures were purchased from invitrogen (Carlsbad, CA, USA) or Finnzymes (Espoo, Finland). Antibodies against p53 and Bcl-X_L were purchased from Santa Cruz Biotech (Santa Cruz, CA, USA). Immun-Star Chemiluminescent protein detection system and protein molecular weight marker were purchased from Bio-Rad Laboratories (Hercules, CA, USA). HiPrep 16/60, 26/60 Sephacryl S-200, HiPrep 26/60 sephacryl S-100 gel filtration columns and Bulk and RediPack GST Purification Module were purchased from Amersham Biosciences (Buckinghamshire, UK). Phenylmethylsulfonyl fluoride (PMSF), reverse transcription-polymerase chain reaction (RT-PCR) kit, restriction enzymes, T4 ligase, expand long PCR system, 1, 4-Dithiothreitol (DTT), and Complete Mini Protease Inhibitor Cocktail Tablets were purchased from Roche (Indianapolis, IN, USA). Lysozyme was purchased from Sigma-Aldrich (St. Louis, Mo, USA). The DNA polymerase *pfu* and site directed mutation kit were purchased from Novagen (Madison, WI, USA). Isoporpyl-Thio-B-D-galactopyranoside (IPTG) was purchased from

Promega (Madison, WI, USA). Ampicillin and kanamycin Sulfate were purchased from US Biological (Massachusetts, USA) or Invitrogen. Bacterial Alkaline Phosphatase was purchased from Fermentas Inc. (Hanover, MD, USA). Isotopes for NMR sample labeling including D_2O, ^{15}N-NH_4Cl, and ^{13}C-glucose were purchased from Cambridge Isotope Laboratories (Andover, MA, USA). MitoTracker® Deep Red 633 and Prolong Antifade reagent, Alexa Fluor® 546 goat anti-rabbit IgG were from Molecular Probes (Eugene, OR, USA). Triton X-100 was bought from Merck KGaA (Darmstadt, Germany). Other common used chemicals were purchased from Sigma-Aldrich (St. Louis, Mo, USA), Merck KGaA (Darmstadt, Germany) or Bio-Rad Laboratories (Hercules, CA, USA). DNA markers for agarose gel electrophoresis, including 100bp ladder and 1kb ladder, were purchased from Bio-Rad or New England Biolabs. Protein molecular weight for SDS-PAGE was from Bio-Rad. Pre-stained protein molecular weight was used for SDS-PAGE followed by western blot analysis to trace the protein transfer to the membrane.

2.1.2. Bacterial strains and mammalian cell lines used in this thesis

Bacterial strain *E.coli* (Escherichia coli) DH5α was used for plasmid amplification and isolation. BL21(DE3) was used for recombinant protein expression and purification. BL21(DE3)pLysS was used to reduce leaky expression and BL21(DE3) Codon Plus was used to increase expression level when needed.

Mammalian cell line NCI-H1299 with a p53-null genotype was used for co-immunoprecipitation experiments and *in vivo* fluorescence resonance energy transfer (FRET) assays.

2.1.3. Vectors

Different vector plasmids were used in this study. pET16b (Ampicilline) was used to express target protein with an N-terminal 10-histidine tag. pET29b (Kanamycin) was used to express target protein with a C-terminal 6-histidine tag. pGEX-4T-m1 (Ampicilline) was used to express target protein with an N-terminal GST tag. pACYC (Chloramphenicol) was used for the co-expression system to express target protein together with another protein from another plasmid. pACDUET (Ampicilline) and pETDUET (Ampicilline) were used to express two target proteins simultaneously in co-expression system to study protein-protein interactions.

pcDNA3.1 (Ampicilline) was used to express target protein in mammalian cells. pECFP and pEYFP were used to express target proteins with fusion protein ECFP and EYFP in mammalian cells for the FRET assay.

2.1.4. Primers

Primers for PCR experiments were purchased from First Base (Singapore, Singapore) or Proligo (Singapore, Singapore). The details of all the primers (including sequencing primers) used in this study are listed in table 2.1.

Table 2-1 Primers used in the study

NAME	USAGE	SEQUENCE
HYD26	FORWARD PRIMER FOR BCL-X_L	CACTCAGCATATGTCTCAGAGCAACCGGGAGCTG (NDE I)
HYD27	REVERSE PRIMER FOR BCL-X_L WITHOUT TERMINATION CODON	GCGATCCTCGAGCTTTCCGACTGAAGAGTGAGCCCAG (XHO I)
HYD28	REVERSE PRIMER FOR BCL-X_L ENDING AT R209 WITHOUT TERMINATION	GCGAAGCTCGAGGCGTTCCTGGCCCTTTCGGCTCTC
HYD29	REVERSE PRIMER FOR BCL-X_L ENDING AT R209 WITH TERMINATION	GCGAAGCTCGAGCTATCAGCGTTCCTGGCCCTTTCGGCTCTC
HYD34	REVERSE PRIMER FOR BCL-X_L WITH TERMINATION CODON –BAM HI	GCGAAGCTGGATCCTTATCATTTCCGACTGAAGAGTGAGCC CAG
HYD40	REVERSE PRIMER FOR BCL-X_L WITH TERMINATION CODON –SALI	GCGAAGCTGTCGACTTATCATTTCCGACTGAAGAGTGAGCC CAG
HYD102	T7 PROMOTOR	TAA TAC GAC TCA CTA TAG G
HYD103	T7 TERMINATOR	GCT AGT TAT TGC TCA GCG G
HYD120	FORWARD PRIMER FOR PGEX SEQUENCING	GGG CTG GCA AGC CAC GTT TGG TG
HYD121	REVERSE PRIMER FOR PGEX SEQUESCING	CCG GGA GCT GCA TGT GTC AGA GG
HYD205	FORWARD PRIMER FOR P53 FROM 62 (NDE I)	C ACT CAG CAT ATG GAA GCT CCC AGA ATG CCA GAG
HYD271	FORWARD PRIMER FOR LOOP DELETION BCL-X_L(45-84)	*P*CTCCGATTCAGTCCCTTCTGG
HYD272	REVERSE PRIMER FOR LOOP DELETION BCL-X_L(45-84)	*P*GCAGTAAAGCAAGCGCTGAGG
HYD324	FORWARD PRIMER FOR PETDUET 1ST PROMOTER SITE	ATG CGT CCG GCG TAG AGG ATC
HYD325	REVERSE PRIMER FOR PETDUET	CGA TTA TGC GGC CGT GTA CAA
HYD326	FORWARD PRIMER FOR PETDUET 2ND PROMOTER SITE	TTG TAC ACG GCC GCA TAA TCG
HYD362	FORWARD PRIMER FOR P53(N1-102) FOR PETDUET (BAMHI)	GC GAA GCT GGA TCC G ATG GAG GAG CCG CAG TCA GAT
HYD363	REVERSE PRIMER FOR P53(N1-102) FOR PETDUET (HINDIII)	C ACT CAG AAG CTT TCA TTA GGT TTT CTG GGA AGG GAC AGA
HYD369	FORWARD PRIMER OF BCL-X_L NO TM (XHO I) FOR ECFP/EYFP	G CGT GAT CTC GAG CT ATG TCT CAG AGC AAC CGG GAG CTG
HYD370	REVERSE PRIMER OF BCL-X_L NO TM (SALI) FOR ECFP/EYFP	GC GAA GCT GTC GAC CTA TCA GCG TTC CTG GCC CT TTC GGC TCT C
HYD372	N-TERMINAL SEQUENCING PRIMER FOR PECFP	GACCCCAAC GAGAAGCGC
HYD373	C-TERMINAL SEQUENCING PRIMER FOR PECFP	ATTCATTTT ATGTTTCAG
HYD374	N-TERMINAL SEQUENCING PRIMER FOR PEYFP	GACCCCAAC GAGAAGCGC
HYD375	C-TERMINAL SEQUENCING PRIMER FOR PEYFP	ATGTTTCAGG TTCAGGGG
HYD403	REVERSE PRIMER OF P53(N1-102) WITH STOP CODON FOR PET16 (XHOI)	GCG AAG CTC GAG CTA TCA GGT TTT CTG GGA AGG GAC AGA
HYD410	FORWARD PRIMER OF P53(N1-102) FOR PEGFP-C2 (XHOI)	GC GAA GCT CTCGAG G ATG GAG GAG CCG CAG TCA GAT
HYD411	REVERSE PRIMER OF P53(N1-102) FOR PEGFP-C2 (SALI)	C ACT CAG GTCGAC TCA TTA GGT TTT CTG GGA AGG GAC AGA
HYD414	FORWARD PRIMER OF BCL-X_L FULL LENGTH FOR PCDNA 3.1 (ECORI)	CACTCAGGAATTCGATGTCTCAGAGCAACCGGGAGCTGGTG
HYD415	REVERSE PRIMER OF BCL-X_L FULL LENGTH FOR PCDNA 3.1 (XHOI)	GCGAAGCTCTCGAGTTATCATCATTTCCGACTGAAGAGTGAG CCCAG
HYD438	FORWARD PRIMER FOR P53(N1-102) FOR PECFP/YFP-C1 (XHO I)	GC GAA GCT CTCGAG GA ATG GAG GAG CCG CAG TCA GAT
HYD439	FORWARD PRIMER OF P53 (N1-102) FOR PET29B (NDEI)	C ACT CAG CAT ATG GAG GAG CCG CAG TCA GAT
HYD440	REVERSE PRIMER OF P53(N1-102) FOR PET29B (XHOI) WITHOUT STOP CODON	GCG AAG CTC GAG GGT TTT CTG GGA AGG GAC AGA
HYD441	FORWARD PRIMER OF P53(N1-102) FOR PCDNA3.1, HINDIII	G CGT GAT AAG CTT ATG GAG GAG CCG CAG TCA GAT
HYD448	REVERSE PRIMER FOR P53(1-102) FOR PECFP/YFP-N1 (SAL I) WITHOUT STOP CODON	C ACT CAG GTC GAC TC GGT TTT CTG GGA AGG GAC AGA
HYD451	SEQUENCING FORWARD PRIMER FOR PEYFP-N1	TAACAACTCCGCCCCATT
HYD452	SEQUENCING REVERSE PRIMER FOR PEYFP-N1	CTCGCCCTCGCCGGACAC
HYD570	REVERSE PRIMER FOR P53 (73) (SAL I) FOR PEYFP-C1	GCGTGATGTCGAC TCACACGCGGGGAGCAGC

2.1.5. Media

2.1.5.1. LB (Luria-Bertani) medium

To make 1 L LB medium, 10 g bacto-tryptone, 5 g bacto-yeast extract, and 5 g NaCl was dissolved into 800 ml H_2O, followed by topping up to 1 L with dd H_2O and autoclave. To make LB agar plates, 2% agar was added into LB medium before autoclave.

To make LB medium with antibiotic, different stock solutions of antibiotics were prepared including ampicillin (100 mg/ml in dd H_2O), kanamycin (30 mg/ml in dd H_2O), and chloramphenicol (15 mg/ml in ethanol). Ampicillin and kanamycin were stored at 4 °C and chloramphenicol at -20 °C. 1 ml of stock solution of corresponding antibiotic was added into 1 L LB or LB agar medium when the medium cool down to below 60 °C after autoclave.

2.1.5.2. SOC medium

SOC Medium was used in the recovery step of *E.coli* competent cell transformations. 2% Bactotryptone, 0.5% yeast extract, 10 mM NaCl, 2.5 mM KCl, 10 mM $MgCl_2$, 10 mM $MgSO_4$, and 20 mM Glucose were dissolved in 800 ml dd H_2O and topped up to 1 L with dd H_2O followed by autoclave. SOC is rich medium which is easy to be contaminated. The prepare procedures were handled with care to avoid contamination.

2.1.5.3. M9 medium

The following stock solutions were prepared before making M9 medium: 0.5 M Na_2PO_4, 1 M KH_2PO_4, 5 M NaCl, 1 M $MgSO_4$, 100 mM $CaCl_2$, 0.5% (w/v) thiamine HCl, 20% glucose, 1 M NH_4Cl. Thiamine HCl was filtered and all other stock solutions were autoclaved.

To make 1 L M9 medium, 105.4 ml 0.5 M Na_2PO_4, 26.5 ml 1 M KH_2PO_4, 2 ml 5 M NaCl, 1.2 ml 1 M $MgSO_4$, 1.2 ml 100 mM $CaCl_2$, 1.2 ml 0.5% (w/v) thiamine HCl, 22.7 ml 20% glucose, 22 ml 1 M NH_4Cl, 1 ml stock solution of antibiotic were mixed and topped up to 1 L with autoclaved H_2O.

To avoid salt precipitation, the $CaCl_2$ was dissolved in 50 ml autoclaved H_2O first before added into the medium. To make uniformly ^{15}N- and/or ^{13}C-labeled M9 medium, 1 g ^{15}N-NH_4Cl and/or 1 g ^{13}C-glucose was added instead of unlabeled NH_4Cl and/or glucose.

The medium was mixed completely and ready for use.

2.1.5.4. Mammalian cell culture medium

Most of the cell lines were routinely maintained in phenol red and high D-glucose-containing Dulbecco's Modified Eagle Medium (DMEM) supplemented with 7.5% fetal calf serum (FCS), 2 mM glutamine and 40 mg/L gentamicin.

2.1.6. Buffers and solutions

2.1.6.1. Buffers and solutions used in DNA agarose gel electrophoresis

50×TAE (Tris-acetate-EDTA) (DNA agarose gel running buffer)

To make 1 L 50×TAE buffer, 242 g Tris base, 57.1 ml glacial acetic acid, 100 ml 0.5 M EDTA were dissolved in 800 ml dd H_2O and pH was adjusted to 8.0. The buffer was then topped up to 1 L with dd H_2O.

TE (Tris-EDTA) buffer

10 mM Tris-Cl and 1 mM EDTA were dissolved in dd H_2O and the pH was adjusted to 7.5 by HCl.

Agarose gel

To make 100 ml 1% (w/v) agarose gel, 1 g agarose powder was added into 100 ml 1×TAE buffer. The solution was carefully boiled in microwave to dissolve. The gel solution was cooled down to room temperature before use.

EtBr (Ethidium bromide)

EtBr stock solution was prepared with 10 mg/ml EtBr in dd H_2O. Final concentration of EtBr in agarose gel was about 0.5 μg/ml. Wearing gloves was compulsory when working with EtBr because EtBr is a mutagen and should be handled as a hazardous chemical.

6×DNA loading dye

0.25% (w/v) bromophenol blue, 0.25% (w/v) xylene cyanol FF, 40% (w/v) sucrose were dissolved in dd H_2O. The loading dye was stored at 4 °C before use.

2.1.6.2. Buffers and solutions used in protein expression

Isopropyl-beta-D-thiogalactopyranoside (IPTG)

IPTG was dissolved in dd H_2O to make 1 M stock solution and stored at -20 °C before use. The IPTG solution was aliquoted to avoid repeating freeze and thaw. 0.1 ml to 1 ml IPTG stock solution was added into 1 L LB medium when inducing target protein expression.

2.1.6.3. Buffers and solutions used in protein purification

For Ni^{2+}-NTA affinity column purification:

Resuspension buffer

20 mM phosphate buffer, 0.5 M NaCl, and 5 mM 2-mercaptoethanol were dissolved into dd H_2O. The pH of the solution was adjusted to 7.8 according to Table 2.2.

Washing buffer

20 mM phosphate buffer, 1 M NaCl, 5 mM 2-mercaptoethanol, and 25 mM imidazole were dissolved into dd H_2O. The pH of the solution was adjusted to 7.2 according to Table 2.2.

Elution buffer

20 mM phosphate buffer, 0.5 M NaCl, 5 mM 2-mercaptoethanol, and 0.5 M imidazole were dissolved into dd H_2O. The pH of the solution was adjusted to 6.0 according to Table 2.2.

Regeneration buffer

6 M guanidinium chloride/0.2 M acetic acid

573.2 g guanidinium chloride was dissolved in 800 ml dd H_2O. 11.5 ml acetic acid (17.4M) was added into the solution and the solution was topped up to 1 L with dd H_2O.

2 %(w/v) SDS (Sodium dodecyl sulfate)

2 g SDS was dissolved in 100 ml dd H_2O. The solution was not allowed to put on ice.

For GST (Glutathione S-transferase) affinity column purification:

Resuspension buffer and washing buffer

PBS (Phosphate Buffered Saline) buffer was used as resuspension and washing buffer. 1×PBS buffer contained 137 mM NaCl, 2.7 mM KCl, 10 mM Na_2HPO_4,

and 2 mM KH_2PO_4, pH 7.3. 1×PBS was diluted from commercial 10×PBS stock buffer in this study.

Elution buffer

0.154 g reduced glutathione was dissolved in 50 ml 50 mM Tris-HCl, pH 8.0. Aliquots of the elution buffer were stored at -20 °C before use. Repeating freeze and thaw were avoided.

Regeneration buffer

Washing buffer 1: 0.1 M Tris-HCl and 0.5 M NaCl were dissolved in dd H_2O, the pH was adjusted to 8.5 using HCl.

Washing buffer 2: 0.1 M sodium acetate and 0.5 M NaCl were dissolved in dd H_2O, the pH was adjusted to 4.5 using acetate acid.

For fast performance liquid chromatography (FPLC) protein purification:

Gel filtration buffer

Running buffer for most NMR samples: 20 mM sodium phosphate, 50 mM NaCl, 1 mM DTT and 0.01% NaN_3 were dissolved in dd H_2O. The pH of the solution was adjusted to 6.5 according to Table 2.2.

PBS buffer for gel filtration purification: 1 mM DTT and 0.01% NaN_3 were dissolved in 1×PBS buffer (137 mM NaCl, 2.7 mM KCl, 10 mM Na_2HPO_4, and 2 mM KH_2PO_4, pH 7.3).

2.1.6.4. Buffers and solutions used in protein characterization

For SDS-PAGE:

5×Tris-glycine electrophoresis buffer

To make 1 L 5×Tris-glycine electrophoresis buffer, 15.1 g Tris, 94 g glycine, and 50 ml 10% SDS were dissolved in 800 ml dd H_2O. The buffer pH was adjusted to 8.3 with HCl and topped up to 1 L with dd H_2O.

SDS-PAGE gel-loading dye (2×)

100 mM Tris-Cl, 200 mM dithiothreitol, 4% SDS, 0.2% Bromophenol blue, and 20% (v/v) glycerol were dissolved in dd H_2O and the pH was adjusted to 6.8 using HCl. The solution was stored at -20 °C before use.

30% acrylamide mix

29 g acrylamide and 1 g N, N'-methylene-bioacrylamide were dissolved in 70 ml dd H_2O and topped up to 100ml with dd H_2O. Final pH of the buffer was controlled to be lower than 7.0. The solution was stored at 4 °C.

10% ammonium persulfate

1 g ammonium persulfate was dissolved in 10 ml dd H_2O and the solution was stored at 4 °C.

Destaining buffer

To make 1 L destaining buffer, 450 ml methanol, 450 ml dd H_2O and 100 ml glacial acetic acid were mixed together completely.

Staining buffer

0.25 g Brilliant Blue R-250 was dissolved in 100ml destaining buffer.

Gel storage buffer

5% methanol and 7.5% glacial acetic acid were dissolved into dd H_2O.

For Western blot:

Transfer buffer

3.03 g Tris and 14.4 g glycine were dissolved in 1 L dd H_2O.

Tris-buffered saline (1×TBS)

20 mM Tris and 500 mM NaCl were dissolved in dd H_2O and the pH was adjusted to 7.5 using HCl.

Washing solution (TTBS)

TTBS contains 20 mM Tris, 500 mM NaCl and 0.1% Tween-20, pH 7.5. 10 ml 10% Tween-20 was added into 1 L TBS to make 1 L TTBS.

Blocking buffer

0.5 g non-fat dry milk was dissolved completely in 100 ml TBS to make 5% milk solution as blocking buffer.

Antibody buffer

0.2 g non-fat dry milk was dissolved completely in 100 ml TTBS to make 2% milk solution as antibody buffer.

2.1.6.5. Stock buffers

1 M Tris buffer pH 8.0

To make 1 L 1 M Tris buffer pH 8.0, 121.12 g Tris was dissolved in 800 ml dd H_2O. The pH was adjusted to 8.0 using HCl, and then the solution was topped up to 1 L with dd H_2O.

1 M Tris buffer pH 7.5

To make 1 L 1 M Tris buffer pH 7.5, 121.12 g Tris was dissolved in 800 ml dd H_2O. The pH was adjusted to 7.5 using HCl, and then the solution was topped up to 1 L with dd H_2O.

5 M NaCl

292 g NaCl was dissolved in 1 L dd H_2O. The solution was stirred until all the NaCl were completely dissolved. The solution was filtered through 0.2 mm membrane.

Sodium phosphate buffer

Sodium phosphate buffer was widely used in this study as the protein sample buffer. Stock solution of 0.2 M NaH_2PO_4 and 0.2 M Na_2HPO_4 were prepared first.

0.2 M NaH_2PO_4: 27.8 g NaH_2PO_4 was dissolved in 1 L dd H_2O.

0.2 M Na_2HPO_4: 28.4 g Na_2HPO_4 was dissolved in 1 L dd H_2O. Use 53.65 g $Na_2HPO_4 \cdot 7H_2O$ or 71.7 g $Na_2HPO_4 \cdot 12H_2O$ if not using Na_2HPO_4.

To prepare sodium phosphate buffer with different pH, mix 0.2 M NaH_2PO_4 and 0.2 M Na_2HPO_4 according to the following table to get the 100 ml 0.2 M different pH stock buffers. A is 0.2 M NaH_2PO_4 and B is 0.2 M Na_2HPO_4.

Table 2-2 Phosphate buffers with different pH

A(ml)	B(ml)	pH	A(ml)	B(ml)	pH
93.5	6.5	5.7	45.0	55.0	6.9
92.0	8.0	5.8	39.0	61.0	7.0
90.0	10.0	5.9	33.0	67.0	7.1
87.7	12.3	6.0	28.0	72.0	7.2
85.0	15.0	6.1	23.0	77.0	7.3
81.5	18.5	6.2	19.0	81.0	7.4
77.5	22.5	6.3	16.0	84.0	7.5
73.5	26.5	6.4	13.0	87.0	7.6
68.5	31.5	6.5	10.5	90.5	7.7
62.5	37.5	6.6	8.5	91.5	7.8
56.5	43.5	6.7	7.0	93.0	7.9
51.0	49.0	6.8	5.3	94.7	8.0

2.2. Methods

2.2.1. Incubation of bacteria

Bacteria were grown on LB medium plates at 37 °C. After transformation, the plates were sealed by laboratory film and stored at 4 °C up to 1 week. In liquid

media (LB or M9 medium), the contained medium volume was less than 1/4 of the flask volume to give better air supply. The media were incubated at 37 °C, 180-250 rpm. The incubation temperature was decreased properly in protein induction process when needed.

2.2.2. Isolation and purification of plasmid DNA from bacteria

Bacteria containing plasmids were inoculated into 2 ml LB medium with corresponding antibiotic and incubated at 37 °C, 220 rpm overnight. The cells were harvested to purify plasmid using Miniprep plasmid purification kit according to the provided protocol.

2.2.3. Agarose gel electrophoresis of DNA

DNA samples were mixed with 6×DNA loading dye and loaded into 0.8%-1.2% agarose gels containing 0.1-0.5 ug/ml EtBr. The gel was running in 1×TAE buffer at 100-120 V for about 30 minutes. The DNA bands were visualized under UV. A DNA marker was often used running beside the DNA sample for estimating the size of the sample.

2.2.4. DNA extraction from agarose gel

DNA samples were separated by running 0.8% agarose gel and the agarose gel containing the band of the target DNA fragment was cut off and weighed up. The DNA was isolated and purified from the gel using Gel Extraction Kit according to the provided protocol.

2.2.5. mRNA extraction from mammalian cells

Mammalian cells were cultured in DMEM medium supplemented with 10% fetal calf serum and incubated at 37 °C with 5% CO_2. The cells were harvested by centrifuging at 500×g for 10 minutes and washed with PBS buffer. The total RNA or mRNA was isolated and purified using the RNeasy RNA Purification Kit according to the provided protocol.

2.2.6. Competent cells preparation

Competent cells are used for the plasmid transformation in the molecular cloning and protein purification. Competent cells of different strains of *E.coli* used in this thesis, including DH5α, BL21(DE3), BL21(DE3)pLysS, and BL21(DE3) Codon Plus were prepared.

To start making competent cells, a colony from LB plate was inoculated into 2 ml LB medium and incubated at 37 °C, 220 rpm overnight. The 2 ml overnight culture was inoculated into another 50 ml fresh LB medium and incubated at 37 °C, 220 rpm to A_{600}= 0.4-0.5. The 50 ml culture was then transferred to sterile centrifuge bottles and put on ice immediately before next step. The cells were harvested by centrifuging at 2600×g (5500 rpm) at 4 °C for 10 minutes. The supernatant was removed carefully and the cell pellet was gently resuspended in 25 ml of ice cold sterile 100 mM $MgCl_2$ solution. This procedure took 3 to 5 minutes. The cells were harvested again by centrifuging at 2600×g (5500 rpm) at 4 °C for 10 minutes. The supernatant was discarded carefully and the cell pellet was resuspended in 5 ml of ice cold sterile 100 mM $CaCl_2$ solution for 2

hours to become transformation competent cells. In stead, the cells can also be put at 4 °C overnight. 2 ml of sterile ice cold 50% glycerol was then added into the cells and mixed briefly. During all the preparation procedures, the cells were remained cold all the times. 20-200 µl aliquot of the cell suspension was put into every ice cold tube and stored at -80 °C. When thawed, the aliquot of competent cells could only be used for once and the remains must be discarded.

2.2.7. Transformation of DNA into *E.coli*

An aliquot of competent cells was taken out from -80 °C and thawed on ice. Approximately 10 ng plasmid DNA and 20 µl competent cells were mixed in a tube and incubated on ice for 30 minutes. The amount of DNA was increased when the BL21(DE3) strain cells were used to do the transformation. The tube was heated for 45 seconds in water bath at 42 °C and put on ice to cool down for 2 minutes. Then the cells were put at room temperature for 1 minute. 500 µl SOC medium or LB medium was added into the tube and incubated at 37 °C, 220 rpm for 45 minutes to 1 hour. 100-200 µl of the culture was plated onto selection LB medium plate and incubated overnight at 37 °C.

2.2.8. DNA concentration measurement

DNA samples were diluted with TE buffer to appropriate final concentration and applied into a 50 µl quartz cuvette. OD_{260} was measured with a UV spectrophotometer. The DNA concentration was calculated by the following equation:

Concentration of DNA (μg/μl) = OD_{260} × dilution factor × 50

Value of OD_{260}/OD_{280} was also measured to valuate the purity of the DNA sample. If the DNA sample is pure, the value of OD_{260}/OD_{280} should be 1.8-2.0. Lower than 1.8 indicates that there may be proteins or/and other UV absorbers in the sample. Higher than 2.0 indicates the sample may be contaminated with chloroform or phenol.

2.2.9. Polymerase Chain Reaction (PCR)

As one of the most important technique in biological sciences, PCR technology was widely utilized to amplify target genes for molecular cloning. In this study, a typical PCR reaction was performed with the components of 1×reaction buffer, 0.2 μM forward primer, 0.2 μM reverse primer, 0.08 mM dNTP mixture, 1 unit DNA polymerase, proper amount of template DNA and topped up with PCR grade dd H_2O. The total volume of the reaction sample is 50 μl. The common used DNA polymerases are Taq polymerase and *pfu* polymerase. Taq polymerase is most used in PCR reaction with high yield and toleration to poor conditions. It lacks a 3' to 5' exonuclease proofreading mechanism so that the mutations generated in the PCR are more than using *pfu* polymerase. Therefore, when high replication fidelity is required, *pfu* polymerase is used in stead of Taq. *pfu* polymerase contains proofreading activity, which decrease the possibility of mutations caused in PCR product. The reaction buffer was determined by the polymerase used in the reaction. The primers were dissolved in dd H_2O. For the dNTP, the amount used in the reaction could be slightly

increased when the target gene was longer than 1 kb. However, the concentration of dNTP was controlled strictly because high concentration of dNTP will increase the possibility to induce mutations in the reaction.

The mixture was added into a 0.2 ml thin-wall PCR tube and put in a GeneAmp® PCR system 9700 (Applied Biosystems, US) PCR machine. A typical PCR reaction cycle contains steps of denature, annealing and extension. A 3-5 minutes first denaturing step was always performed before the actual cycling starts to help denaturing the target DNA completely (especially for the templates which are hard to denature). Also, a final last extension time of 5-10 minutes is used to help finish the elongation of many or most PCR products initiated during the last cycle. Therefore, the following PCR program was mostly used in this work: (1) pre-denature, 95 °C for 3-5 minutes; (2) denature, 95 °C for 30 seconds; annealing, 50-60 °C for 45 seconds; extension, 72 °C/68 °C, 1 minute/kb of target gene; repeat this 3 steps for 25 to 30 cycles; (3) 72 °C/68 °C for 10 minutes to finish the elongation. Set last step of 4 °C for ever to store the sample before collected.

The extending temperature of the program was determined by which polymerase was used, 72 °C for Taq polymerase and 68 °C for *pfu* polymerase. Extending time was decided by the size of the target gene to be amplified, with around 1 minute per 1 kb. In some cases 0.5 µl DMSO was added to the reaction mixture especially in GC rich case. DMSO has been shown to facilitate DNA strand separation (in GC rich difficult secondary structures) because it disrupts base pairing and has been shown to improve PCR efficiency.

2.2.10. Reverse transcriptase PCR (RT-PCR)

RT-PCR was used to amplify cDNAs from mRNA. It contains two steps, RT reaction and PCR reaction. The RT-PCR was performed using a RT-PCR Kit according to the provided protocol. The RT reaction was performed with the components including 1×reaction buffer, 0.2 μM reverse primer, 1 mM dNTP mixture, 1 unit RNase inhibitor, 10 mM DTT, and proper amount of RNA and topped up with PCR grade dd H_2O to 10 μl.

Only reverse primer, not forward primer, was used in the RT reaction. The RNase inhibitor was used to prevent the mRNA template from degradation and digestion. Also the dd H_2O used in RT reaction must be DNase and RNase free. mRNA or total RNA containing mRNA was used as template for the reaction. The mixture was added into a 0.2 ml thin-wall PCR tube and incubated at 65 °C for 10 minutes and put on ice. 1 μl reverse transcriptase was added into the tube and incubated at 42 °C for 1 hour. The RT product was used as template for the following PCR reaction. The subsequent PCR reaction was performed as common PCR reaction according to the protocol described above.

2.2.11. Colony PCR

Colony PCR was used to screen the positive transformant colonies after transformation. After transformation, selected colonies were inoculated into different tubes with 2 ml LB/antibiotic medium individually, one colony in one tube. The cell cultures were incubated at 37 °C, 220 rpm. When the OD_{600} of

the cell culture is above 0.6, 2 μl of the cell culture was used as template for the following PCR reaction. The remaining cell culture was still incubated. In the PCR reaction, Taq polymerase was used and the primers of the target gene or the promoter and terminator sequences from the vector plasmid were used as primers. The PCR products were checked by agarose gel electrophoresis and the cell cultures corresponding to the positive colonies were used for the subsequent plasmid purification and DNA sequencing.

2.2.12. Site-directed and deletion mutagenesis

The site-directed and deletion mutants of target genes were obtained by PCR using the site-directed mutation kit. *pfu* polymerase was used to amplify the gene mutations. 1 μl of DpnI restriction enzyme was added into the purified PCR product to remove the template DNA and then the purified PCR product containing the mutation gene was transformed into XL1-blue competent cells and plated on LB plate with duel antibiotics including Tel and the plasmid selection antibiotic. The positive clones were selected by colony PCR and the mutation genes were confirmed by DNA sequencing.

2.2.13. Clone target gene into vector plasmid

After obtained from PCR reaction, the target genes were cloned into specific vector plasmids to do the following experiments. Both PCR product and plasmid were purified using PCR purification kit according to the provided protocols, and then digested with corresponding restriction enzymes. The

digestion reaction mixtures were incubated at 37 °C for 1.5-2 hours and purified by PCR Purification Kit. Different reaction temperature was used for some special enzymes according to the manuals. For the digested fragment from the vector plasmid less than 100 bp, PCR Purification Kit will remove the small fragment. In case of digested fragment from the vector plasmid bigger than 100 bp, the plasmid digestion sample was separated by agarose gel and the vector band was cut off and purified using Gel Extraction Kit according to the provided protocol. The gene was inserted into the vector by T4 ligase. The ligation reaction mixture contained 2 μl 10×ligation buffer, 1 μl T4 ligase, proper volume of target gene and vector, and topped up to 20 μl with dd H_2O. The reaction was performed at 4 °C for overnight or room temperature for more than 3 hours. The ligation product was directly transformed into *E.coli* DH5α competent cells and colony PCR was used to screen the positive colonies.

2.2.14. Confirmation of insert DNA by DNA sequencing

After cloned into vector plasmids, the target genes were sent for DNA sequencing to confirm the sequence. The PCR mixture for sequencing contained 8.3 μl plasmid, 3.2 μl sequencing primer (T7 promoter/T7 terminator for pET plasmid and specific sequencing primers for other plasmids) and 0.5 μl DMSO. The sequencing data was read and compared with the right DNA sequence of the target gene using Vector NTI software.

2.2.15. Protein expression condition optimization

For the first time to do expression of a new protein, small scale protein expression experiments were performed to test the protein expression efficiency and optimize the induction condition. The plasmid with target gene was transformed into *E.coli* BL21(DE3) competent cells and plated on LB medium plate with corresponding antibiotic. Several transformant colonies were inoculated into different tubes with small volume (usually 2 ml) of LB medium with antibiotic individually. All the cell cultures were incubated at 37 °C, 220 rpm to OD_{600} = 0.6-0.8. Different conditions were applied to do the inductions of the different cell cultures. The conditions to be optimized include ITPG concentration, induction temperature, and induction time. All the cells induced at different conditions were harvested and lysed by sonication. The samples were clarified by centrifuging at 18000 g for 25 minutes. The supernatant and pellet of the cell lysate were checked by SDS-PAGE to compare the target protein yield and solubility.

2.2.16. Large scale protein induction

After the induction condition was optimized, large scale protein induction was performed to produce big amount of proteins. One colony or few colonies from the transformation plate were inoculated into 2 to 10 ml selective LB medium with corresponding antibiotic and incubated at 37 °C, 220 rpm overnight. The overnight cell culture was inoculated into a 2 L flask containing 500 ml selective LB medium and incubated at 37 °C, 220 rpm for several hours to

OD_{600} = 0.6-0.8. IPTG was added into the cell culture and the culture was incubated at the optimized condition with proper ITPG concentration, induction temperature, and induction time. After induction, the cells were harvested by centrifuging at 8000×g for 5 minutes. The cell pellet was immediately used for protein purification or put in -80 °C for storage.

2.2.17. Expression of proteins uniformly labeled with isotope

For some 2D/3D NMR study, the proteins were uniformly labeled with isotope, including ^{15}N and ^{13}C. Minimum M9 medium instead of common LB medium was used to grow cells. ^{15}N-NH_4Cl and/or ^{13}C-Glucose were used with concentration of 1 g/L to take place of normal NH_4Cl and/or Glucose. The cells grow much slower in M9 medium than in LB rich medium. The proteins were commonly induced at 20 °C overnight. The other conditions of expression and the procedure of purification were as same as in LB medium.

2.2.18. Cell lysis

Cell pellets were resuspended in proper volume of resuspension buffer, phosphate buffer for Ni^{2+}-NTA purification and PBS buffer for GST purification. Resuspended cell solution was put on ice and was sonicated for 20 minutes at 20% power until the cells were broken completely. The cell lysate was put on ice all the time to avoid protein degradation and aggregation. The cell lysate was prepared freshly before purification process.

2.2.19. Protein purification by Ni^{2+}-NTA affinity column

Ni^{2+}-NTA affinity column was an efficient tool to purify the target protein. To do the Ni^{2+}-NTA affinity purification, a histidine tag containing six to ten histidines was fused to the N- or C- terminal of target protein during molecular cloning. The recombinant proteins with histidine tag were then purified by Ni^{2+}-NTA affinity columns. Freshly prepared cell lysate was centrifuged at 18000×g for 20-30 minutes and the supernatant was used for the protein purification. The applied amount of Ni^{2+}-NTA resin was decided by the protein amount, 1 ml resin can immobilize about 20 mg proteins. The resin was equilibrated by 10 bed volumes of resuspension buffer before the supernatant of the cell lysate was loaded onto the column. The solution flowed through the resin at a proper rate. 20-30 bed volumes of washing buffer were then applied onto the column to remove the unspecific binding proteins. The immobilized protein on the column was eluted by the elution buffer containing high concentration of imidazole and different fractions were collected and analyzed by SDS-PAGE.

2.2.20. Regeneration of Ni^{2+}-NTA resin

Ni^{2+}-NTA resin can be recycled almost indefinitely if it is washed and regenerated well. If the resin has been oxidized or depleted (loss of light blue color or appearance of yellow/brown color), it is better to be washed with 0.2 M acetic acid in 30% glycerol. The following steps was used for the regeneration of the resin: First the column was washed successively with 2 bed volumes of 6

M guanidinium chloride/0.2 M acetic acid (or other stripping reagent); 5 bed volumes of H_2O; then 2 bed volumes of 2% SDS; 1 bed volume of 25%, 50% and 75% ethanol; 5 bed volumes of 100% ethanol; 1 bed volume of 75%, 50% and 25% ethanol; 1 bed volume of H_2O; 5 bed volumes of 100 mM EDTA; 1 bed volume of H_2O; the column was regenerated with <2 bed volumes of 0.1 M $NiSO_4$, washed with H_2O, and equilibrated with the appropriate chromatographic buffer. The column was white after EDTA wash (or after elution of protein with EDTA) and returned to a pale blue color after regeneration.

2.2.21. Protein purification by GST affinity column

GST affinity column was another device to purify recombinant protein. To use GST column to purify target protein, the protein was fused with a GST tag during molecular cloning. For GST purification, PBS buffer was used to resuspend the harvested cells. Freshly prepared cell lysate was centrifuged at 20000×g for 20-30 minutes. The applied amount of GST resin (Glutatathion Sepharose 4B) was decided by the protein amount. The resin was equilibrated by 10 ml PBS buffer per 1.33 ml of the original slurry of GST beads. The supernatant of cell lysate was loaded onto the column. The solution flowed through the resin at a proper rate. The matrix was washed by 30 bed volumes of PBS buffer to remove the unspecific binding proteins. The immobilized protein on the column was eluted by the elution buffer containing reduced glutathione and different elution fractions were collected and analyzed by SDS-PAGE.

2.2.22. Regeneration of Glutatathion Sepharose 4B

The Glutatathion Sepharose 4B gel can also be regenerated and recycled. The used GST gel was washed with 2 bed volumes of washing buffer 1 (0.1 M Tris-HCl, 0.5 M NaCl, pH 8.5) and 2 bed volumes of washing buffer 2 (0.1 M sodium acetate, 0.5 M NaCl, pH 4.5). The above washing procedure was repeated 4 to 5 times. 3 to 5 bed volumes of PBS buffer were applied to re-equilibrate the gel. The regenerated gel was stored at 4 °C for less than 1 month. For long term storage (> 1 month), the purified gel was washed with 10 bed volumes of PBS buffer followed by repeating washes using 20% ethanol and stored at 4 °C. The regenerated gel was re-equilibrated again by PBS buffer before re-use.

2.2.23. Protein purification using FPLC

After purification using Ni^{2+}-NTA or GST affinity columns, the protein was further purified by FPLC using different columns if the purity is not qualified for the experiments. In this study, gel filtration columns and ion exchange columns were commonly used on the FPLC.

For gel filtration columns including Hiprep 26/60 Sephacryl S-100/S-200 and Superdex 75 10/300 GL from Amersham, appropriate buffers for the target protein were used and the flow rate was normally set at 1 ml/min. More than one bed volume of buffer was used to equilibrate the column before protein was loaded onto the column. The maximum volume of loaded protein was less than

4% of the column bed volume to get a good separation. The fractions of the protein peak were collected automatically and analyzed by SDS-PAGE to check the protein size and purity. The column was washed with at least one bed volume of buffer after purification. For maintenance of the column, more than 1 bed volume of 0.2 M NaOH was usually used to remove the proteins and other molecules blocking in the column and washed using 2 to 3 bed volumes of buffer.

The gel filtration chromatography was also used to measure the molecular weight of protein. Unlike in SDS-PAGE, the proteins were remaining natural in gel filtration purification so that it could tell the polymerization formation of the protein. The molecular weight of the unknown protein was calculated by the standard curve. A serious of molecular weight standard was used to get the standard curve. The molecular weight standard for gel filtration chromatography used in this study contained the following proteins: Thyroglobulin (bovine), 670 kD; R-globulin (bovine), 158 kD; Ovalbumin (Chicken), 44 kD; Myoglobin (horse), 17 kD; Vitamin B12, 1.350 kD. This protein standard mixture was separated in the gel filtration column. According to the gel filtration chromatography, a series of Ve (elution volume of protein) was obtained for all the protein standards. The V_0 (void volume of column) and Vt (total volume of column) were decided by the column specification. Based upon the Ve of each standard, the relationship between Kav ($Kav=(Ve-V_0)/(Vt-V_0)$) and log (molecular weight) should be linear. Based

upon the linear relationship, the molecular weight of the known protein sample was calculated according to its Ve.

Ion exchange columns including anion exchange column and cation exchange column. Ion exchange columns used in this study including Mono Q 5/50 GL from Amersham, and UNO S1 and UNO Q1 from Bio-Rad. Appropriate type of the ion exchange column were chosen according to the protein PI and buffer pH. Before experiment, the column was equilibrated with buffer A with low concentration of salt. The salt concentration of the protein sample was decreased to the same level as buffer A by changing buffer or dilution before the protein was loaded onto the column. After protein sample loaded onto the column, the buffer B with high salt concentration was increased from 0% to 100% in 40-70 ml and the protein was eluted from the column and collected in different fractions. Flow rate was normally set at 1 ml/min. The eluted protein fractions were checked by SDS-PAGE.

2.2.24. Sodium dodecyl sulfate polyacrylamide gel (SDS-PAGE) electrophoresis

SDS-PAGE was extensively used in this study to characterize the molecular weight and purity of purified proteins. Different separation gels were made to detect proteins with different molecular weights. Normally, 10% gel was used for proteins bigger than 60 kD, 15% gel for proteins smaller than 20 kD and 12% gel for proteins in between. The separation gel and stacking gel was made according to the following formula:

Components	Separation gel (5 ml)			Stacking gel (1 ml)
	10%	12%	15%	
H2O	1.9 ml	1.6 ml	1.1 ml	0.68 ml
30% acrylamide	1.7 ml	2.0 ml	2.5 ml	0.17 ml
1.5 M Tris pH8.8 (Separation) or 1.0 M Tris pH 6.8 (Stacking)	1.3 ml	1.3 ml	1.3 ml	0.13 ml
10% SDS	50 µl	50 µl	50 µl	10 µl
10% AP	50 µl	50 µl	50 µl	10 µl
TEMED	2 µl	2 µl	2 µl	1 µl

The protein samples were mixed with same volume of 2× SDS-PAGE loading dye and heated at 90-100 °C for 2-3 minutes. For intact bacteria cells, the heating time was extended to more than 5 minutes to break the cells and denature the total proteins. The heated samples were loaded into the SDS-PAGE gel and run at 30-36 mA for 40-50 minutes. When running finished, the gel was soaked into enough staining buffer for 15 minutes and then washed in destaining buffer until the protein bands were clear.

With a molecular weight standard marker, the protein molecular weight was calculated after SDS-PAGE electrophoresis. The protein molecular weights from Bio-Rad unused in this study contained the following standard proteins: Myosin (20 kD), β-galactosidase (116.25 kD), Phosphorylase b (97.4 kD),

Serum albumin (66.2 kD), Ovalbumin (45 kD), Carbonic anhydrase (31 kD), Trypsin inhibitor (21.5 kD), Lysozyme (14.4 kD), Aprotinin (6.5 kD). A standard curve was generated by plotting the log of the molecular weight of the standard proteins vs. the relative mobility (Rf).

Rf = distance migrated by protein/distance migrated by dye

The curve was used to determine the estimated molecular weights of the unknown proteins.

2.2.25. Protein concentration determination

SDS-PAGE analysis was used to visually estimate the protein concentration according to the protein bands. For relatively accurate determination of the protein concentration, two different methods were used in this study.

Bio-Rad protein assay was used to measure the protein concentration. It can be used for unknown protein and total protein sample containing different proteins. Dye reagent was prepared by diluting 1 part Dye Reagent Concentrate with 4 parts dd H_2O and filtered through Whatman #1 filter (or equivalent) to remove particulates. This diluted reagent was used for approximately 2 weeks when kept at room temperature. Five different dilutions of a protein standard were prepared in advance, which was representative of the protein solution to be tested. BSA was normally used as standard in this assay. The linear range of the assay for BSA is 0.2 to 0.9 mg/ml. 20 µl of each standard and sample solution was added into a clean, dry test tube and 2 ml of diluted dye reagent was

applied to each tube and vortex. Protein solutions are normally assayed in duplicate or triplicate when high accuracy was required. The solution was incubated at room temperature for at least 5 minutes and the absorbance of the sample was measured at 595 nm on a UV spectrometer. A typical standard curve was made using the protein standard data and the protein concentration was calculated according to the curve equation.

For known pure protein, the concentration was also calculated by simply measuring the absorption at 280 nm (A_{280}). The protein was diluted to a proper concentration with an A_{280} between 0.1 and 1. For a pure protein, the protein concentration is in direct proportion to its A_{280}. The factor was calculated by Vector NTI. The protein concentration was calculated as follows:

Conc. = A_{280} × (dilution factor) × Ratio of Con./A_{280}

in which Ratio of Con./A_{280} was obtained from Vector NTI according to the protein sequence.

2.2.26. Buffer exchange of protein sample

After purification, the buffer of the protein solution was changed to the right buffer according to the usage of the protein. Two different methods were used to change the protein buffer. In first method, a centrifugal filter device from Millipore was used. It had a low protein binding membrane which only allows molecules with low molecular weight, like water and salts to pass. Protein solution was applied into the tube and centrifuged at <3000×g to less than 1 ml.

The target buffer was added into the protein solution to 15 ml and the solution was centrifuged to less than 1 ml again. The process was repeated more than three times to get sample with changed buffer. In another method, a commercial desalt column PD-10 Desalting Workmate from GE Healthcare was used. The column was equilibrated with 25 ml target buffer. 2.5 ml protein solution was loaded onto the column and 3.5 ml target buffer was used to elute the protein with changed buffer.

2.2.27. Western blot analysis

Western blot analysis was used to identify specific proteins using corresponding antibodies. The proteins were separated by SDS-PAGE electrophoresis before transfer to the membrane. A pre-stained marker which is visible during running SNS-PAGE and membrane transfer was used to monitor proteins. When the gel was running, a gel-size PVDF membrane was soaked in 100% methanol for 10-15 minutes to equilibrate. Then the PVDF membrane and two gel-size thick filter papers were soaked completely in transfer buffer for about 30 minutes to remove all the bubbles in the filter papers. After the SDS-PAGE electrophoresis was finished, the gel was also soaked in the transfer buffer for 15-30 minutes.

The proteins were transferred from the gel to the PVDF membrane using a semi-dry transfer machine from Bio-Rad. Filter paper, membrane, gel and another filter paper was put on the machine, from bottom to top. The bubbles were excluded by carefully rolling a tube on the surface of the top filter paper. The transfer was run at 15 V and 0.5 A for 20 minutes. If more than one gel was

in the machine, the current will be set 0.5 A per gel. For the proteins with high molecular weight (>134 kD), the running time was extended to 50-60 minutes. The transfer process was monitored using the visible pre-stained marker.

After the proteins transferred from gel to the membrane, the membrane was blocked by 5% non-fat milk in blocking buffer for 1-2 hours at room temperature or overnight at 4 °C. After blocking, the membrane was incubated with protein antibody in antibody buffer, in which the antibody was diluted 1000 to 3000 folds. The solution was incubated at room temperature for 1-2 hours or overnight at 4 °C. Then the membrane was washed in washing buffer for 5 minutes 3-5 times. The membrane was incubated with secondary antibody (1:5000) in antibody buffer for 1-2 hours at room temperature and washed again. Equal amount of western blot detection reagent A and B (0.5 ml each for 1 gel) was mixed together freshly and applied onto the membrane. The protein was detected by exposing to X-ray films.

2.2.28. Circular Dichroism (CD) analysis

After purification, the protein solution was changed to PBS buffer or phosphate buffer with 1 mg/ml and performed CD analysis in a Chirascan Spectropolarimeter (Applied Photophysics Limited, Surrey, UK) to measure its secondary structure. A control sample with buffer only was run as a baseline before the protein sample was run. The samples were added into the cuvette and measured at the wavelength screening from 180-280 nm. The experiments were

repeated 4 times to get an average data. The data from the sample containing buffer only was subtracted from the protein data to minus the buffer effect.

2.2.29. Fourier-transformed infrared spectroscopy (FTIR)

FTIR is another method to measure the secondary structure of protein sample. FTIR spectra were recorded on a Nexus 470 spectrometer purged with N_2 and equipped with a MCT/A detector cooled with liquid nitrogen. For transmission spectra 200 µl of protein (3 mg/ml) were dried on a CaF_2 window (2 cm diameter, 2 mm thick) and also dissolved in D_2O. The dissolved sample was loaded into a transmission of window prepared for liquid samples and a tin space (10 µm thick) was used between the two windows. Spectra were collected at room temperature and without a polarizer. Interferograms recorded were averaged for each sample, with a total of 200 scans. The spectra was deconvoluted to enhance the component bands with FWHH (full width at half-height) = 20 cm^{-1} and a narrowing factor K = 2. Secondary structure content estimation was done by integrating the bands in the deconvoluted spectrum. In the region (1600-1700 cm^{-1}), the different secondary strands content was taken as the percentage of the total area.

2.2.30. Co-expression system to test protein-protein interactions

To identify the interaction between proteins (in this study Bcl-X_L and p53), an *E.coli* co-expression system was used. Both p53NTD and Bcl-X_L were constructed into a dual promoter plasmid pETDuet from Novagen. The

p53NTD contained N-terminal histidine tag while Bcl-X_L contained no tag. The plasmid was transformed into BL21(DE3) cells and both of two proteins were expressed. Then the proteins were purified using a standard Ni^{2+}-NTA affinity column. p53NTD with histidine tag bind to the column and Bcl-X_L without histidine tag was purified only through the interaction with p53NTD. The proteins were characterized by SDS-PAGE and western blot using p53 and Bcl-X_L antibodies.

2.2.31. GST pull-down assay

GST pull-down assay was also used to identify the protein-protein interactions. To test the interaction between two proteins, one of the protein genes was constructed into pGEX-4.1T plasmid to produce a GST fusion protein. Another protein gene was constructed into other vectors such as pET plasmids to expression protein with different tag. The proteins were prepared in PBS buffer after purification. 10 μg of each protein was mixed together and incubated on ice for more than 2 hours. Simultaneity, 20 μl GST resin was washed by PBS buffer for 3-5 times to remove the ethanol and centrifuged at 1000×g and discard the supernatant. The protein sample was then added into the GST resin, gently mixed and incubated at 4 °C for more than 2 hours. The tube containing resin and proteins was kept rotating to avoid precipitation of the resin during incubation. The resin was then washed by 200 μl washing buffer for more than 5 times and eluted by elution buffer containing reduced glutathione. The loading samples and elution samples were detected by western blot.

2.2.32. Tissue culture and transfection

p53-deficient cell line NCl-H1299 cells were cultured at 37 °C under 10% CO_2 in RPMI1640 supplemented with 10% FBS and 100 μg/ml penicillin-streptomycin. Transfections of 1 μg of the plasmid into log-phase growth NCI-H1299 cells were carried out using lipofectamine 2000 reagents from invitrogen according to the provided protocol. Overnight cell cultures were then fixed in 3.7% paraformaldehyde for 20 minutes and mounted on slides. Slowfade antifade kit (Molecular Probes) was used as a mounting solution.

2.2.33. Fluorescence resonance energy transfer (FRET) assay.

FRET assay was performed to test the protein-protein interactions in mammalian cells instead of *in vitro* or in bacterial cell. A Zeiss LSM510 META confocal microscope was employed for FRET analysis using the acceptor photobleaching method as described (Karpova et al., 2003; Kenworthy, 2001) with minor modifications. Both proteins were constructed into the plasmids pECFP and pEYFP respectively to generate fusion proteins with a CFP or YFP tag expressed in mammalian cells. Five images were collected consecutively at 0.15% of the laser intensity in CFP and YFP channels before and after bleaching of YFP by scanning 150 times at 75% laser intensity. An unbleached cell in the same field was used as a background control to determine CFP fluctuations during FRET analysis. Fluorescence intensity was measured in the region where the proteins colocalized. FRET efficiency was calculated as E_F =

$(I_6 - I_5) \cdot 100/I_6$ (Karpova et al., 2003). I_5 and I_6 represent the CFP fluorescence intensities of the fifth and sixth images immediately before and after photobleaching of YFP. The experiment was repeated three times and each set of FRET or control experiments consists of at least 10 cells. The FRET efficiency is presented as the mean percentage of increase in fluorescence intensity with standard deviation.

2.2.34. Peptide synthesis

The p53TAD peptide SN15 (S15 to N29) and SN15p with phosphorylated T18 were purchased from GL Biochem (Shanghai, China). All the alanine mutants of SN15 peptides were chemically synthesized using a Multipep Synthesizer (Intavis). Peptide products were purified by HPLC with a C18 Prep Reversed Phase column. The purity of peptides was tested by HPLC. The molecular weights of all the peptides were measured by mass spectrometer and compared to their real molecular weights to confirm.

2.2.35. Nuclear magnetic resonance (NMR) experiments

NMR experiments were performed on either a Bruker Avance AV700 or AV600 spectrometer, equipped with cryoprobe accessories. Data was acquired and analyzed by Topspin 1.3, Sparky 3.113 and NMRView (Johnson, 2004). Backbone assignment was manually done using Sparky 3.113. The proteins for NMR experiments were purified with >95% purity. 10% D_2O was added into the protein samples. All NMR samples contain 0.01% NaN_3 as a preservative.

1D ^{1}H NMR experiment

Unlabeled proteins were used for the 1D ^{1}H NMR Experiments. The 1D ^{1}H experiment was recorded using water suppression with watergate W5 pulse sequences with gradients. The pulse program is 'zggpw5'. The experiment was performed at 298 K. For the program parameters, TD (size of fid) is 12 K, DS is 4, and sweep width is 16 ppm; the o1p is 4.7 ppm which is decided with the gs mode. The receiver gain was obtained by the command 'rga'. The number of scan was depending on the concentration of the sample and the required definition. For the protein sample with concentration of 0.2-0.5 mM, 8-16 scans were usually used for the data collection. The D19 delay was set to 90-100 us for the water suppression (for 700 MHz, D19=100 us; for 600 MHz, D19=125 us). Other parameters are set as default according to the program from Bruker.

2D ^{1}H-^{15}N HSQC

Uniformly ^{15}N-labeled proteins were used for the 2D ^{1}H-^{15}N HSQC experiments. The 2D ^{1}H-^{15}N HSQC data was collected using the pulse program 'hsqcf3gpph19' with water suppression. The acquisition mode was 'DQD' in the ^{1}H dimension and 'States-TPPI' in the ^{15}N dimension. Program 'hsqcetf3gpsi2' with the acquisition mode of 'Echo-Antiecho' in the ^{15}N dimension was also used. For the program parameters, TD is 256 in the F2 and 4048 in the F2. The CNST4 is set to 90 which is the J (NH). D1 is 1 second. The number of scans was set depending on the concentration of sample and required definition. Usually 2-16 scans were used for most of the experiments.

The spectral width for ^{15}N is 40 ppm and ^{1}H is 16 ppm. The option for 'zg -DLABLE_CN' was used when the ^{15}N and ^{13}C labeled sample was used. The receiver gain was set by the 'rga' command. Other parameters were set as default of the program.

HNCACB

Uniformly ^{15}N, ^{13}C-labeled proteins were used for HNCACB experiments. The pulse program for the experiment is 'hncacbgpwg3d'. The water suppression with watergate was used for the HNCACB experiments. Acquisition mode for the data collection is 'DQD' in the ^{1}H dimension, and 'States-TPPI' in both ^{13}C and ^{15}N dimensions. For the program parameters, the spectral width is 16 ppm for ^{1}H, 34 ppm for ^{15}N and 80 ppm for ^{13}C. The o1p is 4.7 ppm, o2p is 39 ppm and o3p is 119 ppm. The TDs are 2048 for ^{1}H dimension, 128 for ^{13}C dimension and 96 for ^{15}N dimension. The receiver gate was set by command 'rga'. The shaped power (sp1) for water suppression was optimized in the gs mode. Other parameters were obtained by using command getprosol. Also, if the 90 degree pulse for proton is different from the prosol, the command getprosol was used to change it accordingly. The ^{15}N, ^{13}C hard pulse were adjusted according to the standard pulse programs, the water flip pulse and the shape pulse for decoupling were also obtained from the programs provided by Dr. Sattler and Dr. Simon in EMBL.

CBCACONH

Uniformly ^{15}N, ^{13}C-labeled proteins were used for CBCACONH experiments. The experiments were recorded using the same way of that of HNCACB. The pulse program 'cbcaconhgpwg3d' was used with the similar acquisition mode of HNCACB. Other parameters were as same as HNCACB. The scan number was usually 16 for most of the experiments. The shaped power sp1 for water suppression was set in the prosol or re-set in the gs mode.

HNCA and HNCOCA

Uniformly ^{15}N, ^{13}C-labeled proteins were used for HNCA and HNCOCA experiments. The HNCA and HNCOCA experiments were performed using the pulse program 'hncagpwg3d' or 'hncocagpwg3d' with the water suppression using watergate. The acquisition mode was 'DQD' for ^{1}H, 'States-TPPI' for ^{13}C and ^{15}N. The spectral widths for ^{1}H, ^{13}C and ^{15}N were 16 ppm, 32 ppm and 34 ppm. The frequency offset for ^{1}H, ^{13}C and ^{15}N were 4.7 ppm, 54 ppm and 119 ppm. The number of scans was usually 32. The acquisition option 'DLABEL_CN' was used. The receiver gain was set by command 'rga'. Other parameters were obtained by getprosolor or set by the pulse program.

HNCO

The HNCO experiment was performed using the pulse program 'hncogpwg3d' with the water suppression using watergate. The acquisition mode for ^{1}H, ^{13}C and ^{15}N were DQD, States-TPPI and States-TPPI, individually. The spectral widths for ^{1}H, ^{13}C and ^{15}N were 16 ppm, 24 ppm and 34 ppm. The frequency

offset for ^{1}H, ^{13}C and ^{15}N were 4.7 ppm, 54 ppm and 119 ppm. The number of scans was usually 32. The TD in the ^{1}H, ^{13}C and ^{15}N dimensions are 2048, 96, 96. The receiver gain was set by command 'rga'. Other parameters were obtained by getprosol or set by the pulse program.

HNHA

The HNHA experiment was performed using the pulse program 'hnhagp3d'. The acquisition mode for ^{1}H, ^{1}H and ^{15}N were DQD, States-TPPI and States-TPPI, individually. The spectral widths for ^{1}H, ^{1}H and ^{15}N were 14 ppm, 14 ppm and 35 ppm. The frequency offset for ^{1}H, ^{13}C and ^{15}N were 4.7 ppm, 54 ppm and 119 ppm. The number of scans was 32. The TD in the ^{1}H, ^{1}H and ^{15}N are 2048, 128, 96. The receiver gain was set by command rga. Other parameters were obtained by getprosol or set by the pulse program.

2D Nuclear Overhauser Effect (NOE) experiment

The data of 2D NOE experiment were collected using the standard program 'noesyesgpph' from Bruker. The acquisition mode was 'DQD' and 'States-TPPI', individually. The spectral widths were both 14 ppm. The frequency offset for ^{1}H was 4.7 ppm or set by the 'gs' mode. The number of scans was usually 64. The TD in the ^{1}H, ^{1}H were 2048 and 512. The receiver gain was set by command rga. Other parameters were obtained by getprosol or set by the pulse program. The normal sample either in D_2O or H_2O was used for data collection.

2D Total Correlation Spectroscopy (TOCSY) experiment

The data of 2D TOCSY experiment were collected using the bruker standard program 'mlevesgpph'. The acquisition mode was 'DQD' and 'States-TPPI', individually. The spectral widths were both 10 ppm. The frequency offset for ^{1}H was 4.7 ppm or set by the 'gs' mode. The number of scans was usually 16. The TDs in the ^{1}H, ^{1}H were 2048 and 256. The receiver gain was set by command 'rga'. Other parameters were obtained by getprosol or set by the pulse program.

2D Rotating-frame Overhauser Effect Spectroscopy (ROESY) experiment

The data of 2D ROESY experiment were collected using the bruker standard program 'roesygpph19' with water suppression. The acquisition mode was DQD, and States-TPPI, individually. The spectral widths were both 11 ppm. The frequency offset for ^{1}H was 4.7 ppm or set by the gs mode. The number of scans was 64. The TD in the ^{1}H, ^{1}H were 2048 and 512. The receiver gain was set by command rga. The pL11 (f1 channel power level for roesy spin lock) was set to 30 dB. Other parameters were obtained by getprosol or set by the pulse program. The 3-5 mM peptide in buffer was used for data collection with a mixing time 300 ms.

Binding studies by NMR

NMR titration experiment was used to study the protein-protein interactions. ^{15}N uniformly labeled protein was prepared in phosphate buffer of 20 mM

Na-PO_4, 50 mM NaCl, 1 mM DTT, 0.01% NaN_3, 10% D_2O, pH 6.5. The protein concentration was 0.1-0.2 mM. The protein was used to perform 2D ^1H, ^{15}N HSQC experiments at 298 K to get a well separated spectrum. Unlabelled ligand protein or peptide which binds to the ^{15}N labeled protein was prepared. A series of ^1H, ^{15}N HSQC spectra were collected upon adding different amount of ligands.

For the ligand which is a protein, it was purified and prepared in the identical buffer as the ^{15}N labeled protein. When the adding amount of the ligand protein exceeds 10% of the original sample volume, the total sample was taken out from the NMR tube and concentrated to the original volume. For the ligand which is a peptide, the adding amount of peptide was lyophilized before experiment. The right amount of peptide powder was dissolved in the labeled protein solution to get a protein-ligand mixture sample for NMR study. The series of titration experiments were performed continuously using exactly same condition to avoid difference between spectra.

The chemical shift changes of the amino acids upon binding were collected by comparing the spectra. The chemical shift changes of two dimensions were collected separately, and the combined chemical shift changes were calculated according to the following equation

$$\Delta\delta = (\Delta H^2 + (0.154 \times \Delta N)^2)^{0.5}$$

where ΔH and ΔN are chemical shift changes of ^{1}H and ^{15}N channels (Bayer et al., 2003; Kim et al., 2001; Smet et al., 2005).

NMR structure determination of peptide

NMR experiments for determining structures of the peptide SN15 in free state and bound state with Bcl-X_L were carried out on a Bruker Avance 700 equipped with cryo-probe. Two dimensional transferred NOE experiment of 6 mM SN15 was acquired at 298K with mixing time between 100-200 ms in the presence of 0.5 mM Bcl-X_L. The resonance assignment of 2 mM free SN15 was obtained by TOCSY and ROESY. Mixing times of 100 ms for TOCSY and 100-300 ms for ROESY were used. Spectra were processed by Topspin 1.3 (Bruker) and Felix (Accelrys) and analyzed using NMRView.

The ensemble of SN15 structures in free state and bound state with Bcl-X_L was calculated with CYANA, based on both manually and automatically assigned NOEs. Dihedral angle restraints were calculated from chemical shifts using TALOS. The final 20 energy-minimized structures with the lowest target function energy were selected for further analysis. Structures were visualized by PyMOL and SwissPDB viewer.

Complex structure modeling

Modeling of Bcl-X_L/SN15 complex structure was generated using HADDOCK. Chemical shift perturbations observed for Bcl-X_L upon complex formation were used to define ambiguous interaction restraints (AIRs). Active residues of

Bcl-X_L were defined as those having chemical shift perturbations larger than the average +0.5 standard deviation and a relative residue accessible surface area larger than 50% for either side-chain or backbone atoms as calculated with NACCESS. Starting from the minimized average NMR structure of the Bcl-X_L (PDB ID 1bxl, in complex with Bak) and the SN15 structure calculated in the bound state, 1000 rigid-body solutions were generated. The best 200 solutions were selected for semi-flexible refinement and finally refined in explicit water. The clustering was performed using a 1.2 Å cut-off. The 10 lowest energy structures in the lowest energy cluster were accepted as the best representative of the complex.

3. Results

p53 has been discovered for more than 25 years and known as one of the most important tumor suppressor genes. As a transcription activator, its transcription-dependent apoptotic activity has been intensively studied, while transcription-independent apoptotic activity of p53 has a much shorter study history. However, it gains many interests recently with several important evidences published. Mihara et al reported that p53 translocates to mitochondria and directly binds to anti-apoptotic Bcl-2/X_L, resulting in outer mitochondrial membrane permeabilization, subsequent cytochrome c release and apoptosis (Mihara et al., 2003). This study revealed the importance of the p53/Bcl-2 and p53/Bcl-X_L interactions in the transcription-independent apoptosis pathway of p53. To discover the detail of the molecular interaction between p53 and Bcl-2/X_L, especially Bcl-X_L which is easier to work with, different biochemical and biological studies were performed on p53, Bcl-X_L, and its interaction.

3.1. Molecular cloning of p53NTD and Bcl-X_L

The interaction between p53 and Bcl-X_L has been described (Mihara et al., 2003; Petros et al., 2004). To understand the detail information of the interaction, we firstly focused on the N-terminal domain of p53, which is found to be a new binding site for Bcl-X_L. Full length human p53 protein contains 393 amino acid residues. It contains several well-defined functional domains, including an N-terminal domain (NTD), a C-terminal domain (CTD) and a

DNA-binding domain (DBD) in between. NTD contains a transcriptional activation domain from start to amino acid residue 73 and a subsequent proline-rich domain. NTD contributes to the transcription activity of p53. A nuclear export signal also locates here. Amino acid residue 94 to 312 is the DNA binding domain which can interact with specific DNA sequences of p53 target genes. Most of the p53 point mutations found in cancers occur within this domain, suggesting that DNA binding activity is critical for its transcription function and is of importance for the apoptotic activity. A tetramerization domain is localized at CTD which facilitates p53 to form a tetramer. CTD also contains several nuclear-localization signals and a nuclear export signal (Figure 3-1). The numbers displayed in the p53 protein map showed the amino acid residue numbers of the start and end points of different domains.

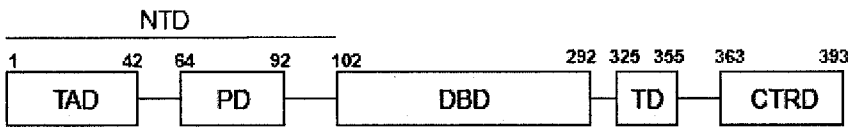

Figure 3-1 Full length wild type p53 protein.

NTD, N-terminal domain; TAD, transcription-activation domain; PD, proline-rich domain; DBD, DNA binding domain; TD, tetramerization domain; CTRD, C-terminal regulation domain. NTD contains TAD and PD. The amino acids of each domain were indicated.

Bcl-X_L is a key member of anti-apoptotic Bcl-2 family proteins. Full length Bcl-X_L protein contains all four Bcl-2 homology domains (BH1 – BH4). A transmembrane domain (TM) was located at the C-terminal of the protein,

which is important for its localization and distribution in cells. Between BH1 and BH4 domains there is a very long flexible loop, which is not critical for its apoptotic activity, but involved in some regulation mechanisms (Kang et al., 2005). Wild type full length Bcl-X_L contains 233 amino acids (Figure 3-2).

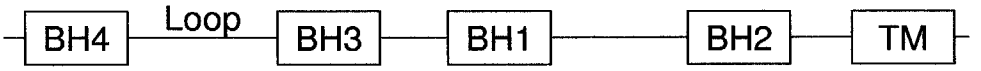

Figure 3-2 Full length wild type Bcl-X_L protein.
BH1 – BH4, Bcl-2 homology domains 1 – 4; TM, transmembrane domain. Loop, flexible long loop between the helices α1 and α2.

To study the interaction between p53NTD and Bcl-X_L, the cDNA of Bcl-X_L and p53NTD domain were cloned from the RNA by RT-PCR or a cDNA library by common PCR reaction. To facilitate the following molecular cloning, the genes were amplified with NdeI and XhoI restriction enzyme sites at the N-terminal and C-terminal primers, respectively. The genes were first cloned into pET16b (for p53NTD) or pET29b (for Bcl-X_L) to generate p53NTD-pET16 and Bcl-X_L-pET29b plasmids. The plasmids were confirmed by DNA sequencing and then used as templates for the following subcloning to generate other plasmids used in this study.

The fragment of p53NTD (N-terminal domain) encoding amino acids from M1 to T102 was amplified by standard PCR using a cDNA library of Hela cells as template (Figure 3-3A). The primers were designed with NdeI enzyme site at 5' and XhoI enzyme site at 3' to generate a p53NTD fragment with restriction

enzyme sites. The PCR product and pET16b vector plasmid were digested with NdeI/XhoI and ligased to generate a pET16b-p53NTD plasmid according to the protocol described in material and method chapter.

The cDNA of Bcl-X_L without C-terminal transmembrane domain was amplified by RT-PCR using a total RNA of MCF-7 cells as template (Figure 3-3B). The transmembrane domain was excluded in PCR to make the Bcl-X_L protein soluble in the following expression and purification processes in bacteria. The primers were also designed with NdeI enzyme site at 5' and XhoI enzyme site at 3'. The RT-PCR product was digested with NdeI/XhoI and inserted into a pET29b vector which was also previously digested by NdeI/XhoI to generate a pET29b-Bcl-$X_L\Delta$TM plasmid.

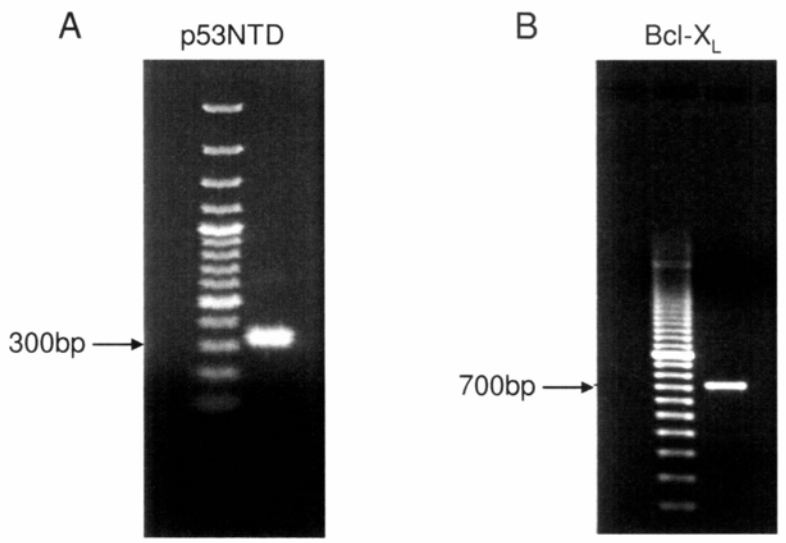

Figure 3-3 Molecular cloning of p53NTD and Bcl-X_LΔTM

A) PCR product of p53NTD. The size of the fragment was more than 300 bp. B) RT-PCR product of Bcl-X_LΔTM. The size of the fragment was about 700 bp. Total volume of the PCR mix was 50 µl. 5 µl of each PCR product was mixed with 1 µl 6×DNA loading dye and loaded into 1% agarose gel. The gel was put in the DNA gel tank and run at 100 V for 30 minutes in 1×TBE buffer. The agarose gel contained EtBr and the DNA bands were visualized under UV spectrometer after run. 100 bp DNA ladders were run beside the target samples to monitor the size.

The PCR products were first confirmed by their molecular weights estimated by the DNA ladder. Then the insert genes were further confirmed by colony PCR using the corresponding primers. After got the plasmids, the insert gene sequences of pET29b-Bcl-X_LΔTM plasmid and pET16b-p53NTD plasmid were confirmed by DNA sequencing using T7 promoter and T7 terminator as sequencing primers. The confirmed plasmids were stored at –20 °C and used

for the following protein purification or subcloning. The plasmids were stable for years when stored at –20 °C.

3.2. Complex formation of p53NTD with Bcl-X_L

It is reported that p53 interacts with Bcl-X_L directly (Mihara et al., 2003). One of the binding sites on p53 was identified to be its DNA binding domain, which was also confirmed by the subsequent NMR study (Mihara et al., 2003; Petros et al., 2004). A model of p53DBD/Bcl-X_L complex structure was proposed based on computer-based modeling. However, detail information of the complex structure is still not available. Interestingly, another report also suggested that the N-terminal domain of p53 alone is necessary and sufficient to induce the transcription-independent apoptosis (Chipuk et al., 2003), which illuminated us to check if p53NTD can interact with Bcl-X_L. To probe the specific molecular interaction between p53NTD and Bcl-X_L, a co-expression system was firstly utilized to perform a binding assay in *E.coli* cells. A dual promoter plasmid pETDuet from Novagen was used in the system. pETDuet vector was designed for the co-expression of two target genes in bacteria cells. It encodes two multiple cloning sites (MCS) each of which is preceded by a T7 promoter/lac operator and ribosome binding site (rbs). The vector also carries the pBR322-derived ColE1 replicon, lacI gene and ampicillin resistance gene. p53NTD and Bcl-X_L cDNA has been cloned into pET system plasmids previously. To do the co-expression, Bcl-X_LΔTM and p53NTD were subcloned from the pET29b-Bcl-X_LΔTM plasmid and pET16b-p53NTD plasmid using

different primers and then constructed under the two different promoters in pETDuet vector to generate a pETDuet-p53NTD-Bcl-X_L plasmid. To facilitate the following purification of the complex, a histidine tag was constructed to the N-terminal of p53NTD while no tag was constructed to any of the Bcl-X_L terminals. Both of the genes were also confirmed by DNA sequencing.

To check the p53NTD/Bcl-X_L interaction and purify the complex, the confirmed pETDuet-p53NTD-Bcl-X_L plasmid was transformed into *E.coli* BL21(DE3) cells and grew at 37 °C. When the A_{600} of the cell culture reached 0.6-0.8, 1 mM IPTG was added and the protein expression was induced at 20 °C, 200 r.p.m for 3 hours. The proteins were purified using Ni^{2+}-NTA columns and the different fractions from the purification procedures were analyzed by 15% SDS-Page using a big size gel (16×20 **cm)** to get a satisfied separation effect. Western blot using both p53 and Bcl-X_L antibodies were also performed to identify the proteins (Figure 3-4).

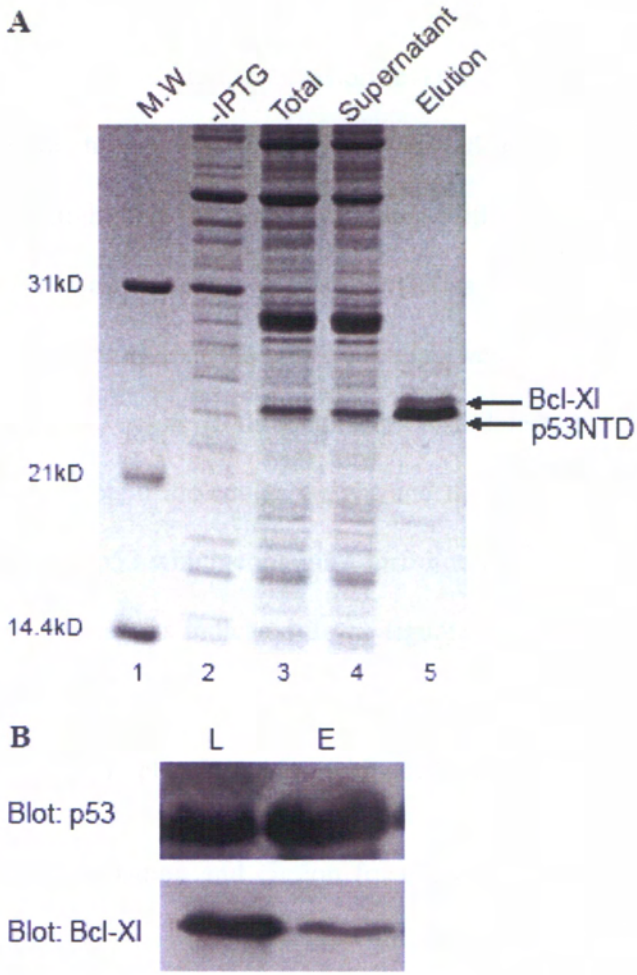

Figure 3-4 Molecular interaction between p53NTD and Bcl-X_L in *E.coli* co-expression system.

A) p53NTD with histidine tag and Bcl-X_L without tag were co-expressed in *E.coli*, purified by Ni^{2+}-NTA affinity column and analyzed by SDS-PAGE. Lane 1, MW marker; lanes 2 and 3, before and after induction by adding IPTG; lanes 4 and 5, loading sample and eluted fraction of Ni^{2+}-NTA affinity column. B) The loading sample (L) and eluted fraction (E) from Ni^{2+}-NTA affinity column were analyzed by Western blot with antibodies to p53 and Bcl-X_L.

Figure 3-4A showed the SDS-PAGE gel of the different fractions in the purification of the co-expressed proteins. Compared with the -IPTG sample, the

expression of p53NTD and Bcl-X_L were obviously induced in lane 3 where IPTG was added. The different expression level of two proteins might due to the differences of the gene position in the plasmid and the N-terminal tag of p53NTD which might help the gene expression. Both protein bands of p53NTD and Bcl-X_L in the supernatant lane were almost as same as the ones in lane 3 (total sample), indicating that these two proteins were soluble when expressed in the co-expression system. Both bands were also detected in elution fraction. According to the protein molecular weight and the band size, the lower band was identified to be p53 which contains a histidine tag and the upper band was Bcl-X_L without any tag, as indicated in the figure. Since Bcl-X_L does not have histidine tag, the only way that it was immobilized on the Ni^{2+}-NTA affinity resin is through the complex formation with p53NTD.

The proteins in the loading and elution fractions from the Ni^{2+}-NTA affinity column purification were further checked by western blot using antibodies to p53 and Bcl-X_L (Figure 3-4B). The western blot result indicated that both proteins of Bcl-X_L and p53 were detected in the loading and elution fractions, confirmed the complex formation of p53NTD/Bcl-X_L in our co-expression system. From the results presented above, the p53NTD/Bcl-X_L complex formation was successfully detected in the co-expression system in *E.coli*, which provided a solid evidence of the molecular interaction between p53NTD and Bcl-X_L. The successful obtaining of the complex in our system also suggested that the p53NTD/Bcl-X_L interaction was stable and resistant to high

salt conditions up to 1 M NaCl during the Ni^{2+}-NTA affinity column purification.

3.3. NMR studies on molecular interaction between p53NTD and Bcl-X_L

The identification of the interaction between p53NTD and Bcl-X_L in the co-expression system in bacteria cells prompted us to check their physical interaction *in vitro*. An NMR-based binding assay was used in this study. To prepare the protein samples for the binding experiments, both p53NTD and Bcl-X_L proteins were expressed, purified, and characterized. Uniformly ^{15}N-labeled p53NTD and Bcl-X_L proteins were also purified for the NMR-based binding assays.

3.3.1. Construction, expression, purification, and characterization of Bcl-X_L loop deletion mutant (Bcl-X_LΔTMΔloop)

As we introduced before, Bcl-X_L contains a very long flexible loop (from M45 to A84) between the first two helices (Figure 3-2). Some of the Bcl-2 family proteins, like Bcl-2, share this loop structure. Flexible region without stable structure always cause a lot of problems in NMR study. The three-dimensional structure of Bcl-X_L was determined using the loop deletion version of Bcl-X_L protein (Muchmore et al., 1996). To get a better performance in NMR study, this loop region was deleted and a Bcl-X_L loop deletion mutant (Bcl-X_LΔTMΔloop) was used in our NMR experiments. It has been reported that the deletion of this loop does not decrease the apoptotic ability of Bcl-X_L

(Muchmore et al., 1996). DNA sequence encoding amino acids from M45 to A84 were deleted using PCR and the DNA fragment of Bcl-X_L loop deletion version was inserted into pET29b vector to generate a pET29b-Bcl-X_LΔTMΔloop plasmid.

The plasmid was then transformed into *E.coli* BL21(DE3) and the protein was induced at $A_{600} = 0.8$ by adding 1 mM IPTG at 30-37 °C, 200 rpm for 2-3 hours. For 2D NMR study, M9 medium containing ^{15}N-NH_4Cl, in stead of LB rich medium, was used to produce uniformly ^{15}N-labeled Bcl-X_LΔTMΔloop protein. Bcl-X_LΔTMΔloop protein was then extracted from the bacteria cells and purified using Ni^{2+}-NTA affinity columns.

The different fractions from the Ni^{2+}-NTA affinity column purification of Bcl-X_LΔTMΔloop were checked by SDS-PAGE. Figure 3-5A showed the SDS-PAGE of the purification fractions. The induction and expression of Bcl-X_LΔTMΔloop protein in *E.coli* cells were quite good and the protein band in supernatant lane indicated that almost all of the expressed Bcl-X_LΔTMΔloop proteins were soluble. The elution fractions on the SDS-PAGE showed that the efficiency of the Ni^{2+}-NTA purification was very good and the purity of around 70-80% was obtained.

To do further purification to get enough pure proteins for NMR study, FPLC purification with a Sephacryl S-200 gel filtration column was performed. The elution fractions from Ni^{2+}-NTA column were loaded onto the gel filtration column. NMR running buffer (20 mM sodium phosphate, 50 mM NaCl, 1 mM

DTT, 0.01% NaN_3, pH6.5) was run at flow rate of 1 ml/min. The column was equilibrated with running buffer previously. After purification, the peak fractions at the appropriate volume were collected and checked by SDS-PAGE. The chromatography of the gel filtration purification of Bcl-X_LΔTMΔloop protein showed a major peak between 100 ml to 200 ml which was the target protein. The peak at around 100 ml contains large proteins and aggregated proteins. The peak coming out after 300 ml was imidazole peak (Figure 3-5B). Figure 3-5C showed the SDS-PAGE of the different fractions of the Bcl-X_LΔTMΔloop protein peak. High efficiency of the Bcl-X_LΔTMΔloop purification was obtained according to the chromatography and the SDS-PAGE result. The purified protein was qualified to do the following NMR experiments. The proteins were concentrated to proper concentration and stored at 4 °C or on ice for short time storage (less than 1 week for Bcl-X_LΔTMΔloop) and at -80 °C for long time storage.

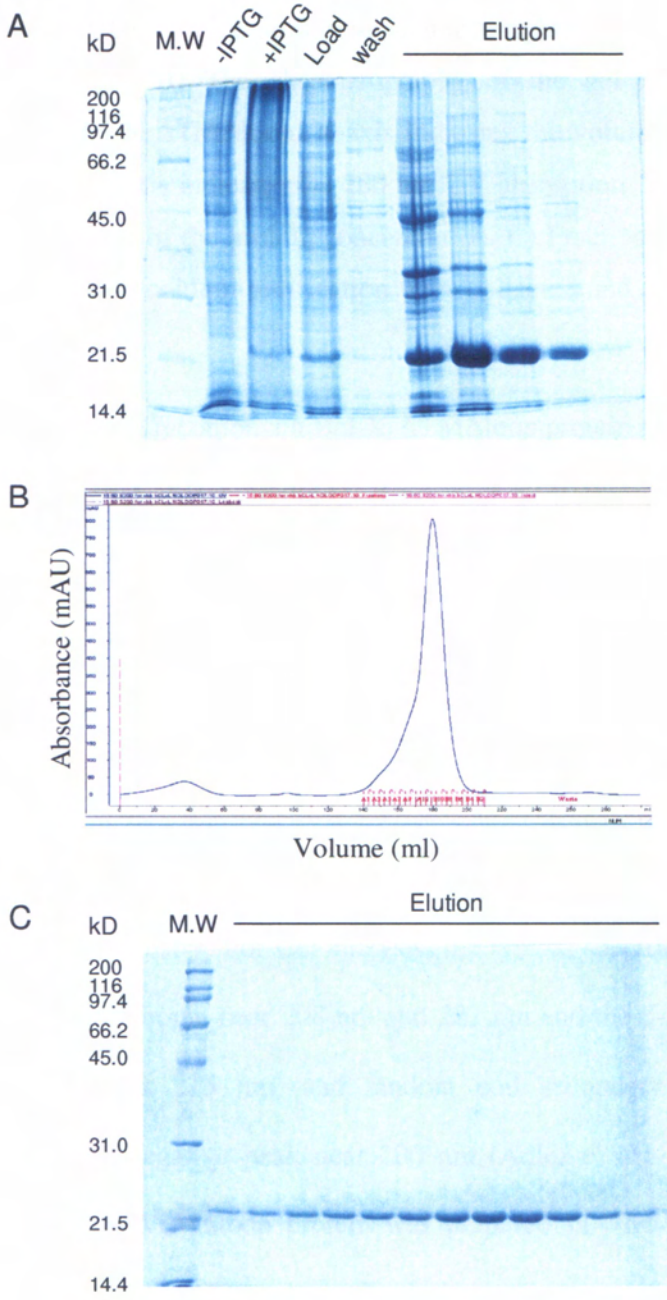

Figure 3-5 Expression and purification of Bcl-X_LΔTMΔloop (M45-A84)

A) Expression and purification of Bcl-X_LΔTMΔloop by Ni^{2+}-NTA affinity column. Fractions from different procedures of protein expression and purification were collected and analyzed by 12% SDS-PAGE. Protein

molecular weight ladder was used as a marker to indicate the target protein size. The size for every band of the protein molecular weight ladder was displayed at the left of the gel. B) The chromatography of the gel filtration column purification of Bcl-X_LΔTMΔloop. X-axis indicates the volume of the running buffer used, and Y-axis indicates the 280 nm UV absorption. The height of the peak is an indication of the protein concentration. C) Fractions from the major peak of gel filtration column purification were collected and analyzed by 12% SDS-PAGE.

After purification, the recombinant Bcl-X_LΔTMΔloop protein was characterized using different biochemical methods. X-ray and NMR structures of Bcl-X_L indicated that Bcl-X_L has a very good secondary structure with several α-helices and no β-sheet (Muchmore et al., 1996). In our study, Circular Dichroism (CD) analysis and Fourier-Transformed Infrared Spectroscopy (FTIR) were used to check the secondary structure of the proteins.

CD analysis is a very common method used to measure the secondary structure of protein in biochemistry. For CD analysis, the typical spectrum of α-helix is characterized by a minima near 208 nm and 222 nm and the β-sheet structures yield a minimum at 215 nm, and random coil secondary structures are characterized by a negative peak near 200 nm (Adler et al., 1973). Purified recombinant Bcl-X_LΔTMΔloop protein was prepared in NMR buffer with 1 mg/ml and performed in CD analysis. Typical α-helical minima were observed in the spectrum indicated the α-helices secondary structure in our recombinant Bcl-X_LΔTMΔloop protein, which was consistent with published data (Figure 3-6A).

FTIR analysis was also used as a common method to measure the protein secondary structure. In the FTIR analysis, the absorption of the amide I spectra arises from the C=O stretching of the peptide bond (1600-1700 cm^{-1}). The correlation between the frequency of the amide I vibrational bands and the type of the secondary structure has been well established before (Byler and Susi, 1986). So the secondary structures of proteins can be assessed through the amide I spectra, which now is widely used for the conformation analysis in proteins. Frequencies in the regions of 1655±4 cm-1 correspond to α-helices, while bands resonating in the regions of 1640-1620 cm^{-1} correspond to β-sheet elements. However, the values may vary slightly according to different families of proteins. In our study, the amide I mode of Bcl-X_LΔTMΔloop protein contained a broad symmetrical band centered at about 1655 cm^{-1}, indicating relatively high α-helices content of the protein (Figure 3-6B). Both of the CD and FTIR results confirmed that the purified recombinant Bcl-X_LΔTMΔloop protein in our study was well folded and remained its natural secondary structure.

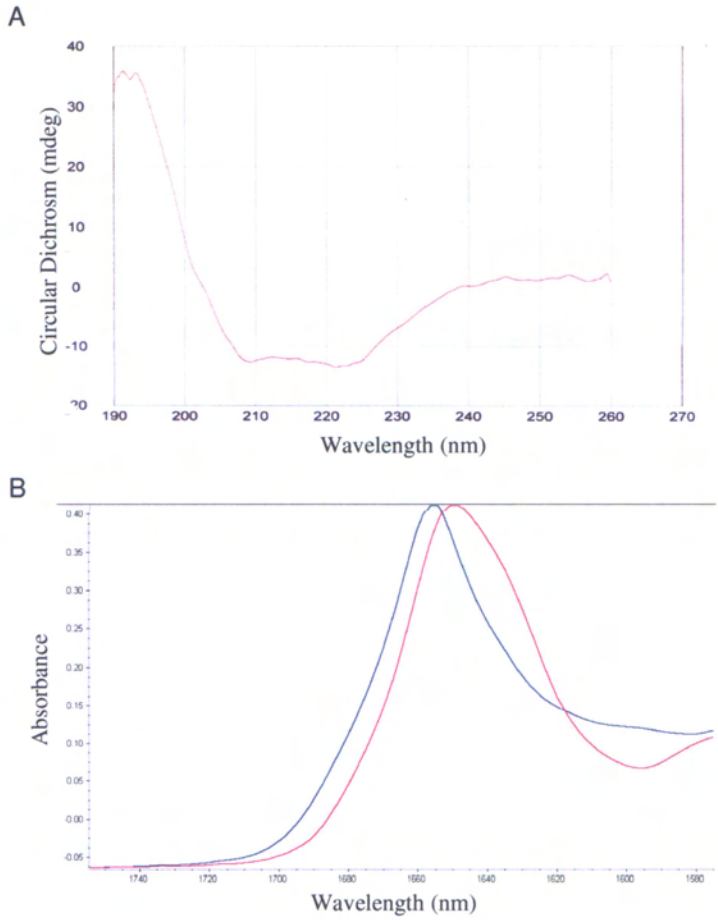

Figure 3-6 CD and FTIR analysis of purified Bcl-X_LΔTMΔloop protein

A) CD analysis of Bcl-X_LΔTMΔloop. Purified Bcl-X_LΔTMΔloop was prepared with concentration of 1 mg/ml. A blank sample with same buffer but no protein was used as control. The data measured using control sample was subtracted from the data of protein to remove the background effect. B) FITC analysis of Bcl-X_LΔTMΔloop. Red curve was obtained from original measurement. Blue curve was modified by the software.

Before the protein was used in NMR binding assay, 1D ^{1}H and 2D ^{1}H-^{15}N HSQC experiments were performed using unlabeled and uniformly ^{15}N-labeled Bcl-X_LΔTMΔloop proteins to check their performance in NMR spectrometers.

In an NMR spectrum, the dispersion of the NMR resonance signals in the regions of methyl protons (-0.5-1.5 ppm), α-protons (3.5-6 ppm), and amide protons (6-10 ppm) is a very good indicator of folded globular proteins (Page et al., 2005). In this meaning, 1D ^{1}H and 2D ^{1}H-^{15}N HSQC experiments were often used to identify the folding status of proteins. In the spectrum of 1D ^{1}H NMR experiment using unlabeled Bcl-X_LΔTMΔloop, very obvious signal peaks of the methyl protons were observed, indicating that the protein was well folded (Figure 3-7A). In the 2D ^{1}H-^{15}N HSQC experiments using uniformly ^{15}N-labeled Bcl-X_LΔTMΔloop, the spectrum presented very good dispersion of the peaks, confirmed that the protein was well folded and qualified for the NMR-based binding assay (Figure 3-7B).

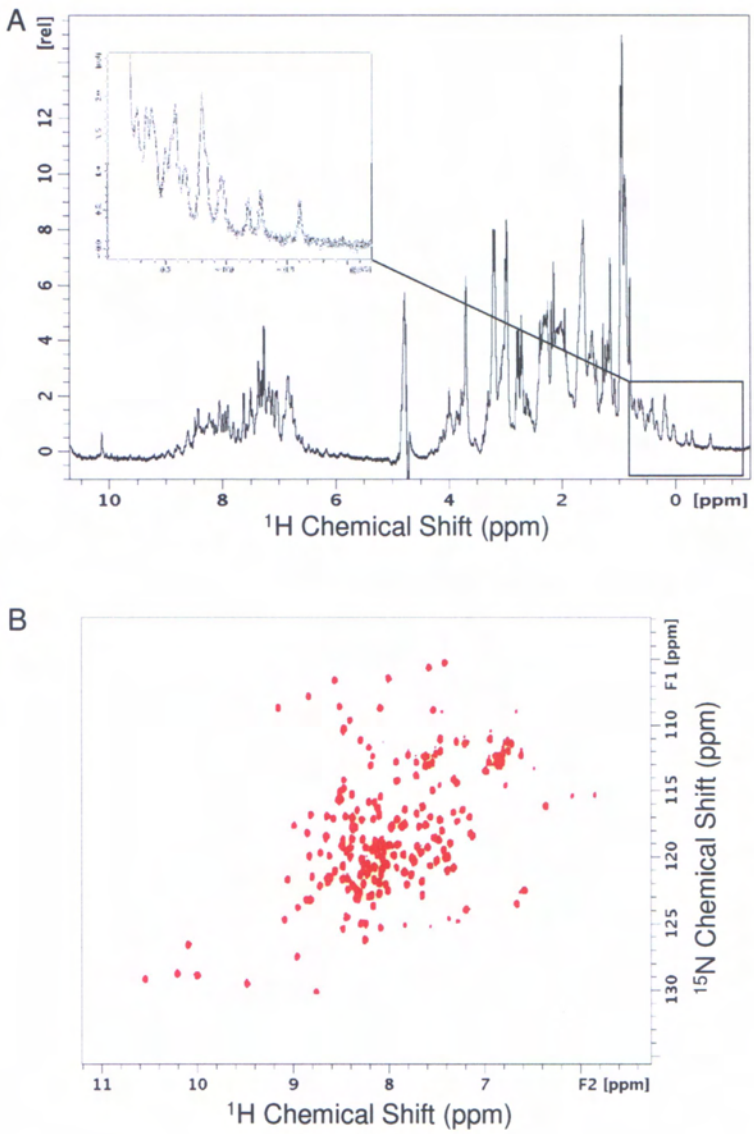

Figure 3-7 1D and 2D NMR analysis of purified Bcl-X_LΔTMΔloop

Purified unlabeled and ^{15}N-labeled Bcl-X_LΔTMΔloop proteins were prepared in NMR running buffer with concentration of 0.2 mM for NMR experiments. A) 1D ^{1}H NMR experiment of Bcl-X_LΔTMΔloop. B) 2D ^{1}H-^{15}N HSQC experiment of uniformly ^{15}N-labeled Bcl-X_LΔTMΔloop.

3.3.2. Expression, purification, and characterization of p53NTD.

p53NTD consists of 102 amino acids from the N-terminal of p53, containing the transcriptional activation domain (TAD) from residue 1 to 73 and proline-rich domain (PPD) after the TAD. p53NTD was reported to be necessary and sufficient to induce the transcription-independent apoptosis (Chipuk et al., 2003). To study the involvement of p53NTD in the interaction with Bcl-X_LΔTMΔloop *in vitro*, the p53NTD protein was also expressed, purified and characterized.

The pET16b-p53NTD plasmid, containing p53NTD with an N-terminal histidine tag, was transformed into BL21(DE3) and the protein was induced at A_{600} = 0.8 by adding 1 mM IPTG at 20-25 °C, 220 rpm for 2-3 hours. For 2D NMR study, M9 medium containing ^{15}N-NH_4Cl in stead of LB rich medium was used to produce uniformly ^{15}N-labeled p53NTD. The protein was then extracted from the bacteria cells and purified using Ni^{2+}-NTA affinity columns.

The different fractions from the Ni^{2+}-NTA affinity column purification of p53NTD were checked by SDS-PAGE. The induction and expression of p53NTD in *E.coli* cells were not very high but still satisfied. The p53NTD band in supernatant lane was similar as the band in total sample, indicating that most of the expressed p53NTD proteins were soluble. The elution fractions on the SDS-PAGE showed a satisfied efficiency of the Ni^{2+}-NTA purification and the purity of around 80% was obtained (Figure 3-8A).

To do further purification to get enough pure proteins for NMR study, FPLC purification with a Sephacryl S-200 gel filtration column was also performed. The eluted fractions from Ni^{2+}-NTA column were concentrated to a proper concentration and loaded onto the column. NMR running buffer (20 mM sodium phosphate, 50 mM NaCl, 1 mM DTT, 0.01% NaN_3, pH6.5) was used at flow rate of 1 ml/min. After purification, the peak fractions at the appropriate volume were collected and checked by SDS-PAGE.

Figure 3-8B showed the chromatography of the gel filtration purification of p53NTD. The target protein peak was collected in different fraction tubes and tested by SDS-PAGE (Figure 3-8C). The results indicated that p53NTD was purified with high efficiency using gel filtration column. The purified protein was qualified to do the following NMR experiments. The proteins were concentrated to proper concentration and stored at -80 °C before use.

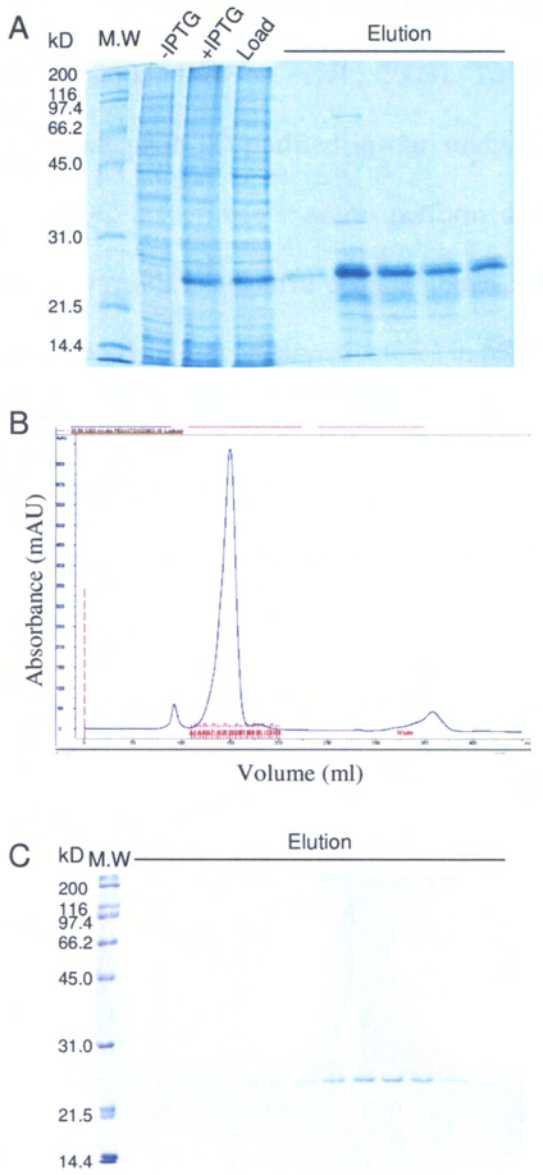

Figure 3-8 Expression and purification of p53NTD(1-102)

A) Purification of p53NTD by Ni^{2+}-NTA affinity column. Fractions from different procedures of protein purification were collected and analyzed by 12% SDS-PAGE. B) The chromatography of the gel filtration column purification of p53NTD. C) Fractions from the gel filtration column purification were analyzed by 12% SDS-PAGE.

Structure study on the N-terminal domain of p53 indicated that it was natively unfolded (Bell et al., 2002; Dawson et al., 2003). To check the secondary structure of recombinant p53NTD purified in our study, CD analysis, 1D ^{1}H and 2D ^{1}H-^{15}N HSQC experiments were performed to do the protein characterization. In CD result, a negative peak at about 200 nm was observed, indicating the major disordered secondary structures in p53NTD protein (Figure 3-9A). Similar results were also obtained in 1D and 2D NMR experiments. Signals in the methyl protons region (-0.5 ppm to 1.5 ppm) in 1D ^{1}H NMR spectrum were not detected (Figure 3-9B) and the 2D ^{1}H-^{15}N HSQC spectrum showed a very narrow dispersion in the backbone amide proton resonance signals which only covered about 7.5 ppm to 8.5 ppm (Figure 3-9C). The CD and NMR results confirmed that our recombinant p53NTD protein remains disordered, which is consistent with its native state.

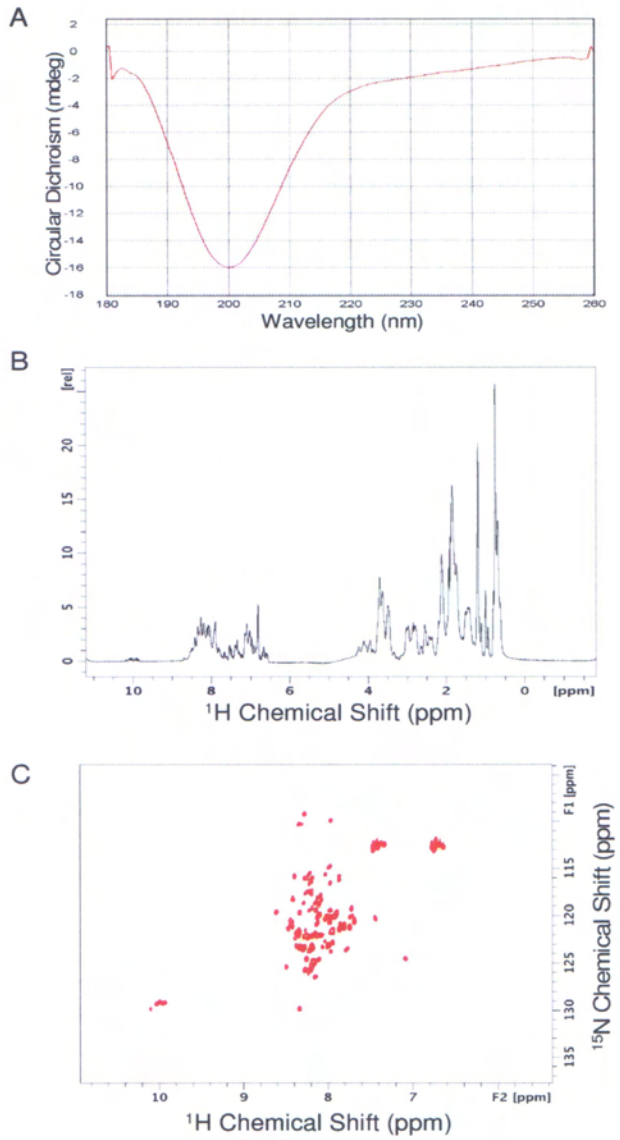

Figure 3-9 Characterization of purified p53NTD

Purified recombinant p53NTD protein was characterized using CD, 1D and 2D NMR experiments. A) CD analysis of p53NTD. Purified p53NTD was prepared with concentration of about 1 mg/ml. A blank sample with same buffer but no protein was used as control. The data measured using control sample was subtracted from the data of protein to remove the background effect. B) 1D ^{1}H NMR experiment result of p53NTD. C) 2D ^{1}H-^{15}N HSQC experiment of uniformly ^{15}N-labeled p53NTD.

3.3.3. NMR studies on the interaction between p53NTD and Bcl-X_L

With purified p53NTD and Bcl-X_LΔTMΔloop proteins, an NMR-base binding assay was used to study the interaction between p53NTD and Bcl-X_L. ^{15}N-labeled Bcl-X_LΔTMΔloop was purified and finally prepared in 90% H_2O/10% D_2O containing 20 mM sodium phosphate, 50 mM NaCl, 1 mM DTT, and 0.01% NaN_3, pH 6.5 with concentration of 0.2-0.5 mM. The unlabeled p53NTD protein was also purified and prepared in the same NMR running buffer. A 2D ^{1}H-^{15}N HSQC experiment was first performed using ^{15}N-Bcl-X_LΔTMΔloop protein without p53NTD protein. Different amount of p53NTD protein was then added into the Bcl-X_L sample. A series of ^{1}H-^{15}N HSQC spectra were collected with increasing p53NTD amount and the chemical shift perturbations were monitored. The NMR sample was concentrated to its original volume when the volume of added p53NTD exceeded 10% of the initial sample. The different spectra were analyzed and compared using Bruker Topspin software and Sparky.

The chemical shift changes of Bcl-X_LΔTMΔloop upon adding p53NTD were obviously detected (Figure 3-10A). The results did not show tremendous overall chemical shift changes of Bcl-X_L, indicating that no major conformational change was induced by p53NTD. While some noticeable chemical shift changes from amino acids of Bcl-X_L revealed the physical interaction between p53NTD and Bcl-X_L. Enlarged section of some amino acids involved in the interaction was also presented, showing that the chemical shift changes of L112 and E129 are specifically perturbed in the presence of

p53NTD (Figure 3-10B). Gradient chemical shift changes were obtained by titrating with increasing amount of p53NTD. The concentrations of different amount of p53NTD were indicated (Figure 3-10B).

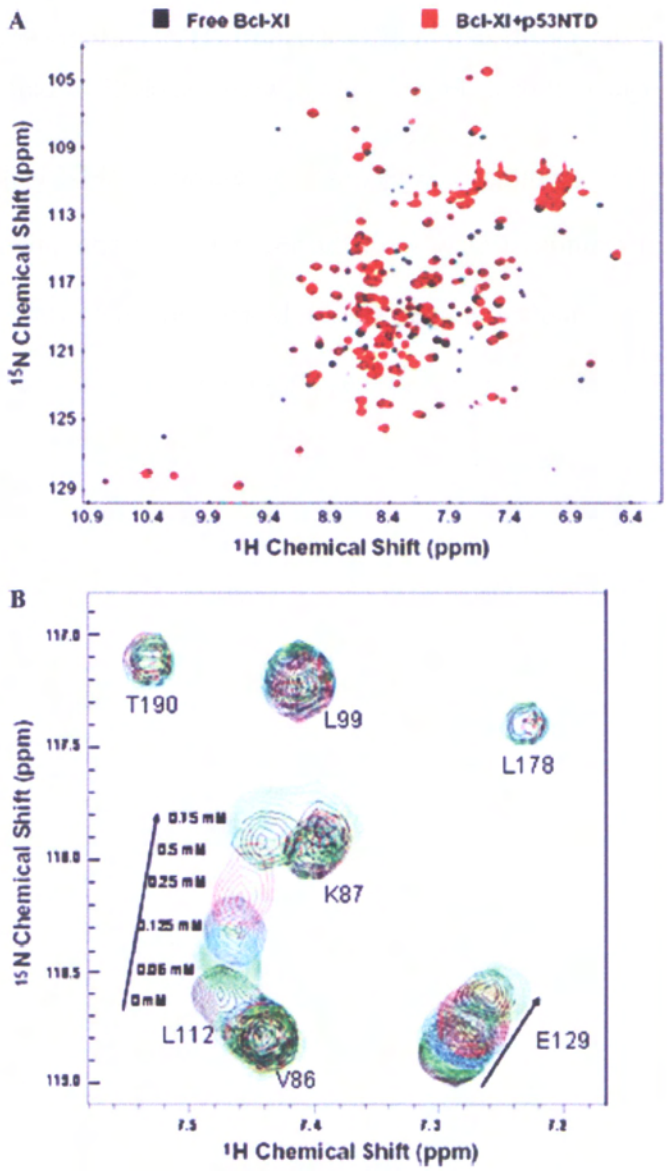

Figure 3-10 Bcl-X_L interacts with p53NTD in an NMR-based assay.

A) ^{15}N-labeled Bcl-X_L was monitored on a 2D ^{1}H–^{15}N HSQC upon the addition of unlabeled p53NTD. Spectrum of Bcl-X_L alone is presented in black.

Spectrum of Bcl-X_L with the addition of p53NTD is presented in red. Concentration of ^{15}N-labeled Bcl-X_L was 0.5 mM. Concentrations of ^{15}N-labeled Bcl-X_L and p53NTD were 0.5 and 0.25 mM, respectively. B) Section of a ^{15}N HSQC NMR titration spectrum. Chemical shift changes were observed on the peaks of amino acid L112 and E129 upon the addition of increasing amount of p53NTD from 0 to 0.75 mM as displayed. V86, K87, L99, E129, L178, and T190 do not show obvious chemical shift changes.

With published NMR structure and backbone assignment of Bcl-X_L, Bcl-X_L residues showing chemical shift perturbations were preliminarily summarized. The residues affected are located in the region including α4, the N- and C-termini of α3, the N-terminus of α5, and the central part of α2 (Figure 3-11).

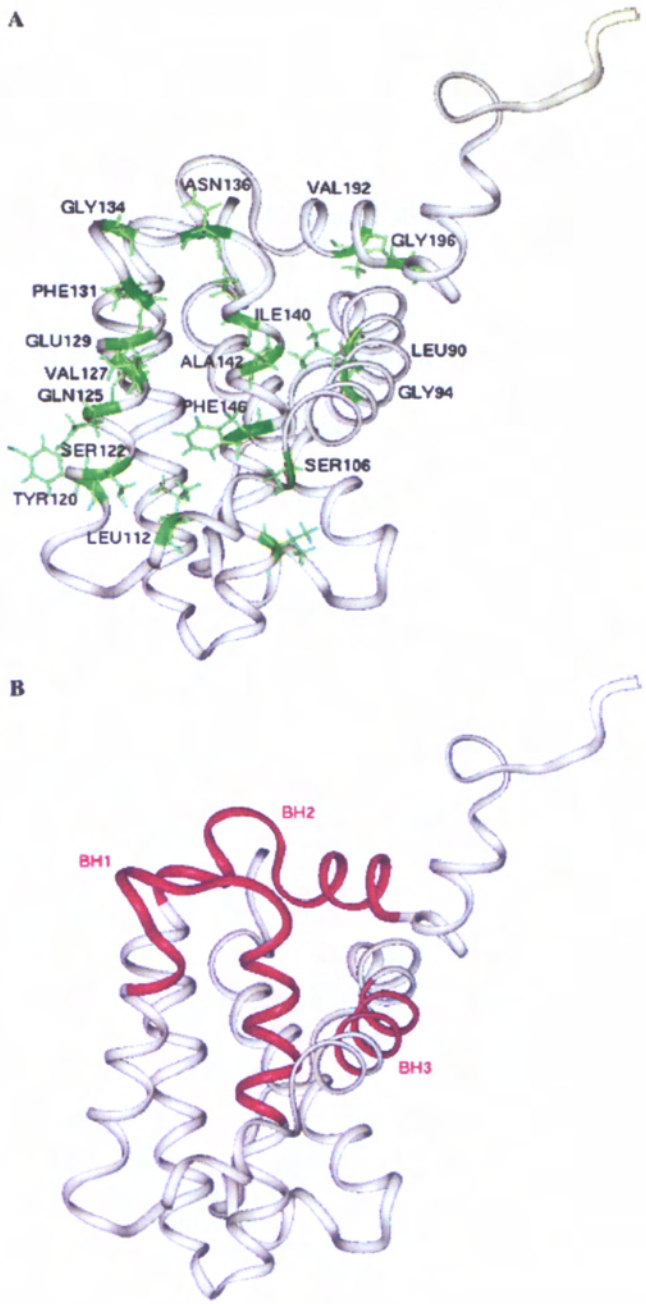

Figure 3-11 Mapping of p53NTD/Bcl-X_L interaction on Bcl-X_L.

A) Ribbon representation of Bcl-X_L. Amino acids perturbed upon the addition of p53NTD are shown in green. B) Ribbon representation of Bcl-X_L (PDB1BXL). BH1, BH2, and BH3 regions are shown in pink.

In addition, the NMR-based binding assay was also performed with ^{15}N-labeled p53NTD and titrated with unlabeled Bcl-X_LΔTMΔloop. The spectra of the 2D ^{1}H-^{15}N HSQC experiments before and after adding Bcl-X_LΔTMΔloop were overlaid to compare (Figure 3-12). Chemical shift changes were observed upon the addition of Bcl-X_LΔTMΔloop. Signals of several amino acids disappeared after binding. The result confirmed the physical interaction between p53NTD and Bcl-X_L. Not like Bcl-X_L, p53NTD do not have published backbone assignment data. Therefore we were not able to get the interface on p53NTD from the NMR binding assay.

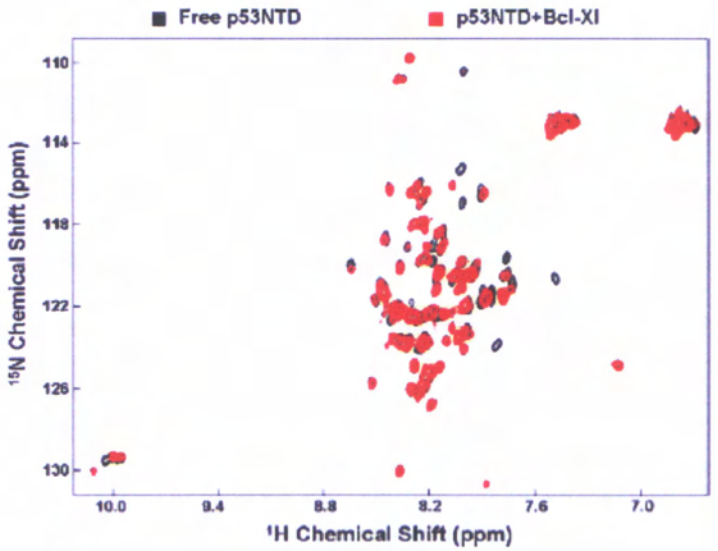

Figure 3-12 Bcl-X_L interacts with p53NTD in an NMR-based assay.
2D ^{1}H-^{15}N HSQC spectrum recorded on ^{15}N-labeled p53NTD in the absence (in black) and presence (in red) of unlabeled Bcl-X_LΔTMΔloop protein. Concentrations of ^{15}N-labeled p53NTD and unlabeled Bcl-X_LΔTMΔloop were 0.25 and 0.375 mM, respectively.

3.4. p53NTD and Bcl-X_L interact in cells

To further confirm the molecular interaction between p53NTD and Bcl-X_L we observed in *E.coli* cells and *in vitro* NMR binding assay, we performed a FRET assay to test their interaction in mammalian cells. p53-deficient cell line NCI-H1299 was used in the assay. p53NTD was fused to a yellow fluorescent protein (YFP) as acceptor molecule and Bcl-X_L was fused to a cyan fluorescent protein (CFP) as donor molecule. Both of the two proteins were overexpressed in NCI-H1299 cells. The amount of FRET was calculated as a percentage increase in the donor (CFP) fluorescence intensity after photobleaching the acceptor (YFP) in a small part of the cell as seen in Figure 3-13A. When the YFP acceptor fluorophore was at least 85% selectively bleached, an increase in fluorescence signal in the donor CFP in the region of interest was observed, indicating the occurrence of FRET. The increase in CFP fluorescence intensity in the bleached region (Figure black dashed box) was compared to the CFP fluctuation in the unbleached (control) region (Figure white dashed box). From the data, the FRET efficiency for the bleached and unbleached samples was 5.11% and 0.54%, respectively (Figure 3-13B). Taken together, our FRET data suggest that the FRET is seen between the donor CFP-Bcl-X_L and acceptor YFP-p53NTD, which appears to be attributed to the molecular interaction between p53NTD and Bcl-X_L in NCI-H1299 cells.

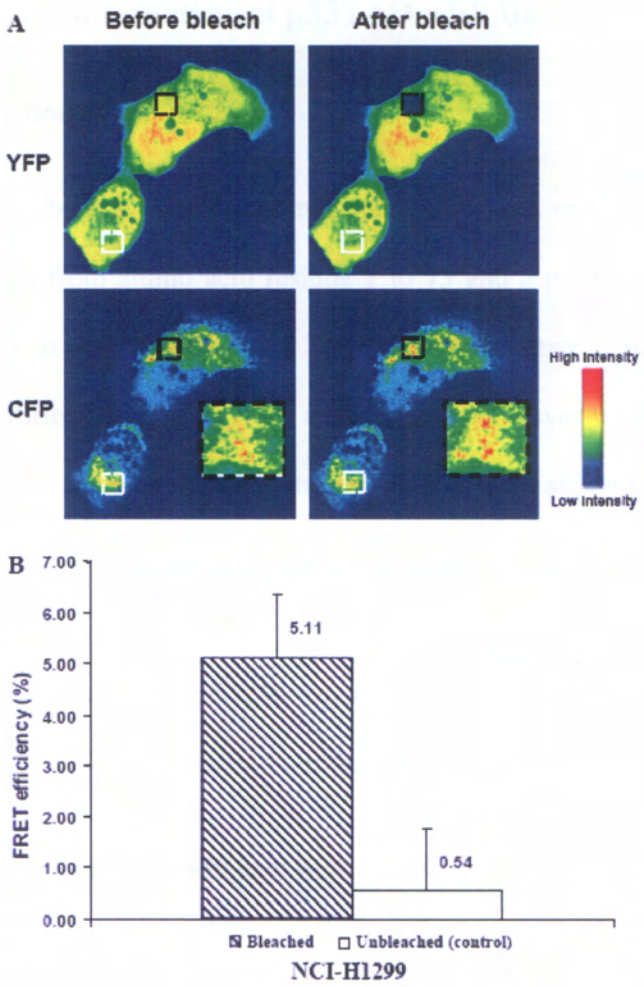

Figure 3-13 Molecular interaction between p53NTD and Bcl-X_L in a FRET assay.

A) FRET assay was used to illustrate the existence of the binding between p53NTD and Bcl-X_L. NCI-H1299 cells co-expressing p53NTD-YFP and Bcl-X_L-CFP were cultured at 37 °C for 16-18 hours before FRET assay. Images of NCI-H1299 cells in CFP and YFP channels before and after acceptor photobleaching are shown. The bleached region was outlined by black dashed square box, whereas white dashed box indicates the unbleached (control) region. B) Histogram shows quantification of FRET. The increase in CFP fluorescence intensity in bleached (black columns) and control unbleached (white columns) cells. The data represent the average of three experiments.

3.5. Molecular interaction of p53TAD with Bcl-X_L

3.5.1. Construction of p53TAD

As we introduced before, p53 N-terminal domain consists of a transcriptional activation domain from amino acid residue 1 to 73 and a proline rich domain from residue 73 to 102 (Figure 3-3). The interaction between p53NTD and Bcl-X_L was confirmed in our previous experiments. However whether both of these two domains are necessary for the interaction were still not known. To further study the binding site on p53NTD, the proline rich domain was truncated from p53NTD by PCR. p53TAD gene containing first 73 amino acids of p53 was constructed into pET16b vector to generate a pET16b-p53TAD plasmid. Binding studies were carried out on p53TAD and Bcl-X_L.

3.5.2. p53TAD is enough to interact with Bcl-X_L

To check whether p53TAD binds Bcl-X_L, GST pull-down assay was used to study the physical interaction *in vitro*. Bcl-X_LΔTMΔloop protein was purified as mentioned above. p53NTD and p53TAD were constructed into a pGEX vector to generate pGEX-p53NTD and pGEX-p53TAD plasmids which produce GST fusion proteins.

Both of the pGEX-p53NTD and pGEX-p53TAD plasmids were transformed into BL21(DE3) *E.coli* cells and the recombinant proteins were expressed and purified. The induction condition was OD_{600}=0.8, IPTG=1 mM, 25 °C, 220 rpm for 3 hours. The proteins were first purified with a GST affinity column. Gel

filtration columns were also used to get satisfied purity after affinity columns. PBS buffer was used in the gel filtration purification of GST fusion proteins.

Figure 3-14 showed the SDS-PAGE results of purification of GST-p53TAD and GST-p53NTD. The molecular weights of proteins were added by GST molecular weight, which made them bigger than the proteins alone. GST-p53TAD expressed with high yield in *E.coli* cells and was completely soluble (Figure 3-14A). GST-p53TAD was purified using GST affinity column and then further purified by gel filtration column to get satisfied purity. Chromatography of gel filtration column purification and SDS-PAGE result of elution fractions showed high efficiency of the purification (Figure 3-14B and 3.14C). The PBS buffer was used as gel filtration purification running buffer to purify GST-fused proteins. The GST-p53TAD protein after gel filtration was qualified and used to do the following assay. Expression of GST-p53NTD was also good and nice purification efficiency was gained by GST affinity column purification (Figure 3-14D). The last two elution fractions from the GST affinity column purification were quite pure (>95%) and qualified for the GST pull-down assay (Figure 3-14D). Therefore, these two fractions were collected and changed buffer to PBS. Both GST-p53TAD and GST-p53NTD proteins were prepared in PBS with concentration of 1 mg/ml. Fresh proteins were used in the assay.

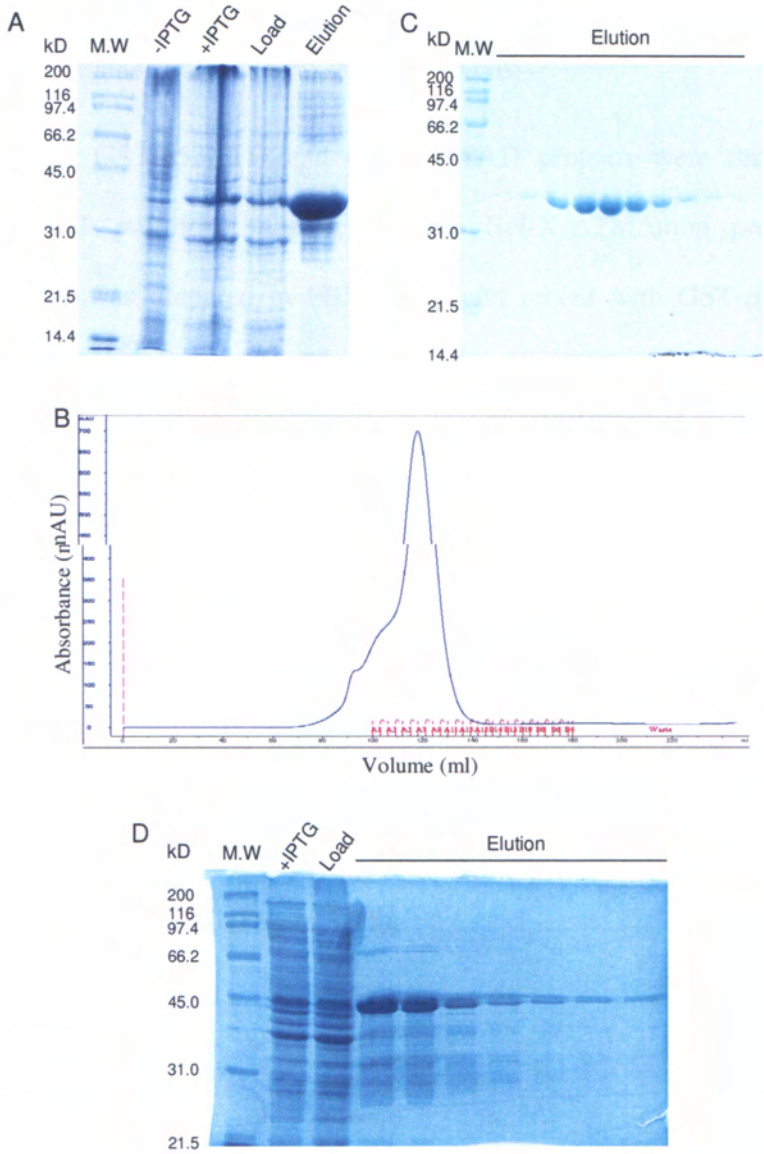

Figure 3-14 Expression and purification of GST-p53TAD and GST-p53NTD fusion proteins.

A) Purification of GST-p53TAD by GST affinity column. Fractions from different procedures of protein purification were collected and analyzed by 12% SDS-PAGE. B) The chromatography of the gel filtration column purification of GST-p53TAD. C) Fractions from the gel filtration column purifications were analyzed by 12% SDS-PAGE. D) Purification of GST-p53NTD by GST

affinity column. Fractions from different procedures of protein purification were collected and analyzed by 12% SDS-PAGE.

The purified GST-p53NTD and GST-p53TAD proteins were then used to perform GST pull-down assays. Purified Bcl-X_LΔTMΔloop protein with histidine tag was prepared in PBS buffer and mixed with GST-p53NTD or GST-p53TAD and GST beads. The loading and elution samples were analyzed with western blot using anti-Bcl-X_L antibody. GST without any fusion protein was used as control in this assay. Bcl-X_L was detected in the elution fraction of GST-p53NTD and GST-p53TAD samples, but not in GST sample (Figure 3-15). p53TAD was enough to interact with Bcl-X_L, which suggested that proline rich domain was dispensable for the interaction. No obvious difference of the amount of eluted Bcl-X_L was observed between GST-p53NTD and GST-p53TAD, revealing that p53TAD, not proline rich domain, contains the binding site with Bcl-X_L (Figure 3-15).

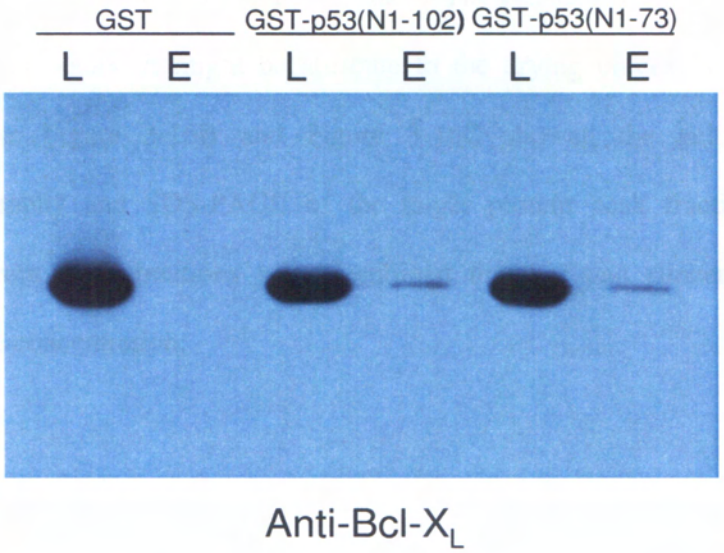

Figure 3-15 Interaction between p53TAD and Bcl-X_L.
Comparison of p53NTD/Bcl-X_L and p53TAD/Bcl-X_L interactions using GST pull-down assay. GST was used as a control. Loading samples and eluted samples of GST beads were analyzed by western blot using anti-Bcl-X_L antibody.

NMR-base binding assay was also used to confirm the p53TAD/Bcl-X_L interaction *in vitro*. To prepare p53TAD protein for the assay, the DNA fragment encoding the first 73 amino acids was constructed into pET16b vector to generate a pET16b-p53TAD plasmid. The plasmid was transformed into BL21(DE3) *E.coli* cells and the p53TAD protein with a 10 histidine tag at the N-terminal was expressed. The induction condition was OD_{600}=0.8-1.0, 1 mM IPTG, 25 °C, 220 rpm for 3 hours. The protein was purified using Ni^{2+}-NTA column and further purified with gel filtration column. Figure 3-16A showed the SDS-PAGE of the Ni^{2+}-NTA affinity column purification. The yield was

fine and the purification effect was acceptable. The gel showed protein bands of two different colors. It might be attribute to the drying process at a higher temperature. Figure 3-16B and Figure 3-16C showed the gel filtration chromatography and SDS-PAGE of the target protein peak fractions. The proteins from peak fractions were combined together and concentrated to appropriate concentration.

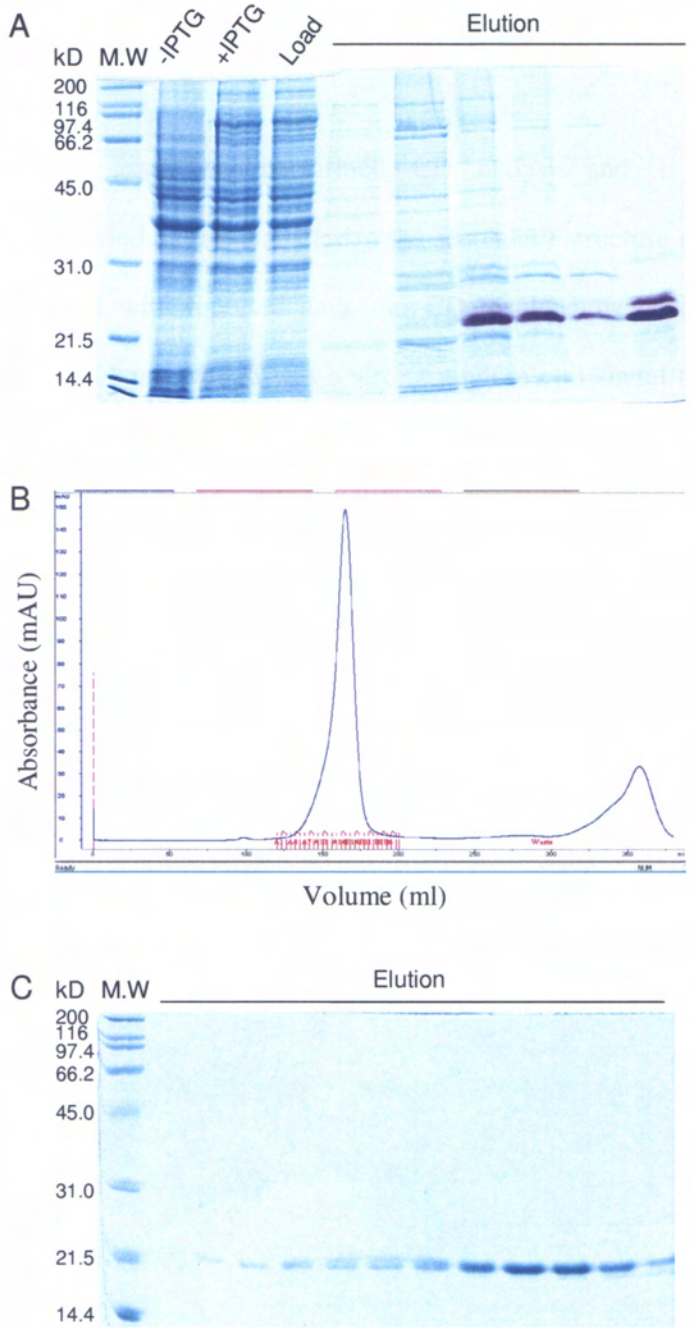

Figure 3-16 Expression and purification of p53TAD proteins.

A) Purification of p53TAD by Ni^{2+}-NTA affinity column. Fractions from different procedures of protein purification were collected and analyzed by 12%

SDS-PAGE. B) The chromatography of the gel filtration column purification of p53TAD. C) Fractions from the gel filtration column purification were analyzed by 12% SDS-PAGE.

Before the binding assay was performed, CD analysis and ^{1}H 1D NMR experiment were carried out to characterize the secondary structure elements of p53TAD. Consistent with reported data, our CD result showed a significant minimum peak at 200 nm, which was a strong random coil signal of p53TAD (Figure 3-17A). 1D NMR experiment also indicated that the protein was mostly unfolded (Figure 3-17B).

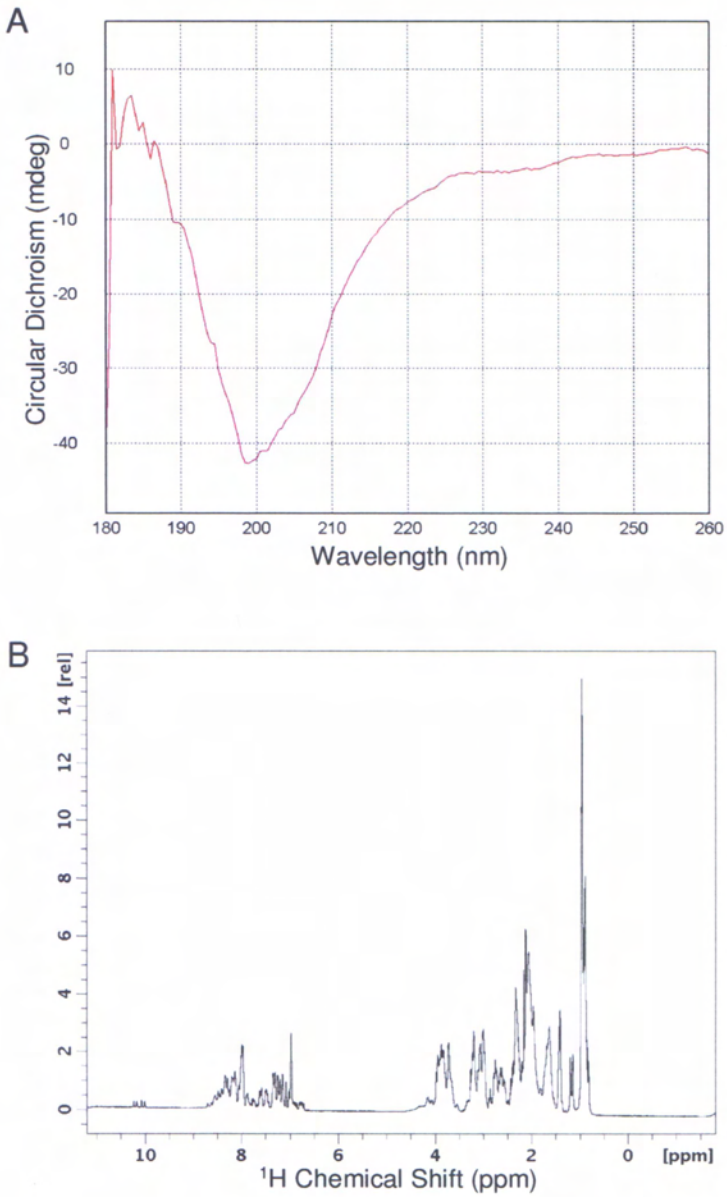

Figure 3-17 Characterization of p53TAD protein using CD and 1D NMR.

A) CD analysis of p53TAD. Purified p53TAD was prepared with concentration of about 1 mg/ml. A blank sample with same buffer but no protein was used as control. The data measured using control sample was subtracted from the data of protein to remove the background effect. B) 1D ^{1}H NMR experiment of p53TAD.

p53NTD is able to induce obvious chemical shift changes on Bcl-X_L in our NMR titration experiment. To confirm that p53TAD is enough to interact with Bcl-X_L, NMR titration experiment was performed using ^{15}N-labeled Bcl-X_LΔTMΔloop with unlabeled p53TAD. Different 2D ^{1}H-^{15}N HSQC spectrua of ^{15}N-labeled Bcl-X_LΔTMΔloop were collected with absence and presence of different amount of unlabeled p53TAD. The spectra were overlaid to visualize the chemical shift changes (Figure 3-18). Similar as p53NTD, the chemical shift changes were obviously detected after adding p53TAD. Most involved amino acids of Bcl-X_L in the interaction of p53NTD were also detected with relatively high chemical shift changes, indicating that their binding pattern was similar. GST pull-down data and the NMR binding assay together confirmed the physical interaction between p53TAD and Bcl-X_L. The proline rich domain of p53NTD may not be important for the interaction from our results.

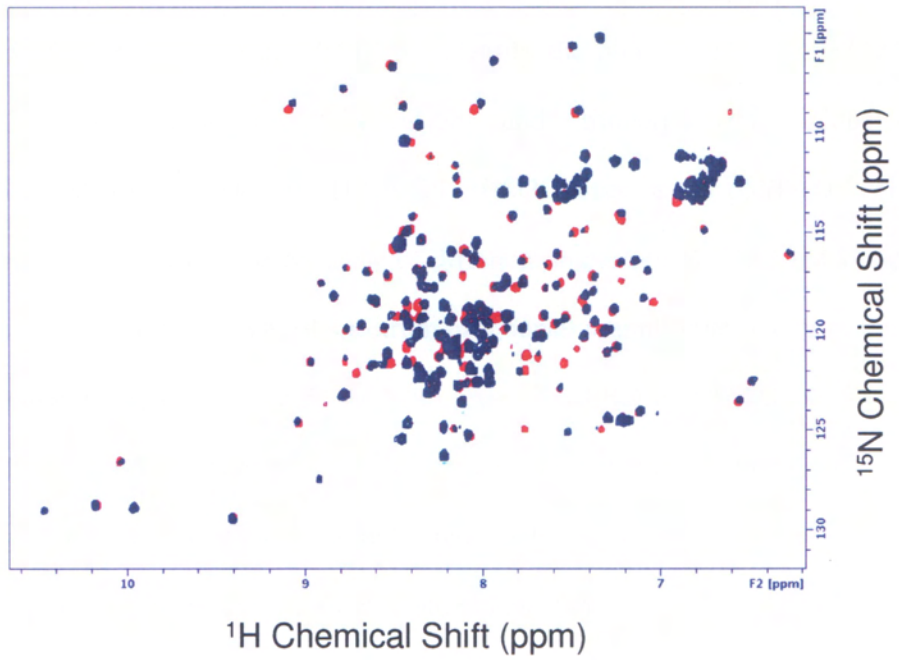

Figure 3-18 p53 interacts with Bcl-X_L in NMR titration experiment.
Bcl-X_LΔTMΔloop was uniformly ^{15}N-labeled and monitored on a 2D ^{1}H-^{15}N HSQC experiment upon the addition of unlabeled p53TAD. Spectrum showed overlaid HSQC spectra recorded on ^{15}N-labeled Bcl-X_L in the absence (red) or presence (black) of unlabeled p53TAD.

p53TAD is important for the transcription activity of p53. In the transcription-dependent apoptosis, p53TAD initiates the transcription of target genes when p53 was localized to the DNA through its DNA binding domain. Here we confirmed that it also played important role in the interaction with Bcl-X_L, which suggested that it is also important in transcription-independent apoptotic activity of p53.

The backbone assignment of p53TAD has been published by different groups (Chi et al., 2005; Lee et al., 2000). To identify the binding site on p53TAD, p53TAD was uniformly ^{15}N-labeled and titrated with unlabeled Bcl-X_LΔTMΔloop. Different ^{1}H-^{15}N 2D HSQC spectra of p53TAD were collected with absence and presence of different amount of Bcl-X_LΔTMΔloop. p53TAD present a very typical spectrum of a nonstructural protein with narrow dispersion of signals (Figure 3-19). With presence of Bcl-X_LΔTMΔloop, major signals remained unchangeable while signals from several amino acids were strongly affected or even disappeared (Figure 3-19). It indicated that the overall conformation of p53TAD does not change upon binding, and that the binding site located in a minor region of p53TAD. The amino acids involved in the interaction were assigned according to the published backbone assignment data. As shown in Figure 3-19, these amino acids include T18, S20, W23, K24 and L26. As we introduced, p53TAD was reported to be natively unfolded. However, it also contains structural element, especially upon binding to other proteins (Kussie et al., 1996). NMR studies revealed that p53TAD contains α-helix structure. From our NMR experiments, it is easy to note that all those involved amino acids are from S15 to N29, which is in the potential α-helix region of p53TAD. This region of potential α-helix is reported to be very important for p53 to bind its partner proteins. MDM2/p53 complex structure has showed that MDM2 bind to p53 on this region (Kussie et al., 1996). Our data here figure out that this region is also the binding site on p53TAD for Bcl-X_L.

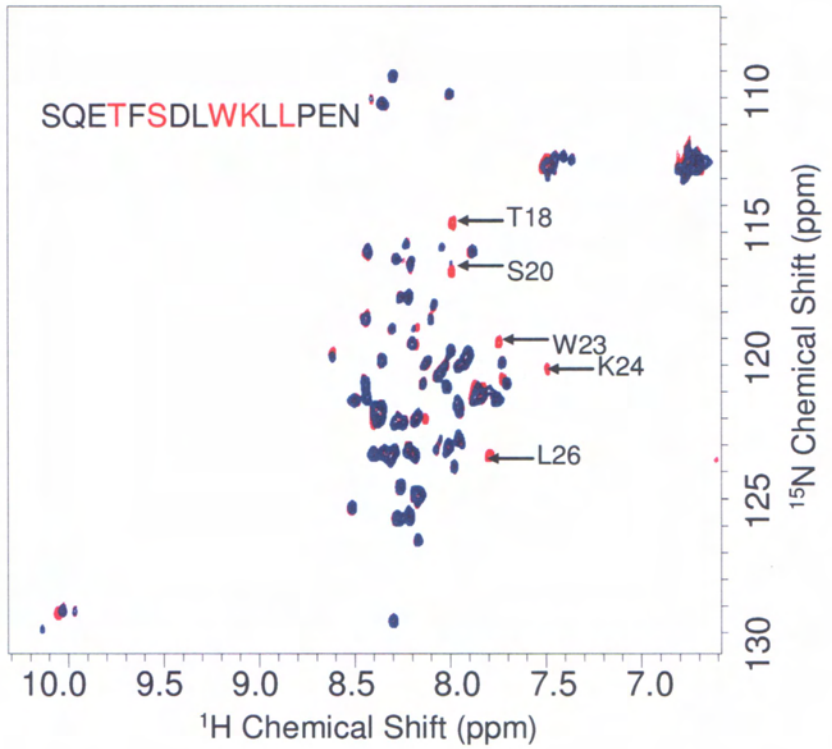

Figure 3-19 Bcl-X_L interacts with p53TAD on its SN15 peptide region.
The 2D ^{1}H-^{15}N HSQC spectra of p53TAD in the absence (in red) and presence (in blue) of Bcl-X_LΔTMΔloop are overlaid. 0.2 mM p53TAD and 0.2 mM Bcl-X_LΔTMΔloop were used in experiments. Residues from SN15 with disappeared signals are indicated.

3.6. Residues (S15-N29) of p53TAD (hereafter referred as SN15) are involved in binding to Bcl-X_L

3.6.1. SN15 binds to Bcl-X_L

To further study the binding site on p53TAD, we chemically synthesized the peptide of S15 to N29 from p53, which is here named SN15. This peptide is also used as a binding site of p53 to form a complex with MDM2, whose structure has been determined using X-ray crystallography (Kussie et al., 1996).

SN15 peptide contains about 2.5 turns with some extra amino acids in the p53/MDM2 complex.

To identify if Bcl-X_L directly binds to peptide of SN15, the peptide was used in the NMR-based binding assay to titrate with Bcl-X_L. Different 2D ^{1}H-^{15}N HSQC spectra of ^{15}N-labeled Bcl-X_LΔTMΔloop were collected with absence and presence of different amount of SN15 peptide. The chemical shift changes were similar with the result of experiments in which p53TAD was used to titrate with ^{15}N- Bcl-X_LΔTMΔloop, indicating that SN15 seems to be the binding site on p53TAD with Bcl-X_L. The chemical shift changes in the spectra indicated that the affinity constant of the Bcl-X_L/SN15 complex is medium (Figure 3-20).

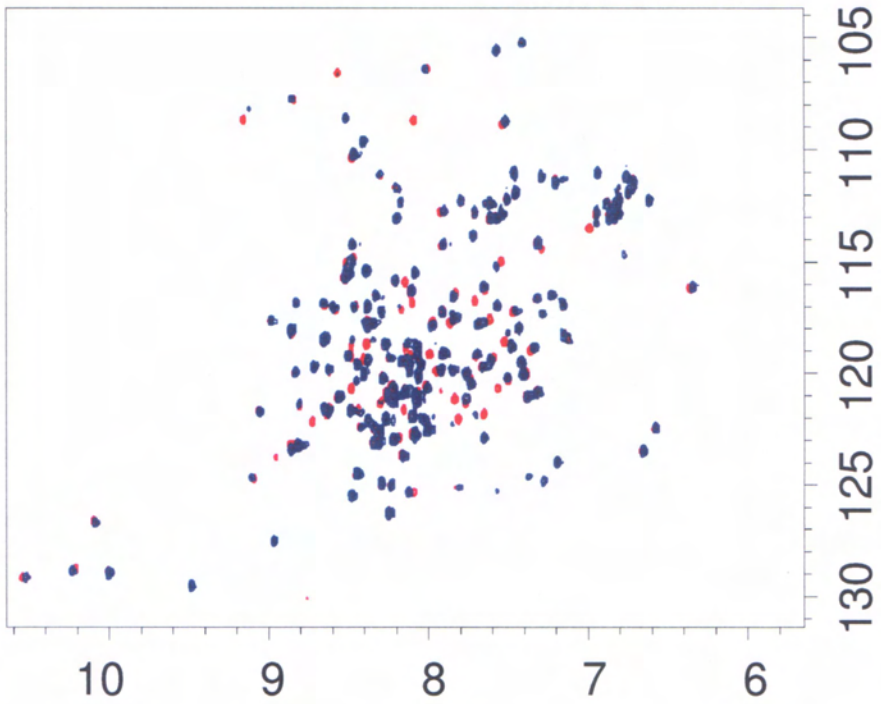

Figure 3-20 SN15 interacts with Bcl-X_L.

The 2D ^{1}H-^{15}N HSQC spectra of Bcl-X_LΔTMΔloop in the absence (in red) and in the presence (in blue) of SN15 peptide. 0.2 mM Bcl-X_LΔTMΔloop and 0.2 mM SN15 peptide were used in experiments.

3.6.2. Backbone assignment of Bcl-X_L

The binding site on p53NTD was identified from the study of the interactions between Bcl-X_L and different parts of p53 NTD protein (p53NTD, p53TAD and SN15). The α-helix peptide SN15 from p53NTD was confirmed to play critical role in the p53NTD/Bcl-X_L interaction. On the other side, NMR-based binding assay displayed the chemical shift changes of the amino acids from Bcl-X_L which were involved in the Bcl-X_L/SN15 interaction. These amino acids directly contributed to the complex conformation or indirectly affected the

interaction. The binding interface should be located around the region containing these amino acids on Bcl-X_L. With the backbone assignment of Bcl-X_L, these amino acids can be assigned and the binding interface on Bcl-X_L can be preliminarily determined.

The Bcl-X_L backbone assignment is available with published solution structures (Muchmore et al., 1996; Sattler et al., 1997). However, our spectrum was found to be a little bit different from the published assignment. Since the protein used in our study is exactly identical with the published one, this difference may due to the different NMR machines and some minor differences of the experiment conditions. To get an accurate assignment data for our experiments to figure out the binding interface on Bcl-X_L, the backbone assignment of Bcl-X_LΔTMΔloop was done on our NMR machine with our specific conditions.

The assignment of proton, nitrogen and carbon chemical shifts of molecules were allowed with the introduction of three and four dimensional NMR experiments and the availability of ^{13}C-, ^{15}N-labeled samples (Kang et al., 2006). ^{13}C-Glucose and ^{15}N-NH_4Cl were used as the only carbon and nitrogen source in the M9 minimum medium to produce ^{13}C-, ^{15}N-labeled Bcl-X_LΔTMΔloop protein. The protein was expressed and purified using the same protocol as ^{15}N-labeled Bcl-X_LΔTMΔloop protein except the medium. The purified protein was prepared in NMR buffer (10% D_2O, 20 mM sodium phosphate, 50 mM NaCl, 1 mM DTT, 0.01% NaN_3, pH 6.5) with concentration of 0.5 mM.

Series of 3D NMR experiments were performed with double labeled Bcl-X_LΔTMΔloop sample to do the backbone assignment. HNCACB experiment provides $C_{\alpha i}$, $C_{\alpha i-1}$, $C_{\beta i}$, and $C_{\beta i-1}$ information and CBCACONH provides $C_{\alpha i-1}$, and $C_{\beta i-1}$ information. The assignment was performed mainly on these two data with the supplementary of HNCA which provides $C_{\alpha i}$ and $C_{\alpha i-1}$ information and HNCOCA which provides $C_{\alpha i}$ information as correction and confirmation data.

Sparky was used to analyze the 3D NMR data and finish the backbone assignment. The published backbone assignment data of Bcl-X_LΔTMΔloop was used as a reference to help the new assignment. More than 90% of the amino acids have been assigned and the new backbone assignment was used in the following analysis of the binding interface determination (

Figure **3-21**).

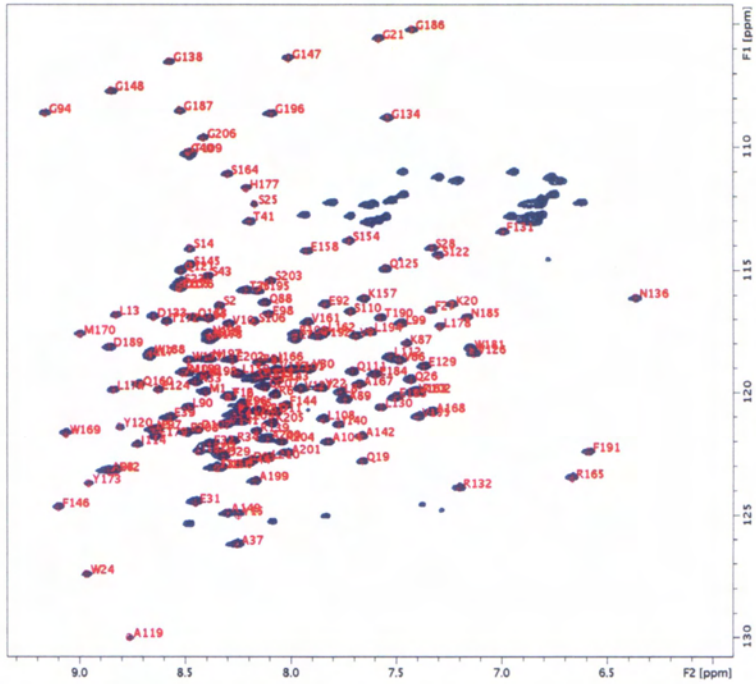

Figure 3-21 ^{1}H-^{15}N backbone assignment of Bcl-X_LΔTMΔloop.

The backbone assignment of the ^{1}H-^{15}N HSQC spectrum of Bcl-X_LΔTMΔloop was presented with the name and number of amino acid residues from the protein with the corresponding peak on the spectrum.

3.6.3. Binding interface on Bcl-X_L of Bcl-X_L/SN15 interaction

With the new backbone assignment and the titration experiments of the Bcl-X_L/SN15 interaction, the involved amino acids on Bcl-X_L were figured out. The chemical shift changes of each amino acid residue from Bcl-X_L in nitrogen and proton channels were plotted (Figure 3-22). It was shown that the amino acids from BH3, BH1, BH2 domains and α3 and α4 helices between BH3 and BH1 were mostly involved in the interaction. BH1, BH2 and BH3 domains of Bcl-X_L formed a hydrophobic groove (Muchmore et al., 1996). Bcl-X_L/Bak complex structure indicated that BH3 domain peptide from Bak protein adopts

an amphipathic α-helix that interacts with this hydrophobic groove through hydrophobic and electrostatic interactions (Sattler et al., 1997). Our data suggested that the overall binding pattern of p53 peptide with Bcl-X_L is similar with BH3 domain peptide from pro-apoptotic proteins, such as Bak, with Bcl-X_L.

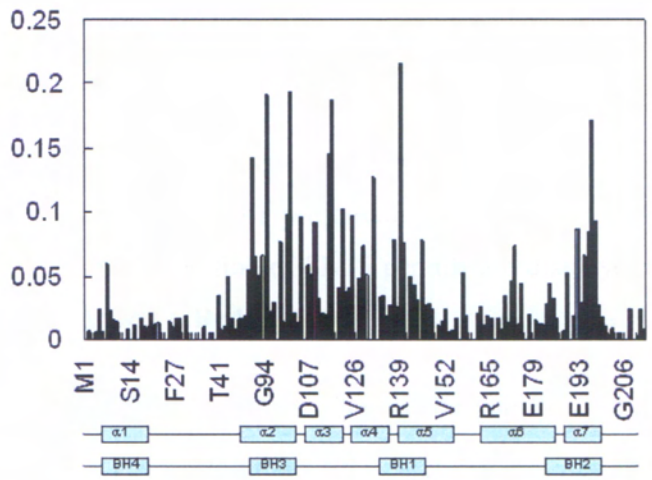

Figure 3-22 Chemical shift changes of Bcl-X_LΔTMΔloop residues upon binding to SN15 peptide.

The chemical shift change data was calculated when the molar ration of SN15 to Bcl-X_LΔTMΔloop is 1:1. The secondary structure and BH domains region corresponding to the amino acid residues were presented.

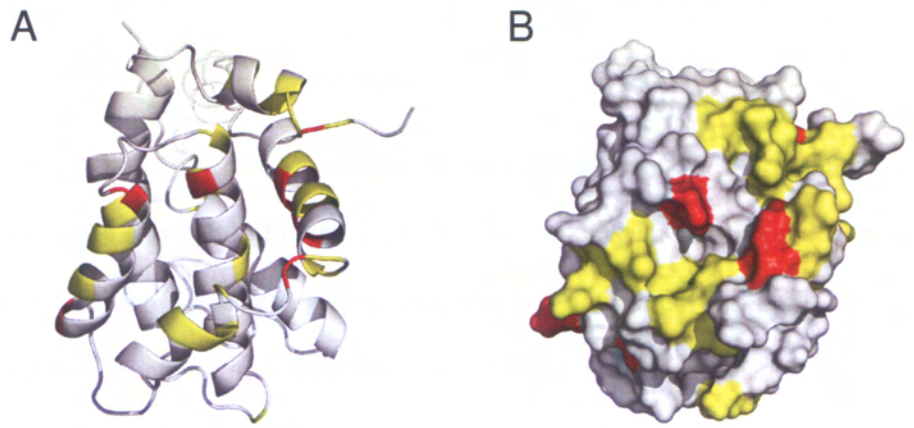

Figure 3-23 Mapping the interaction of Bcl-X_L/SN15 on Bcl-X_L.
Surface (left) and ribbon (right) presentation of Bcl-X_LΔTMΔloop. Amino acids perturbed upon the addition of SN15 peptide are displayed in yellow and red. Yellow: $0.05<\Delta\delta c<0.1$, Red: $\Delta\delta c>0.1$.

To visualize the binding interface on Bcl-X_L, the published three-dimensional structure of Bcl-X_L was presented in surface and ribbon mode. The amino acids involved in the interaction were highlighted with yellow and red colors (Figure 3-23). From the Bcl-X_L structure, an obvious groove exist on the surface, surrounded by the α-helices forming BH1, BH2 and BH3 domains of Bcl-X_L. Most of the involved amino acid residues with yellow and red colors located around the pocket, suggesting that the ligand binds to this hydrophobic pocket and induces the chemical shift changes of the amino acids nearby.

3.7. The flexible loop of Bcl-X_L is not critical for Bcl-X_L/SN15 interaction

As we introduced, Bcl-X_L contains a very flexible loop in its structure from residue A45 to M84 (Figure 3-2). Bcl-X_L remains its anti-apoptotic activity when this loop was deleted, suggesting that it is not critical for its anti-apoptotic function (Muchmore et al., 1996). Both of the loop deletion and loop intact version of Bcl-X_L are completely soluble without the C-terminal transmembrane domain. However, the loop intact Bcl-X_L performs poorly in NMR study with such a long nonstructural region (Muchmore et al., 1996). Therefore, loop deletion Bcl-X_L was used in the structure determination of Bcl-X_L and complexes of Bcl-X_L and other proteins or peptides (Muchmore et al., 1996; Petros et al., 2000; Sattler et al., 1997). In our study, loop deletion version of Bcl-X_LΔTMΔloop with deletion of amino acid residues from A45 to M84 was also used and found to interact with p53 on SN15.

3.7.1. Cloning, expression, purification, and characterization of the Bcl-X_LΔTM protein

To check whether this loop region affects the Bcl-X_L/SN15 interaction, the interactions between SN15 with Bcl-X_L loop intact and deletion version were compared using NMR binding assay. Bcl-X_LΔTM (loop intact) protein was cloned, expressed, purified and characterized before doing the binding assay. DNA fragment of Bcl-X_LΔTM containing loop region was cloned into pET29b plasmid to generate pET29b-Bcl-X_LΔTM plasmid. The plasmid was then

transformed into BL21(DE3) *E.coli* cells and the protein was induced at A_{600}=0.8 by adding 1 mM IPTG at 37 °C, 220 rpm for 2 hours in M9 medium containing $^{15}NH_4Cl$ as the only Nitrogen source.

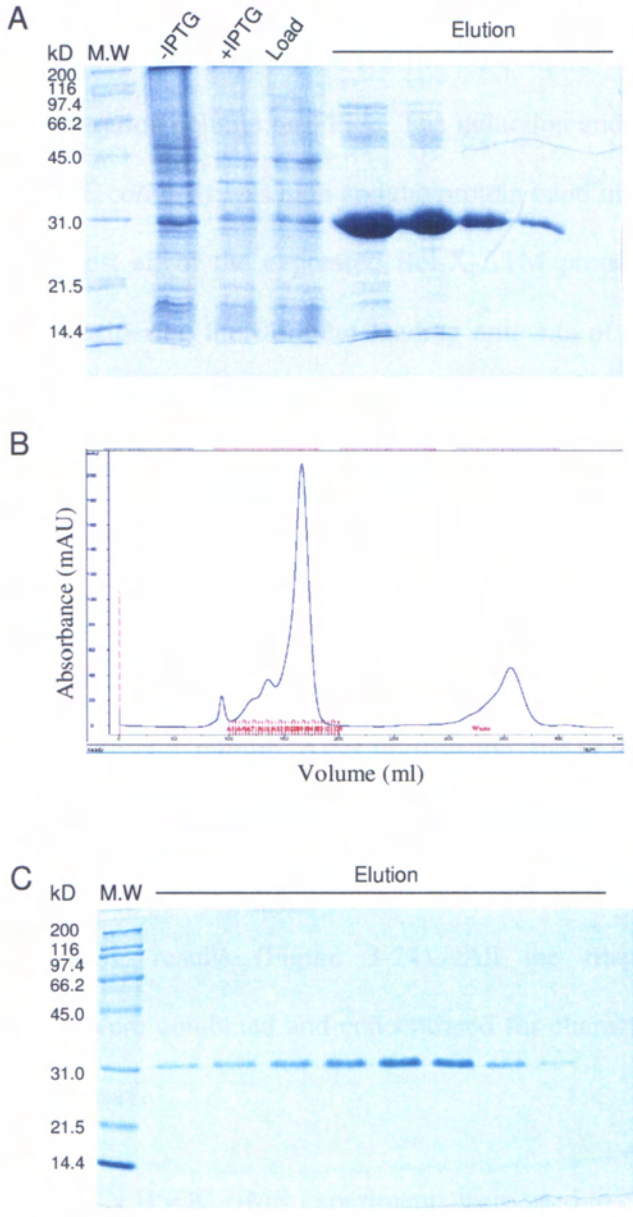

Figure 3-24 Expression and purification of Bcl-X_LΔTM protein.

A) Expression and purification of Bcl-X_LΔTM by Ni^{2+}-NTA affinity column. Fractions from different procedures of protein purification were collected and analyzed by 12% SDS-PAGE. B) The chromatography of the gel filtration column purification of Bcl-X_LΔTM. C) Fractions from the gel filtration column purifications were analyzed by 12% SDS-PAGE.

The expressed Bcl-X_LΔTM protein was purified by Ni^{2+}-NTA affinity column followed by gel filtration column on FPLC. The induction and expression level of Bcl-X_LΔTM in *E.coli* cells was high and the protein band in supernatant lane indicated that almost all of the expressed Bcl-X_LΔTM proteins were soluble (Figure 3-24). Considering the different loading amounts of protein samples, the ratio of the target protein to total protein were similar in the IPTG-induced sample and the control (IPTG-uninduced) sample. The elution fractions showed that the efficiency of the Ni^{2+}-NTA purification was quite good and the purity of around 80% was obtained. In gel filtration purification, NMR running buffer (20 mM sodium phosphate, 50 mM NaCl, 1 mM DTT, 0.01% NaN_3, pH 6.5) was used at flow rate of 1 ml/min. After purification, the peak fractions at the appropriate volume were collected and checked by SDS-PAGE. High efficiency of the Bcl-X_LΔTM purification was obtained according to the chromatography and the SDS-PAGE results (Figure 3-24). All the fractions from the Bcl-X_LΔTM peak were combined and concentrated for characterization before used in the NMR assay.

1D ^1H and 2D ^1H-^{15}N HSQC NMR experiments were used to check the folding state of Bcl-X_LΔTM protein. 1D ^1H spectrum showed that the purified protein was well folded, with obvious peaks in the region of methyl protons (-0.5 ppm

to 1.5 ppm) as enlarged in Figure 3-25. 2D ^{1}H-^{15}N HSQC spectrum of Bcl-$X_L\Delta TM$ also showed very good dispersion of the peaks, confirming that the protein was well folded.

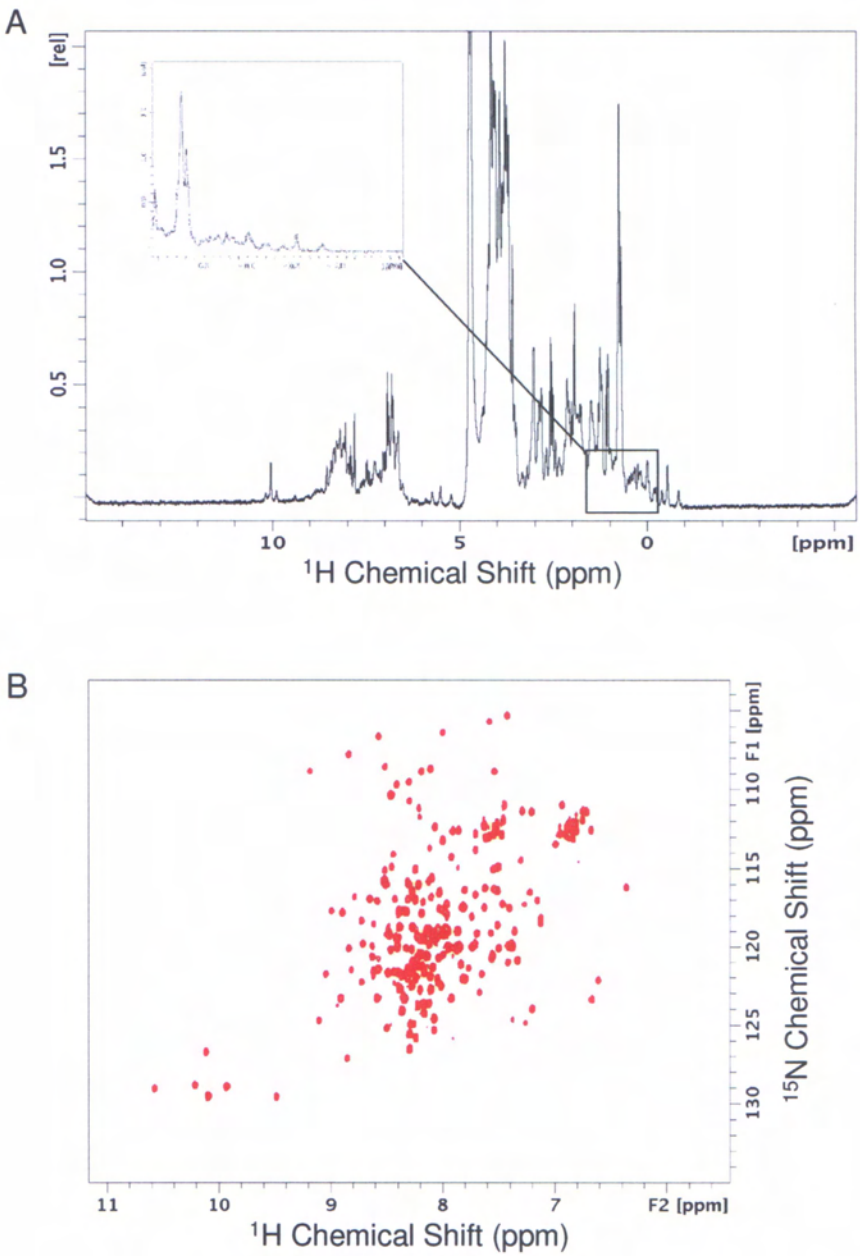

Figure 3-25 Characterization of Bcl-X_LΔTM protein by NMR.
A) 1D ^{1}H NMR experiment of Bcl-X_LΔTM. B) 2D ^{1}H-^{15}N HSQC experiment of uniformly ^{15}N-labeled Bcl-X_LΔTM.

However, unlike Bcl-X_LΔTMΔloop, more signals crowded at the middle part of the spectrum (7.5 ppm to 8.5 ppm), which indicated more amino acid residues from flexible regions in the protein (Figure 3-25). The signals from the flexible loop caused the peaks heavily overlapping, making the chemical shifts poorly resolved. The proteins were concentrated to proper concentration and stored at -80 °C before use.

3.7.2. Bcl-X_L flexible loop is not critical for the Bcl-X_L/SN15 interaction

To compare the interactions of SN15 with Bcl-X_LΔTM and Bcl-X_LΔTMΔloop, NMR binding assays were performed parallel with both of them. ^{15}N-labeled Bcl-X_LΔTM and Bcl-X_LΔTMΔloop were monitered on 2D ^{1}H-^{15}N HSQC upon the addition of SN15 peptide. The spectra before and after adding peptides were overlaid to show the chemical shift changes of Bcl-X_L amino acids (Figure 3-26). Obvious chemical shift changes were detected on both loop intact and loop deletion version of Bcl-X_L proteins. However, when compared to each other, there was big difference between loop intact and loop deletion Bcl-X_L. The number of amino acids with noticeable chemical shift change on Bcl-X_LΔTM spectrum was much less than on Bcl-X_LΔTMΔloop spectrum. It is an evident indication that SN15 affects less on loop intact version of Bcl-X_L than loop deletion one. Loop might cover some of the binding site on Bcl-X_L, which weakened the interaction. It is also possible that the difference of

chemical shift changes were due to their different performance in NMR experiment. Our data here supported that the loop deletion of Bcl-X_L in our study did not abolish or decrease the interaction with SN15 from p53. Loop might have some negative regulation activity on the p53/Bcl-X_L interaction, but the exact role of loop in the interaction is not clear and requires more intensive studies.

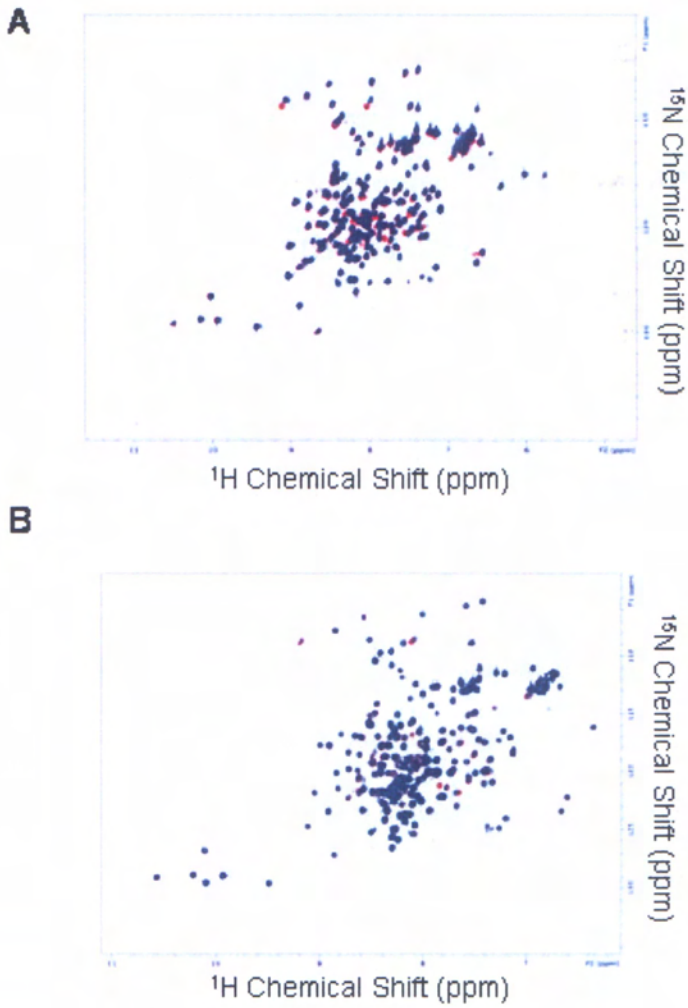

Figure 3-26 Loop region of Bcl-X_L is not critical for the interaction with SN15 peptide.

A) Bcl-X_LΔTMΔLoop was uniformly ^{15}N-labeled and monitored on a 2D ^{1}H-^{15}N HSQC experiment upon the addition of SN15 peptide. Overlaid HSQC spectra recorded on ^{15}N-labeled Bcl-X_LΔTMΔLoop in the absence (red) or presence (blue) of SN15 peptide were shown. B) Bcl-X_LΔTM was uniformly ^{15}N-labeled and monitored on a 2D ^{1}H-^{15}N HSQC experiment upon the addition of SN15 peptide. Overlaid HSQC spectra recorded on ^{15}N-labeled Bcl-X_LΔTM in the absence (red) or presence (blue) of SN15 peptide were shown.

3.8. BH3 peptide abolishes p53TAD/Bcl-X_L interaction

The identification of the binding interface on Bcl-X_L using chemical shift changes data indicated that the region including BH3, BH1, BH2 domains and α3 and α4 helices between BH3 and BH1 were mostly involved in the interaction (Figure 3-22, Figure 3-23). As an anti-apoptotic protein of Bcl-2 family, Bcl-X_L forms heterodimers with pro-apoptotic proteins of the same family, including Bak and Bad. Complex structures showed that the BH3 domain from Bak or Bad adopts an amphipathic α-helix and bind to a hydrophobic groove of Bcl-X_L consisting of BH1, BH2, and BH3 domains (Petros et al., 2000; Sattler et al., 1997). The similar secondary structure of the ligand (α-helix) and the analogous binding interface on Bcl-X_L suggested that the binding pattern of Bcl-X_L/SN15 is compatible with Bcl-X_L/BH3. To prove this hypothesis, a competition binding experiment was performed using GST pull-down assay. GST-p53TAD protein was cultured with Bcl-X_LΔTMΔloop protein. In another two samples, BH3 peptides from Bak (GR16) or Bad (NK25) were added into the protein mix, respectively. The molar ratios of added

peptides to GST-p53TAD protein were 1:1. GST without p53TAD fusion protein was used as negative control. The protein mixes were incubated and immobilized on GST beads followed by washing and elution.

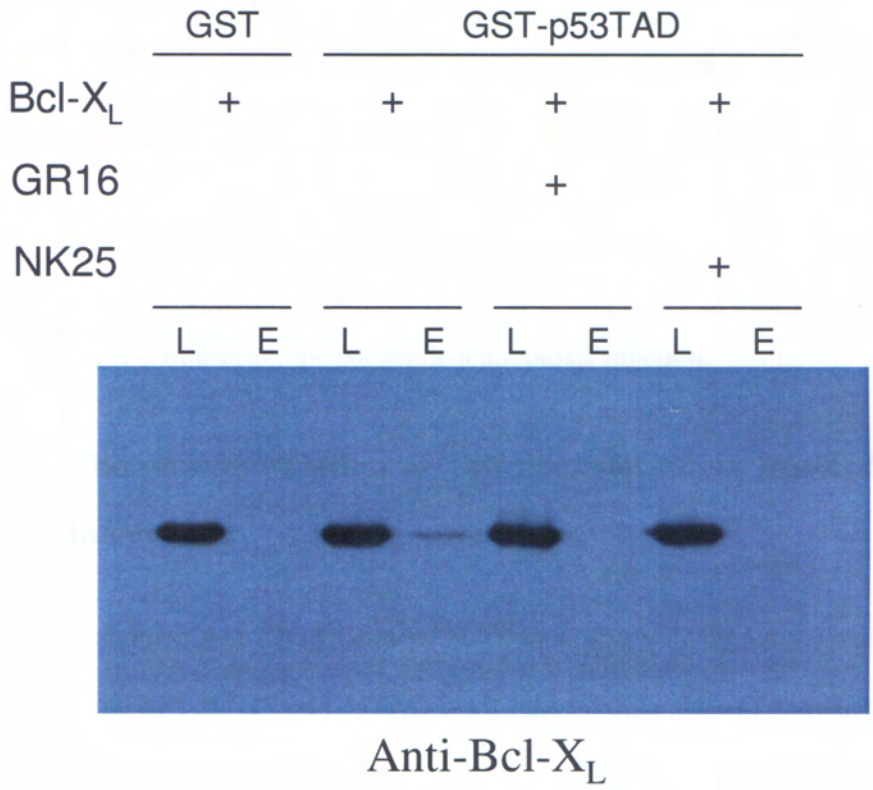

Figure 3-27 BH3 peptides compete Bcl-X_L from p53TAD/Bcl-X_L complex. GST pull-down assay performed using GST-p53TAD with Bcl-X_L protein in the absence or presence of GR16 (from Bak BH3 domain) or NK25 (from Bad BH3 domain) peptides. GST was used as a negative control. Loading samples and eluted samples of GST beads were analyzed by western blot using anti-Bcl-X_L antibody.

The loading and elution fractions of each sample were checked by western blot using anti-Bcl-X_L antibody (Figure 3-27). Bcl-X_L was detected in elution

fraction of GST-p53TAD alone, but not in GST-p53TAD with GR16 or NK25, indicating that p53TAD/Bcl-X_L interaction was abolished by presence of GR16 or NK25. It confirmed our hypothesis that BH3 peptides from Bcl-X_L binding proteins Bak and Bad compete with p53TAD to bind Bcl-X_L. Considering their similar binding site on Bcl-X_L, we believe that they have similar binding pattern or at least overlapping binding site on Bcl-X_L. The results also indicated that the binding affinity of Bcl-X_L/SN15 interaction is relatively low compared to Bcl-X_L/BH3 peptide with Kd of nM level. This competition also correlated p53 into the Bcl-2 family protein regulation system, which might be a part of p53-dependent transcription-independent apoptosis function.

3.9. The phosphorylation of T18 does not affect Bcl-X_L/SN15 interaction

Our data showed that SN15 from p53TAD interacts with Bcl-X_L. This SN15 peptide from S15 to N29 on p53TAD is also the binding site of p53 to associate with its cellular down-regulator, MDM2. As we introduced, MDM2 is one of the most important cellular negative regulators of p53 that keeps a balanced p53 level (Momand et al., 1992). It interacts with p53TAD and induce the p53 degradation via the ubiquitin-proteasome pathway (Michael and Oren, 2003). The p53/MDM2 complex structure was determined using a MDM2/SN15 complex (Kussie et al., 1996). SN15 peptide contains several phosphorylation sites including S15, T18, and S20. Previous work showed that phosphorylation of T18, but not S15 and S20, abrogates p53/MDM2 binding (Schon et al., 2002).

Phosphorylation of T18 was also observed *in vivo* which results in MDM2 binding reduction and p53 stabilization (Sakaguchi et al., 2000). To check if p53/Bcl-X_L has similar regulation mechanism, peptide SN15p which the T18 in SN15 was phosphorylated was synthesized to compare its binding affinity with non-phosphorylated SN15. Unlike MDM2, SN15p still interacts with Bcl-X_L (Figure 3-28). The chemical shift changes on Bcl-X_L spectrum after adding SN15p were quite similar with that after adding SN15, indicating that the phosphorylation of T18 does not decrease the Bcl-X_L/SN15 interaction. Bcl-X_L and MDM2 share the same binding site on p53TAD but have different detailed binding pattern. It is possible that the T18 phosphorylation of p53 on TAD abrogates the p53/MDM2 interaction, resulting in p53 stabilization and accumulation. And the "stable" p53 still remains its ability to interact with Bcl-X_L, which is critical for the transcription-independent apoptosis activity of p53.

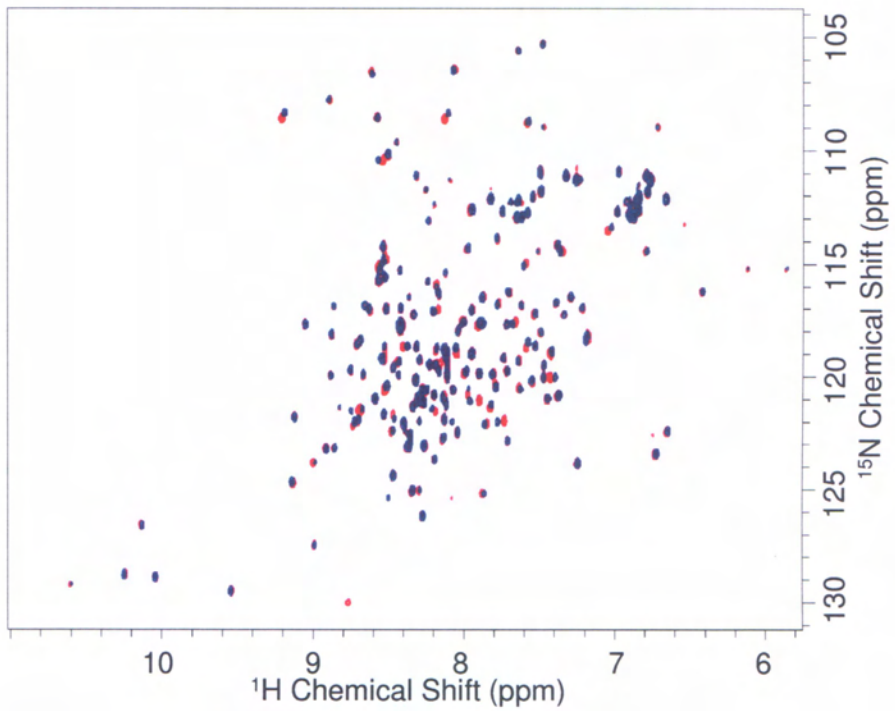

Figure 3-28 Phosphorylation of T18 on p53 does not abrogate Bcl-X_L/SN15 interaction.

Overlaid 2D ^{1}H-^{15}N HSQC spectra recorded on ^{15}N-labeled Bcl-X_L in the absence (red) or presence (blue) of SN15p peptide with phosphorylated T18.

3.10. W23 and K24 of SN15 peptide are critical for the binding to Bcl-X_L

Our results indicated that SN15 peptide from p53TAD interacts with Bcl-X_L. To further identify the critical residues in SN15 for the binding, we synthesized all 15 alanine mutants of SN15 peptide in which each one of the amino acid residue was replaced by alanine. All these alanine mutants were applied in the NMR titration experiments to check their binding with Bcl-X_L (Figure 3-29). In all these 15 residues, W23 and K24 were most critical for the interaction. No

obvious chemical shift changes were detected on the NMR titration experiments using peptides W23A and K24A, showing that both of them lost the ability to interact with Bcl-X_L. These two amino acid residues also belong to the five residues whose signals disappear on 2D ^{1}H-^{15}N HSQC spectra upon binding to Bcl-X_L (Figure 3-19). From the chemical shift change data of all the titration experiments, except W23 and K24, Q16, E17, T18, L22 and L26 are also important for the interaction. All the alanine mutants of these residues significantly decreased their binding affinity to Bcl-X_L. Like W23 and K24, T18 and L26 also disappears in NMR titration experiments upon binding to Bcl-X_L. F19, D21, L25 and N29 are involved in the interaction with less effect on Bcl-X_L residues chemical shift changes. Mutants of S15A, S20A, P27A, and E28A still interact with Bcl-X_L, suggesting that these amino acids residues are not critical for binding.

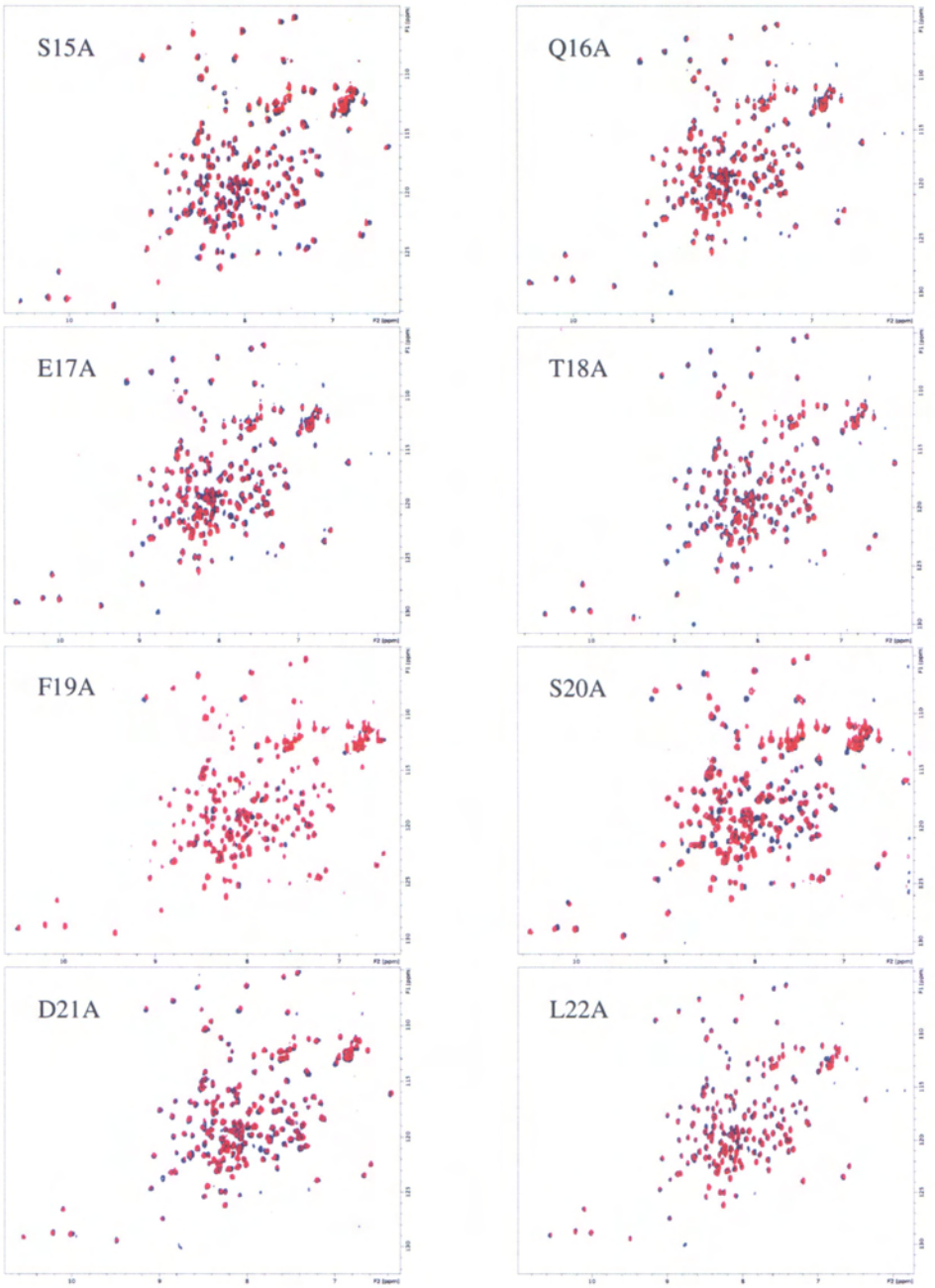

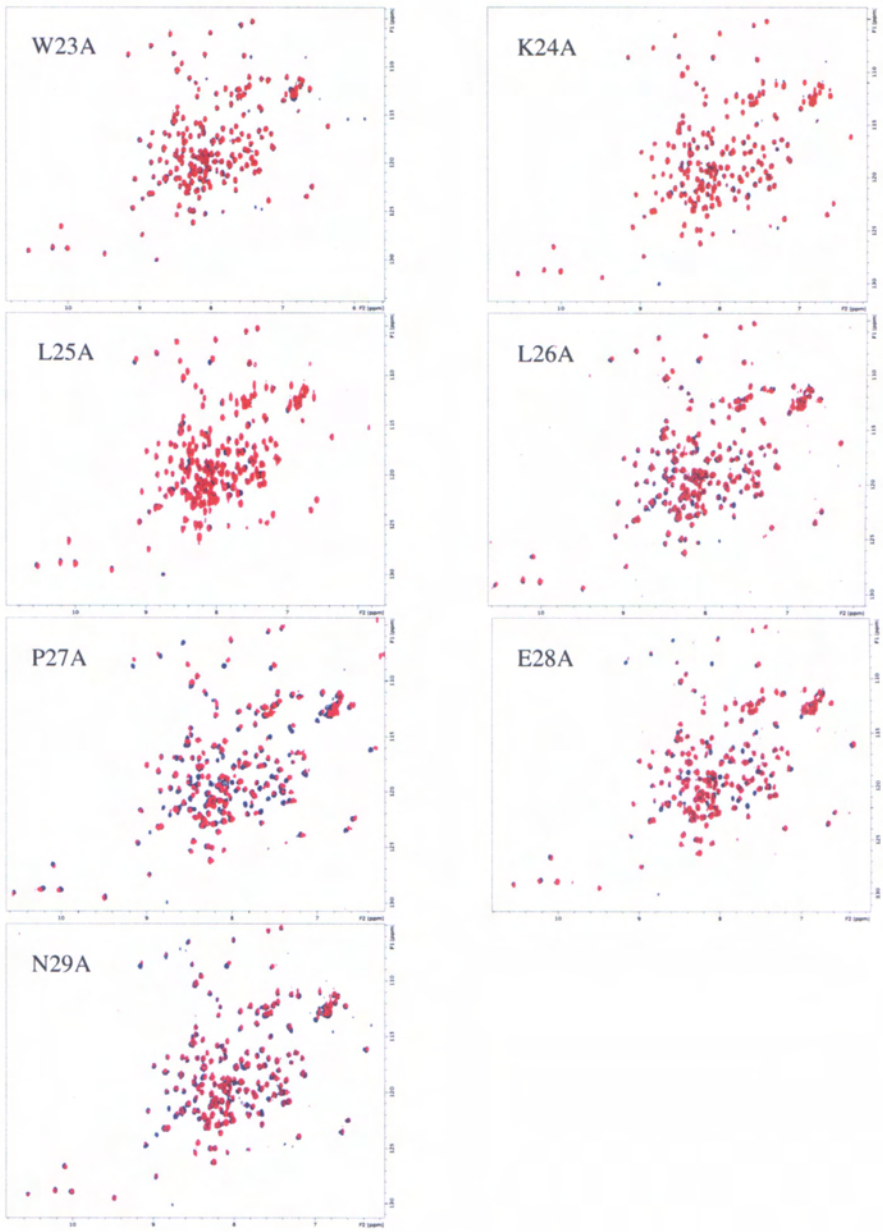

Figure 3-29 NMR titration experiments using alanine mutation SN15 peptides.

The 2D ^{1}H-^{15}N HSQC spectra of Bcl-X_LΔTMΔloop in the absence (in red) and in the presence (in blue) of all 15 alanine mutants of SN15 peptide. 0.2 mM ^{15}N- Bcl-X_LΔTMΔloop and 0.2 mM peptide were used in all the experiments.

3.11. Structure determination and comparison of free SN15 and SN15 in complex with Bcl-X_L

To study the protein interaction of SN15 and Bcl-X_L in more detail and understand the complex formation, we studied the NMR structures of the SN15 peptide in free mode and in complex mode with Bcl-X_L. NOEs for the free and bound SN15 structures calculation were derived from the 2D ^{1}H-^{1}H ROESY and 2D ^{1}H-^{1}H transferred NOE spectra recorded with a mixing time of 200 ms. Dihedral angle restraints were calculated from chemical shifts using TALOS. The ensembles of SN15 structures in free state and bound state with Bcl-X_L were calculated with CYANA based on both manually and automatically assigned NOEs. NOE restraints were grouped into four distance ranges: strong 1.8-2.8 Å, medium 1.8-4.0 Å, weak 1.8-5.0 Å and very weak 1.8-6.0 Å. Standard torsion angle dynamics protocol was used. The number of NMR-derived distance restraints was 118 for free SN15 and 259 for bound SN15. More distance restraints were observed in SN15 with presence of Bcl-X_L, especially for the sequential and medium range distance restrains. The final 20 energy-minimized structures with the lowest target function energy were selected for further analysis. The ensemble for bound SN15 contained no NOE violation greater than 0.1Å and no dihedral angle violation greater than 5°. The average root-mean-square deviation (RMSD) values for bound SN15 were determined to be 0.23 Å for the backbone atoms and 0.80 Å for heavy atoms residues, respectively. Structural quality of the NMR ensemble was analyzed using PROCHECK showing that 91.2% of the residues of the bound SN15 in

the most favored and 6% in the additionally allowed regions of the Ramachandran map (Figure 3-30). The structure data of free SN15 without binding partner indicated that the α-helix structure is very unstable and transient. It is consistent with known structural features the p53 transactivation domain. When in present of Bcl-X_L, the structure of SN15 peptide become more stable and the helix extended. This conformational change induced by Bcl-X_L confirmed the interaction between Sn15 and Bcl-X_L. The complex formation stabilized the structure of the peptide. It is also similar mode with the interaction between SN15 and MDM2.

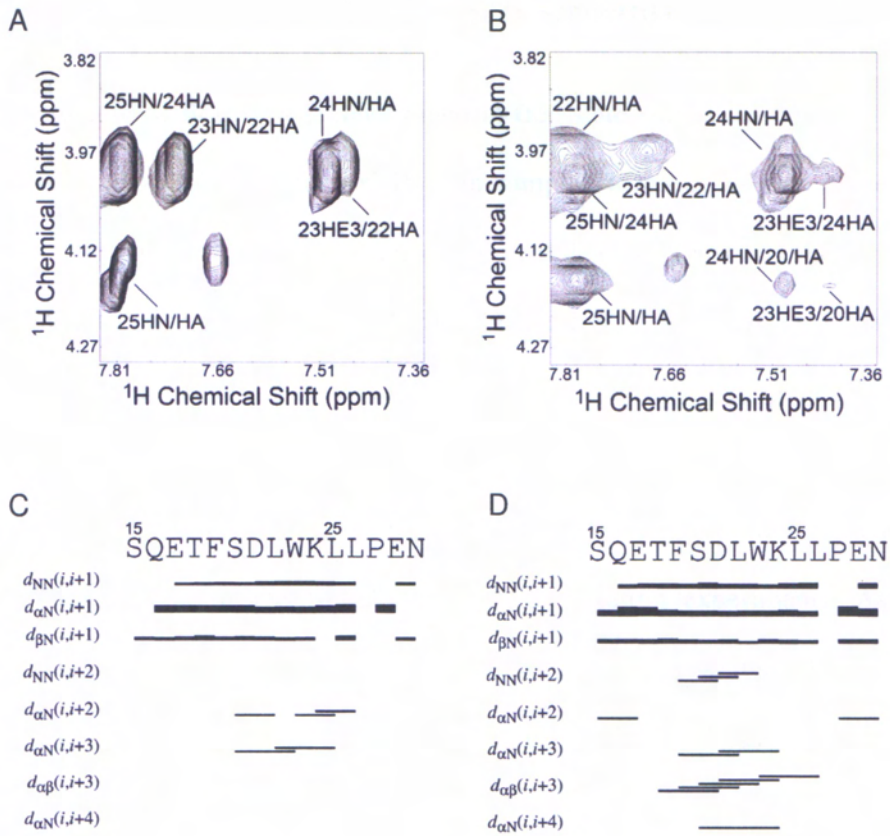

Figure 3-30 NOE data show differences of SN15 peptide structure in the absence and presence of Bcl-X_L.

A) 2D ^{1}H-^{1}H ROESY spectrum recorded with a mixing time of 200 ms shows NOEs in the amide/aliphatic fingerprint for the free peptide. B) As a comparison, 2D ^{1}H-^{1}H transferred NOESY spectrum recorded with a mixing time of 200 ms shows NOEs in the same region for the peptide in presence of Bcl-X_L. C) and D) summarized NOEs for SN15 in absence and presence of Bcl-X_L. Summary of short and medium range NOEs show differences of SN15 peptide structure upon binding Bcl-X_L. The thickness of the bar presents relative intensity (*i.e.* strong, medium or weak) of NOEs.

3.12. Model of Bcl-X_L/SN15 complex structure

The structure of Bcl-X_L was determined in free state and in the complex with BH3 peptide of Bak. Structure of SN15 in complex with Bcl-X_L was studied by NMR. The binding site of the interaction on Bcl-X_L was also identified using the NMR titration experiments, which is on the BH1, BH2, and BH3 domains of Bcl-X_L. BH1, BH2 and BH3 domains of Bcl-X_L form a hydrophobic pocket binding the Bak BH3 peptide. Thus, we performed Bcl-X_L/SN15 complex structure modeling using both structures of SN15 and Bcl-X_L, with the chemical shift change data of the Bcl-X_L/SN15 NMR titration experiments. As we expected, the complex structure model of Bcl-X_L/SN15 showed similar binding pattern with Bcl-X_L/Bak peptide complex structure. The SN15 peptide interacts with the hydrophobic pocket of Bcl-X_L. Like BH3 peptide, hydrophobic side chains (F19, L22, W23, L25, and L26) of the SN15 peptide are directed into the hydrophobic cleft of Bcl-X_L. The complex structure model indicated that BH3 peptide from pro-apoptotic Bcl-2 family proteins and SN15 peptide from p53 share the similar binding site on Bcl-X_L, explained the competition binding experiments result (Figure 3-31). However, the orientation of SN15 peptide in complex with Bcl-X_L is opposite compared to the Bak peptide complexed with Bcl-X_L. In the structural models, SN15 and Bak peptides share the similar binding modes (α-helix binding to hydrophobic groove on the surface) but are opposite in the directional sense. In the structure of another pro-apoptotic Bcl-2 family protein Bax, the helix α9 of Bax is also located in its hydrophobic pocket. The direction of this α9 helix in the hydrophobic pocket is also opposite

to that of the Bak peptide in Bcl-X_L/Bak complex, and is same as the orientation of SN15 peptide in Bcl-X_L/SN15 complex.

The comparison of SN15 peptide structure with present and absent of Bcl-X_L and the model of Bcl-X_L/SN15 complex structure suggested some of the kinetics in the Bcl-X_L/SN15 interaction. Free SN15 peptide presents a loose structure with an unstable α-helix. When the peptide interacts with Bcl-X_L on the hydrophobic pocket, its α-helix structure was stabilized and extended. This model explained what we observed in the Bcl-X_L/SN15 interaction, suggesting that the p53TAD is also important in the interaction with anti-apoptotic Bcl-X_L. However, more biological study in vivo need to be done to explain the relationship between its binding ability and the transcription-independent apoptotic function.

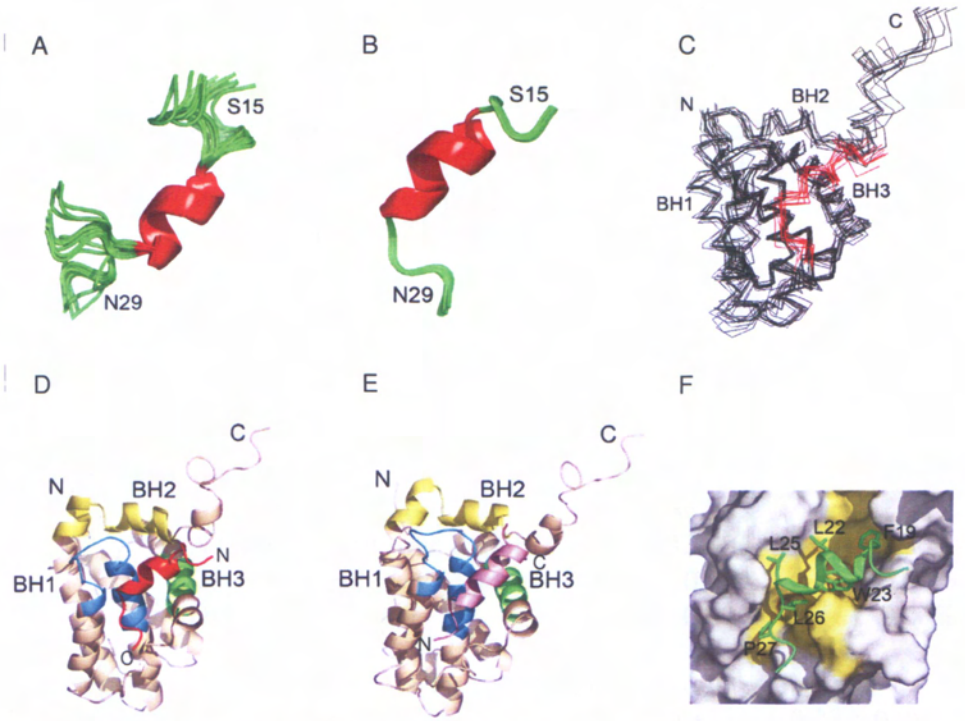

Figure 3-31 NMR structures of SN15 and model of Bcl-X_L/SN15 complex.

A) Ensemble of top 20 NMR-derived structures of free SN15 peptide. B) Ensemble of top 20 SN15 structures in presence of Bcl-X_L. C) Model of Bcl-X_L complexed with SN15 built by NMR-based docking is shown as backbone. D) Ribbon depiction of the complex model. BH1, BH2 and BH3 regions of Bcl-X_L are shown in blue, yellow, green respectively, and SN15 is shown in red. E) NMR structure of Bcl-X_L/Bak complex is shown as a comparison (PDB ID 1bxl). F) Surface representation of the hydrophobic pocket of Bcl-X_L bound to the SN15 peptide. Hydrophobic residues of Bcl-X_L are colored in yellow and SN15 peptide is show in green.

	Free state	Bound state
Distance restrains	118	259
Intraresidual (i=j)	58	78
Sequential (|i-j|=1)	46	105
Medium-range (1<|i-j|<5)	14	76
Long-range (|i-j|>4)	0	0
Dihedral angle restraints (φ and ψ)	14	16
Total number of restraint violations > 0.1 Å	1	0
Total number of dihedral angle violations > 5 °	0	0
Ramachandran plot (% of all residues)		
Most favored regions	86.70%	91.20%
Additionally allowed regions	13.30%	8.80%
Generously allowed regions	0.00%	0.00%
Disallowed regions	0.00%	0.00%
Average RMSD (Å) to Mean for the top 20 structures (all residues)		
Backbone atom	1.49 ± 0.34	0.23 ± 0.08
Heavy atom	2.47 ± 0.39	0.80 ± 0.10

Table 3-1 Structural statistics for SN15 in free state and bound state with Bcl-X_L.

NOEs for the free and bound SN15 structure calculation were derived from the 2D ^{1}H-^{1}H ROESY and 2D ^{1}H-^{1}H transferred NOE spectra recorded with a mixing time of 200 ms at 298K, respectively. Dihedral angle restraints were calculated from chemical shifts using TALOS. The ensembles of SN15 structures in free state and bound state with Bcl-X_L were calculated with CYANA based on both manually and automatically assigned NOEs. Standard torsion angle dynamics protocol was used. The number of NMR-derived distance restraints was 118 for free SN15. It was 259 for bound SN15 and was more than that of free SN15, especially for the sequential and medium range distance restrains. The final 20 energy-minimized structures with the lowest

target function energy were selected for further analysis. The ensemble for bound SN15 contained no NOE violation greater than 0.1Å and no dihedral angle violation greater than 5°. The average root-mean-square deviation (RMSD) values for bound SN15 were determined to be 0.23 Å for the backbone atoms and 0.80 Å for heavy atoms residues, respectively. Structural quality of the NMR ensemble was analyzed using PROCHECK showing that 91.2% of the residues of the bound SN15 in the most favored and 6% in the additionally allowed regions of the Ramachandran map. Comparisons of the free and bound SN15 on the structural statistics data suggested that the peptide became more stable and well-defined upon binding Bcl-X_L.

4. DISCUSSIONS

p53 has been known as a critical tumor suppressor for very long time. It receives the cellular stresses and activates different downstream effectors for different cell type and stress. As a transcription factor, p53 executes its anti-cancer activity by regulating the transcription of several target genes. These genes control the process of cell death and cell survival. However, p53 also undergoes transcription-independent apoptosis pathway without induce or inhibit any gene transcription. Recent paper reported that p53 executes this pathway by forming complexes with several other proteins. Particularly, Bcl-2 family proteins, including Bcl-2/X_L, Bak, Bax, Bad, and PUMA, are described to interact with p53. These protein-protein interactions, together with the regulations between Bcl-2 family proteins, form a complicated matrix to activate and control the p53-dependent transcription-independent apoptosis pathway. Nevertheless, the details of these protein interactions were still unclear. Here we studied the interaction between p53 and Bcl-2/X_L, which are the first members of Bcl-2 family discovered to interact with p53.

Both p53 and Bcl-2 family proteins are the most important proteins in the apoptosis system, associating with many different proteins and molecules to precisely keep the balance of cell survival and apoptosis. Thus it is understandable that the discovery of p53/Bcl-2 and p53/Bcl-X_L interactions gains so many interests from researchers. p53 directly induces permeabilization

of the outer mitochondrial membrane by forming complexes with Bcl-2/X_L, resulting in cytochrome c release and subsequent apoptosis. The p53/Bcl-2 and p53/Bcl-X_L pathway suggested a first model of p53-dependent transcription-independent apoptosis mechanism. Details of the p53/Bcl-2 and p53/Bcl-X_L interactions will help the understanding of the p53 transcription-independent apoptosis pathway and the role of Bcl-2/X_L in this pathway.

Among the different p53 domains including transcriptional activation domain (TAD), DNA binding domain (DBD), and C-terminal domain (CTD), p53DBD was firstly identified to be the binding site of p53/Bcl-X_L interaction, reported in the first paper describing the interaction and confirmed by another group based on NMR experiments (Mihara et al., 2003; Petros et al., 2004). However, the detailed structure information of the complex is still lacking. In this study, we found another binding site on p53 transcriptional activation domain of the interaction with Bcl-X_L. We first observed that the N-terminal domain of p53 interacts with Bcl-X_L. The physical interaction was confirmed by different *in vitro* and *in vivo* experiments including GST pull-down, co-expression assay, FRET assay and NMR titration experiments. Further study revealed that p53TAD alone without the proline rich domain is enough to bind to Bcl-X_L. NMR titration experiment indicated that the amino acids from S15 to N29 from p53TAD were involved in the interaction. The following binding study indicated that this SN15 peptide is the binding site on p53TAD for Bcl-X_L. The binding pattern was compared with the interactions of Bcl-X_L/BH3 and

p53/MDM2. NMR experiments showed the binding site on Bcl-X_L consists of BH1, BH2 and BH3 domains. The mutagenesis experiment on SN15 peptide designate that the W23 and K24 were critical for the interaction. Finally we measured the structure of SN15 peptide in free and complex mode, indicating that the peptide undergo conformational change upon binding to Bcl-X_L. A compute-based model of the Bcl-X_L/SN15 complex structure showed that SN15 peptide adopts a α-helix to bind the hydrophobic groove on Bcl-X_L.

Both of Bcl-2 and Bcl-X_L were discovered to form complex with p53 (Mihara et al., 2003). Bcl-2 and Bcl-X_L are ones of the most important anti-apoptotic subfamily members of Bcl-2 family proteins. They have quite similar three-dimensional structures and share many biological functions (Muchmore et al., 1996; Petros et al., 2001). They both have all the four BH domains (BH1 to 4). Their structures consist of seven α-helices and a very long flexible loop between α1 and α2, which is different from other Bcl-2 family proteins. Both of them are soluble when the transmembrane domains at C-terminal were removed. However, the performances in solution are quite different between them. Bcl-X_L is quite stable in solution and tolerates very high concentration, especially when the flexible loop is removed. Bcl-2 performs poorly in solution. It is soluble but very easy to precipitate when concentrated, even the loop is removed. It brought big problem for the structure determination and its structure was solved five years later than Bcl-X_L. A part of Bcl-X_L loop was used to replace the own loop of Bcl-2 to make a hybrid protein which performs better than wild type Bcl-2 and the hybrid protein was used to solve the

three-dimensional structure of Bcl-2. Considering the difficulty, we decided to start with studying p53/Bcl-X_L interaction, which is easier for the *in vitro* studies. Further more, the loop region between α1 and α2 was removed in our *in vitro* study. This loop is a very long (more than 60 amino acids) and flexible. The loop intact version of Bcl-X_L performed poorly in NMR or X-ray crystallography studies due to the instability caused by the long nonstructural loop. This problem was solved by deletion of this loop. The anti-apoptotic activity of Bcl-X_L remains after remove of the loop (Muchmore et al., 1996). Therefore, the loop deletion Bcl-X_L was used in this study, especially *in vitro* experiments.

Initially, DNA binding domain was identified as the binding domain on p53 to bind Bcl-X_L. The interaction was reported by co-IP experiment and confirmed by subsequent NMR titration experiments (Mihara et al., 2003; Petros et al., 2004). In parallel, several papers reported that the N-terminal domain of p53 is involved in the transcription-independent apoptosis. p53NTD is necessary and sufficient to induce transcription-independent apoptosis, while DNA binding domain is dispensable (Chipuk et al., 2003). In mammalian cells, p53 can be cleaved through a caspase-dependent pathway. Two out of four generated fragments of p53, p53-(1-186) and p53-(22-186), which contains entire N-terminal domain and part of DNA binding domain, translocate to mitochondria and induce mitochondrial membrane depolarization in the absence of transcriptional activity (Sayan et al., 2006). These interesting results indicated that p53 NTD is important for its transcription-independent apoptosis.

It also implied that p53NTD might correlate the p53/Bcl-X_L interaction with its transcription-independent apoptosis.

According to our results, the p53NTD/Bcl-X_L interaction was successfully detected in our experiments. From a co-expression system which expresses p53NTD and Bcl-X_L proteins simultaneously in *E.coli* cells, the p53NTD/Bcl-X_L complex was obtained from a Ni^{2+}-NTA affinity column. The complex formation tolerates the high salt condition in the purification process, suggesting that the interaction is a specific protein-protein interaction. And the interaction is not fully depending on the charge-charge interaction which is easy to be broken by high ion. This p53NTD/Bcl-X_L interaction was also confirmed by different systems. GST pull-down assay confirmed their physical interaction i*n vitro*; and *in vivo* FRET assay confirmed that the process also occurs in mammalian cells.

After confirmation of the existence of the interaction, we performed NMR experiments to get more information about the detail. NMR was a high effective tool in protein structure determination and protein-protein interaction study. So far, the most widely used NMR method to map the protein interaction is NMR titration experiment using 2D HSQC (normally 2D ^{1}H-^{15}N HSQC) experiments to monitor the chemical shift changes on the spectrum upon binding to the ligands (Zuiderweg, 2002). 2D ^{1}H-^{15}N HSQC is a two dimensional NMR experiment that correlate the ^{15}N frequency with amide ^{1}H. It displays chemical shift change of amide ^{15}N with its directly attached amide ^{1}H for every amino acid, which is presented as a cross peak on a ^{1}H-^{15}N HSQC

spectrum. Therefore, every amino acid residue from the protein has its specific peak on the spectrum, and every protein has its specific pattern of peaks on the spectrum. The correlation of the amino acid residues to the cross peaks on the spectrum can be assigned by backbone assignment through several 3D NMR experiments. The peak position on the HSQC spectrum of each amino acid is depending on the chemical environment of the amide from the amino acid. The chemical environment of protein amides are extremely sensitive to the changes including pH, temperature and binding to some molecules, resulting in chemical shift changes on the spectrum. Therefore, for protein-protein interactions, chemical shift changes usually occurred on the amino acids which are directly involved in or near the binding site; or involved in the induced conformational rearrangement in case of strong bindings. Thus, the distribution of amino acids with chemical shift changes upon binding ligand will give information about the binding site and binding pattern of the interaction. The requirement of using this method includes: i) The protein must be soluble with enough high concentration to perform 2D NMR experiments and get qualified signals; ii) The protein must be uniformly ^{15}N-labeled; iii) Backbone assignment of the protein is available.

In our study, p53NTD and Bcl-X_LΔTMΔloop were ^{15}N-labeled to run NMR titration experiments. To get different information of the interaction on both p53NTD and Bcl-X_L, the experiments were executed using ^{15}N-Bcl-X_LΔTMΔloop titrated with unlabeled p53NTD and ^{15}N-p53NTD titrated with unlabeled Bcl-X_LΔTMΔloop, respectively. In the experiment of

^{15}N-Bcl-X_LΔTMΔloop titrated with unlabeled p53NTD, no major conformational change was detected, indicating that the binding does not break or induce secondary structure of Bcl-X_LΔTMΔloop. This is consist with the interaction patterns of Bcl-X_L with other ligands, such as the BH3 peptides from Bak and Bad, in which no major conformational change was observed either. Obvious chemical shift changes were noticed on amino acids from Bcl-X_L though. According to the backbone assignment published by other group, we preliminarily mapped the binding site on Bcl-X_L depending on the distribution of the involved amino acids.

NMR titration experiments were also done on ^{15}N-labeled p53NTD titrated with unlabeled Bcl-X_LΔTMΔloop to get the binding information on p53NTD. Major part of p53NTD amino acids remains unchangeable upon Bcl-X_L binding. However, several amino acids signals disappeared after binding Bcl-X_L, suggesting that conformational change might occur on minor region of p53, which is induced by Bcl-X_L association. Unfortunately we are unable to locate this region on p53 at this step due to the lack of p53NTD backbone assignment. Different NMR titration experiments both confirmed the interaction between p53NTD and Bcl-X_L.

As we introduced, p53NTD is able to induce apoptosis without transcriptional activity (Chipuk et al., 2003). A proline rich domain deletion mutant of p53, p53Δpp, lost the ability to induce apoptosis. Proline rich domain and transcriptional activation domain together compose the N-terminal domain of p53. Our results showed that p53NTD binds Bcl-X_L. Is proline rich domain

essential for the interaction like its role in the p53 apoptotic activity? Our data revealed that p53TAD alone, without proline rich domain, is able to bind Bcl-X_L. The binding affinities of p53TAD and p53NTD are at similar level, according to the Bcl-X_L amount that binds p53NTD and p53TAD in a GST pull-down assay. Our NMR titration experiment on ^{15}N-Bcl-X_LΔTMΔloop titrated with p53TAD showed similar spectrum as p53NTD. These data suggested that p53TAD, not the proline rich domain, contains the Bcl-X_L binding site. Proline rich domain might be important for other critical steps of p53-dependent transcription-independent apoptosis pathway. The biological functions of different domains of p53 in its apoptotic activity and their different roles in the interaction with Bcl-X_L are still controversial and need more investigation both *in vitro* and *in vivo*.

The identification of p53TAD/Bcl-X_L interaction makes us put our attention on the transcriptional activation domain of p53. Extensive structural studies have been done on the p53 DNA binding domain and C-terminal oligomerization domain. Their three-dimensional structures have been successfully determined by X-ray crystallography and NMR long time ago (Cho et al., 1994; Clore et al., 1995; Lee et al., 1994). However, the information about the structure of p53TAD is still accumulating. It was firstly reported that the N-terminal domain of p53, including p53TAD, is natively unfolded (Bell et al., 2002; Dawson et al., 2003). p53TAD consists of first 73 amino acids of the N-terminal domain of p53. As one of the transcription domains, it is rich in acidic amino acids which make it easy to interact with many DNA-binding proteins to function its

transactivity (Fields and Jang, 1990; Ptashne and Gann, 1997). Like many of the transcriptional activation domains of other proteins, p53TAD contains fragments which is able to be induced to α-helices upon binding to partner proteins, such as MDM2 (Kussie et al., 1996; Triezenberg, 1995). A fragment of p53TAD adopt a α-helix to interact with the hydrophobic cleft of MDM2 in the complex structure, confirmed the structural element in p53TAD which can be induced by protein-protein interactions (Kussie et al., 1996). Further more, recent NMR studies on the full length p53TAD also revealed that unbound p53TAD also contains local structural elements, including helix and turns (Chi et al., 2005; Lee et al., 2000). These include an amphipathic helix formed by residues from T18 to L26 and two nascent turns which are formed by residues from M40 to M44 and D48 to W53. Deep structural study revealed that beside the known SN15 peptide, these two potential nascent turns also be able to bind to MDM2 with different binding affinities (Chi et al., 2005). Taken together, the p53TAD may not be fully unfolded protein, but partially folded or loosely folded. It contains secondary structural elements in unbound state. These structural elements, including helix and turns, are transient or unstable in unbound state, and sometimes difficult to detect. With present of partner proteins, these regions tend to be the binding site and their secondary structures are induced and stabilized upon binding.

In our experiments, p53TAD showed no stable secondary structure in the biochemical assays, including CD, 1D ^{1}H and 2D ^{1}H-^{15}N NMR experiments. The NMR titration experiments on ^{15}N-p53TAD titrated with Bcl-X_L showed

no overall conformational change. However, obvious chemical shift changes or even signals disappearance on small amount of amino acids were observed, suggesting possible conformational change on minor part of p53TAD. More interestingly, backbone assignment data figured out that these involved amino acids (including T18, S20, W23, K24 and L26) belong to a region from S15 to N29. This SN15 peptide from p53TAD was reported to be the binding site with MDM2 (Kussie et al., 1996; Oliner et al., 1993). The complex structure of MDM2/SN15 peptide revealed that SN15 peptide adopts an amphipathic α-helix to bind a deep hydrophobic groove on MDM2 (Kussie et al., 1996). This region of S15 to N29 also belongs to the reported potential local structural elements in p53TAD (Lee et al., 2000). Further more, Bcl-X_L also contains a hydrophobic groove binding the α-helix peptide from BH3 domains of pro-apoptotic proteins, like Bak and Bad (Petros et al., 2000; Sattler et al., 1997). Thus, it is also possible that the SN15 peptide from p53TAD also adopts a α-helix, like it does in p53/MDM2 interaction, and binds to the hydrophobic groove of Bcl-X_L.

The SN15 peptide was then chemically synthesized to study the interaction with Bcl-X_L. Unsurprisely, the Bcl-X_L/SN15 interaction was detected in NMR titration experiments on ^{15}N-Bcl-X_LΔTMΔloop titrated with the SN15 peptide. Chemical shift changes were detected upon adding different amount of peptide. Thus, the binding site on Bcl-X_L was able to be mapped according to the backbone assignment of Bcl-X_LΔTMΔloop protein. We have utilized published backbone assignment data in our study. However, even though the constructs of

Bcl-X_L are exactly same, minor difference was still observed between our spectra with published one. This might due to the different NMR machines the experiments run on, or some minor experiment conditions differences. To get precise binding site information from the experiments, we did the backbone assignment on our working condition. The ^{1}H-^{15}N backbone assignment was done basically based on four 3D NMR experiments including HNCACB (providing $C_{\alpha i}$, $C_{\alpha i-1}$, $C_{\beta i}$, and $C_{\beta i-1}$ information), CBCACONH (providing $C_{\alpha i-1}$ and $C_{\beta i-1}$ information), HNCA (providing $C_{\alpha i}$ and $C_{\alpha i-1}$ information) and HNCOCA (providing $C_{\alpha i}$ information). All the experiment data were correlated to decide the value of $C_{\alpha i}$, $C_{\alpha i-1}$, $C_{\beta i}$, and $C_{\beta i-1}$. More than 90% of all amino acids are assigned.

The backbone assignment data facilitated the binding site mapping on Bcl-X_L. The chemical shift changes of amino acids from Bcl-X_L were summarized and plotted. From the plot, it is clear that amino acids from BH1, BH2, BH3 domains and α3 and α4 helices between BH3 and BH1 displayed significant chemical shift changes. These amino acids are mostly involved upon binding to SN15, directly or indirectly affected by interactions with SN15 peptide residues. Three-dimensional structure of Bcl-X_L indicated that BH1, BH2 and BH3 domains form a hydrophobic cleft (Muchmore et al., 1996). In Bcl-X_L/Bak BH3 peptide and Bcl-X_L/Bad BH3 peptide complexes, both of the peptides adopt α-helices to interact with this hydrophobic groove (Petros et al., 2000; Sattler et al., 1997). Our results here indicated that the binding site on Bcl-X_L located to its hydrophobic groove too, which is similar with the interaction of Bcl-X_L with

Bak and Bad. On the ribbon and surface presentation of three-dimensional structure of Bcl-X_L, the amino acids involved in the interaction mostly surround the hydrophobic pocket.

Moreover, the Bak peptide from its BH3 domain is mainly random coil when free in solution. It forms an α helix after binding to Bcl-X_L (Sattler et al., 1997). Similar binding pattern was also observed in Bcl-X_L/Bad peptide interaction (Petros et al., 2000). Further more, both of the complex structures and mutagenesis experiments revealed that the ability to form an α helix is a critical factor for binding to Bcl-X_L (Petros et al., 2000; Sattler et al., 1997). As we discussed above, SN15 peptide from p53TAD is able to be induced to a α-helix upon binding to partners. The possible conformational change on this region was observed by the NMR titration experiment. Also, the binding site on Bcl-X_L of Bcl-X_L/SN15 interaction is the hydrophobic pocket. All these data together suggest that the SN15 peptide from p53TAD might also adopt a α-helix to bind to Bcl-X_L on its hydrophobic pocket. The binding pattern of Bcl-X_L/SN15 interaction is similar as Bcl-X_L/Bak and Bcl-X_L/Bad peptide interactions.

This hypothesis was confirmed by a competition binding experiment. In a competition GST pull-down binding assay, p53TAD/Bcl-X_L interaction was reduced or abolished by presence of GR16 or NK25. GR16 and NK25 are peptides from BH3 domains of pro-apoptotic Bcl-2 family proteins Bad and Bak. GR16 is a 16-mer peptide from Bak and NK25 is a 25-mer peptide from Bad. They were also used to solve the complex structure with Bcl-X_L (Petros et

al., 2000; Sattler et al., 1997). As we introduced before, GR16 and NK25 peptides were induced to adopt α helices upon binding to Bcl-X_L. And the binding site is on the cleft consists of BH1, BH2, and BH3 domains of Bcl-X_L. The competition GST pull down binding assay results showed that both of them bind to Bcl-X_L strongly and inhibit the p53TAD/Bcl-X_L interaction. It confirmed our results from the NMR study that Bcl-X_L/SN15 interaction shares similar binding site on Bcl-X_L with Bcl-X_L/Bak and Bcl-X_L/Bad peptide interactions. It also suggested that the binding constant of Bcl-X_L/SN15 is lower than Bcl-X_L/Bak and Bcl-X_L/Bad peptide.

To further understand the Bcl-X_L/SN15 interaction deeply, we also compared it with MDM2/SN15 interaction. As we introduced, MDM2 is one of the most important cellular regulator of p53. p53 induces the MDM2 expression by activating its gene transcription. On the other hand, MDM2 protein inhibits the p53 activity by binding to p53 on the transcriptional activation domain. Thus, MDM2 and p53 form a negative feedback loop to control the expression level of p53 in healthy cells (Wu et al., 1993). MDM2 binds to p53TAD to inhibit its transcriptional activity directly or to induce an ubiquitin-proteasome pathway of p53 degradation (Fang et al., 2000; Honda and Yasuda, 2000; Momand et al., 1992; Oliner et al., 1993). Thus, bypassing the MDM2-dependent p53-degradation is a critical step for the activation of p53 apoptotic function. Biological studies indicated that several post-translation regulation mechanisms of p53 were utilized for the p53 stabilization by breaking the p53/MDM2 interaction. Particularly, a phosphorylation of T18 on p53, which is one of the

amino acid from SN15 peptide, was critical for breaking the p53/MDM2 interaction (Schon et al., 2002). SN15 peptide with phosphorylated T18 was unable to bind MDM2. *In vivo* T18 phosphorylation was also observed with following effect of p53/MDM2 binding reduction and p53 stabilization (Sakaguchi et al., 2000). Considering that SN15 is also the binding site of p53TAD/Bcl-X_L interaction, it is interesting to compare the Bcl-X_L/SN15 interaction with MDM2/SN15 interaction by checking the effect of T18 phosphorylation of p53 on Bcl-X_L/SN15 interaction. We used a chemically synthesized SN15 peptide with phosphorylated T18, SN15p, to check its binding affinity with Bcl-X_L. In our NMR titration experiments, obvious chemical shift changes were observed in the HSQC spectra of ^{15}N-Bcl-X_LΔTMΔloop with absence and presence of SN15p peptide. The spectrum pattern is similar with the SN15 wild type peptide. This result showed that phosphorylation of T18 did not abolish the interaction of Bcl-X_L/SN15 *in vitro*. T18 phosphorylated p53 remains its Bcl-X_L binding ability. The post-translation of T18 phosphorylation is a critical mechanism for p53 stabilization. This phosphorylated p53 becomes an active mode, which bypassed the MDM2-mediated degradation pathway. It is thus understandable that this active mode p53 remains its ability to form complex with Bcl-X_L, which is believed to be important for its transcription-independent apoptotic activity. It is consistent with the published models of p53 stabilization and activation mechanisms and supports the possible mechanism of Bcl-X_L dependent p53 transcription-independent apoptosis.

We also did a SN15 alanine screening assay to further study the role of every amino acid residues in the Bcl-X_L/SN15 interaction. We synthesized a series of peptide mutants in which each of the amino acid residues from SN15 was replaced by alanine. All the mutant peptides were used in NMR titration experiments of ^{15}N-Bcl-X_LΔTMΔloop. Result showed that most critical amino acids are W23 and K24. Both W23A and K24A peptides can not bind to Bcl-X_L. Q16, E17, T18, L22 and L26 are also important for the interaction, and alanine mutant of these amino acids significantly decrease their binding affinity to Bcl-X_L. Among these most important amino acids, T18, W23, K24, and L26 belong to the five amino acids whose signals disappear on 2D ^{1}H-^{15}N HSQC spectra upon binding to Bcl-X_L. F19, D21, L25 and N29 are involved in the interaction with less effect on Bcl-X_L residue chemical shift changes. Mutants of S15A, S20A, P27A, and E28A still interact with Bcl-X_L, suggesting that these amino acids residues are not critical for binding.

Although we found that p53NTD and p53TAD interact with Bcl-X_L, a recently published paper reported that the interaction was not detected in their experiment (Sot et al., 2007). The binding of Bcl-X_LΔTM to fluorescein-labeled N-terminal p53 (residues 1-93) was checked by the fluorescence anisotropy assay. No obvious interaction between them was observed. In our studies, molecular interaction was examined using different assays, including FRET assay and NMR binding assay. The FRET assay was performed in mammalian cells, which is physiologically relevant in checking protein-protein interactions. NMR assay is a reliable method to measure weak bindings that might be missed

in other methods such as fluorescence-based anisotropy. So it is possible that the interaction may not be detected under their experimental conditions. Our SN15 peptide mutagenesis experiments identified critical residues responsible for the interaction between SN15 and Bcl-X_L, suggesting that the interaction detected in our studies is not due to nonspecific bindings. Therefore, the disagreement between the results reported by Sot, B et al and our results might be due to the low binding affinity of the interaction and different experimental methods and conditions used.

We observed that several amino acids peaks from SN15 disappeared upon binding to Bcl-X_L in 2D ^{1}H-^{15}N NMR HSQC titration experiments. It is a signal that minor conformational change on this region might occur. Further more, the SN15 peptide of p53TAD is known as a loose structural region with some structure elements. It is able to induce conformational change upon binding to some partner proteins, such as MDM2. To investigate the binding mode of Bcl-X_L/SN15 interaction, we determined the NMR structure of SN15 peptide in free state and compound state with presence of Bcl-X_L. Our structure data consists with the performance of SN15 peptide in other complex structures. The free SN15 peptide shows a short α-helix. The structure statistic indicated that the α-helix structure of free SN15 is loose and unstable. With presence of Bcl-X_L, the α-helix structure of SN15 is extended and stabilized, compared with the free peptide. This comparison of the structures in different state confirmed that the α-helix of SN15 peptide is induced, extended and stabilized

upon binding Bcl-X_L. This might be a common binding mode of the p53TAD, which also occurred in other complex formations.

Based on both structures of SN15 and Bcl-X_L, and the binding interface on Bcl-X_L identified by the chemical shift change data, a Bcl-X_L/SN15 complex structure model was obtained by computer-based docking. In the model, SN15 peptide adopts a α-helix to interact with the hydrophobic pocket of Bcl-X_L. The hydrophobic side chains of F19, L22, W23, L25, and L26 from SN15 peptide are directed into the hydrophobic cleft of Bcl-X_L. This binding mode is very similar with the Bcl-X_L/Bak peptide interaction, with same binding site on Bcl-X_L. It also explained our binding competition result that BH3 peptide of Bak and Bad efficiently abolished the p53TAD/Bcl-X_L interaction.

In Bcl-X_L/Bak complex, in addition to the hydrophobic interactions, the electrostatic interactions between Bak peptide (Arg76, Asp83 and Asp84) and Bcl-X_L (Glu129, Arg139, and Arg100, respectively) also play critical role to stabilize the complex formation. In our study, SN15K24A mutant peptide showed the loss of binding with Bcl-X_L, suggesting that K24 may play an important role in recognizing Bcl-X_L. However, in our complex structural model of Bcl-X_L/SN15, K24 does not make direct contacts with any negatively charged residues. This suggested that no electrostatic interaction is involved in the molecular interaction between K24 of SN15 and Bcl-X_L. The loss of binding affinity between the mutant peptide and Bcl-X_L might be attributable to the loss of secondary structure through the mutation.

On the other hand we have noticed that the position of D21 from SN15 in the Bcl-X_L/SN15 complex resembles that of D83 from Bak in the Bcl-X_L/Bak complex; D83 was shown to form an electrostatic interaction with R139 of Bcl-X_L and contribute to stabilizing Bcl-XL/Bak complex. Indeed our HSQC experiment using the mutant peptide (SN15D21A) showed a decrease in the binding affinity to Bcl-X_L, suggesting that D21 might be important in stabilizing the Bcl-X_L/SN15 complex through an electrostatic interaction. L78 from Bak in the Bcl-X_L/Bak complex is critical for the complex formation through hydrophobic interaction. In our Bcl-X_L/SN15 structural model, interestingly L26 from SN15 exhibits a similar topological arrangement to what was seen with L78 of Bak in the hydrophobic pocket. Taken together, our results suggest that the mode of interaction between Bcl-X_L and SN15 is similar to that of Bcl-X_L/Bak interaction in which both hydrophobic and electrostatic interactions are involved in the complex formation.

The interaction between p53 and Bcl-X_L is important for the transcription-independent apoptotic function of p53, especially when more and more Bcl-2 family proteins besides Bcl-2 and Bcl-X_L (Bax, Bak, Bad, and PUMA) were found to associate with p53 during its transcription-independent apoptotic pathway. The ability to interact with p53 might be universal function of Bcl-2 family proteins as part of its apoptotic regulation function. Studies on the association between p53 and Bcl-X_L enable us to understand the complexity of p53 function and discover novel anti-cancer drugs targeting on p53 function deficient.

Conclusions

In this thesis, cDNAs of Bcl-X_L with or without loop, p53NTD and p53TAD were cloned and constructed into different vector plasmids. The proteins of Bcl-X_LΔTM, Bcl-X_LΔTMΔloop, p53NTD, p53TAD, GST-p53NTD and GST-p53TAD were expressed, purified by different methods and characterized by different assays.

Binding assays including GST pull-down, co-expression system, NMR titration experiments and FRET assay confirmed that p53NTD interacts with Bcl-X_L *in vitro*, in *E.coli* cells and in mammalian cells. The binding interface on Bcl-X_L was preliminarily defined. Further experiments showed that the p53TAD alone without PPD domain can bind Bcl-X_L. The NMR titration experiments indicated a possible conformational change occurs on small region of p53TAD upon binding to Bcl-X_L. This region was figured out to be S15 to N29 according to p53TAD backbone assignment data.

Then SN15 peptide was chemically synthesized and confirmed to interact with Bcl-X_L. With the 2D ^{1}H-^{15}N backbone assignment of Bcl-X_LΔTMΔloop and its chemical shift change data upon binding to SN15 peptide, the binding site on Bcl-X_L was identified. BH1, BH2 and BH3 domains of Bcl-X_L are involved in the interaction, implying that similar as Bak or Bad BH3 peptide, SN15 also binds to the hydrophobic pocket on Bcl-X_L. Competition binding experiments also showed that peptides from Bak/Bad BH3 domains compete and abolish

Bcl-X_L/SN15 interaction, indicating that they share similar or overlaid binding site on Bcl-X_L.

Binding experiments also showed that SN15 interacts with both Bcl-X_LΔTM with loop and Bcl-X_LΔTMΔloop. The loop deletion does not decrease the binding affinity with SN15. Further more, phosphorylated T18 on SN15 also binds to Bcl-X_L, which is different from the MDM2/SN15 binding. Mutagenesis study on SN15 peptide indicated that amino acids W23 and K24 are most critical for the binding.

With further study on the details of Bcl-X_L/SN15 binding, 3D NMR experiments indicated that SN15 showed a loose and unstable α-helix in unbound mode. When binds to Bcl-X_L, it adopts an extended α-helix to form complex. In a compute-based complex structure model, SN15 peptide forms a α-helix and binds to the hydrophobic pocket of Bcl-X_L, which is consistent with our previous results.

List of Publications

Articles:

Huibin Xu, Jeff Tai, Hong Ye, Cong Bao Kang, Ho Sup Yoon, The N-terminal domain of tumor suppressor p53 is involved in the molecular interaction with the anti apoptotic protein Bcl-X_L, Biochemical and Biophysical Research Communications 341 (2006) 938-944.

Huibin Xu, Hong Ye, Nur Eliza Osman, Kristen Elizabeth Sadler, Ho Sup Yoon, The MDM2-binding region in the transactivation domain of p53 also acts as a Bcl-XL-binding motif, Ready for submission.

Conference Paper

Xu, H., Tai, J., Ye, H., Kang, C.B., Yoon, H.S. The involvement of the N-terminal domain of p53 in the molecular interaction with the anti-apoptotic protein Bcl-X_L. Protein Science 15 (Supplement 1): 134:A220 (August, 2006).

References

Abrams, J.M. (1999). An emerging blueprint for apoptosis in Drosophila. Trends Cell Biol *9*, 435-440.

Adams, J.M., and Cory, S. (1998). The Bcl-2 protein family: arbiters of cell survival. Science *281*, 1322-1326.

Adimoolam, S., and Ford, J.M. (2003). p53 and regulation of DNA damage recognition during nucleotide excision repair. DNA Repair (Amst) *2*, 947-954.

Adler, A.J., Greenfield, N.J., and Fasman, G.D. (1973). Circular dichroism and optical rotatory dispersion of proteins and polypeptides. Methods Enzymol *27*, 675-735.

Arima, Y., Nitta, M., Kuninaka, S., Zhang, D., Fujiwara, T., Taya, Y., Nakao, M., and Saya, H. (2005). Transcriptional blockade induces p53-dependent apoptosis associated with translocation of p53 to mitochondria. J Biol Chem *280*, 19166-19176.

Ashcroft, M., and Vousden, K.H. (1999). Regulation of p53 stability. Oncogene *18*, 7637-7643.

Ashkenazi, A., and Dixit, V.M. (1998). Death receptors: signaling and modulation. Science *281*, 1305-1308.

Bakhshi, A., Jensen, J.P., Goldman, P., Wright, J.J., McBride, O.W., Epstein, A.L., and Korsmeyer, S.J. (1985). Cloning the chromosomal breakpoint of t(14;18) human lymphomas: clustering around JH on chromosome 14 and near a transcriptional unit on 18. Cell *41*, 899-906.

Barak, Y., Juven, T., Haffner, R., and Oren, M. (1993). mdm2 expression is induced by wild type p53 activity. Embo J *12*, 461-468.

Bayer, E., Goettsch, S., Mueller, J.W., Griewel, B., Guiberman, E., Mayr, L.M., and Bayer, P. (2003). Structural analysis of the mitotic regulator hPin1 in solution: insights into domain architecture and substrate binding. J Biol Chem *278*, 26183-26193.

Bell, S., Klein, C., Muller, L., Hansen, S., and Buchner, J. (2002). p53 contains large unstructured regions in its native state. J Mol Biol *322*, 917-927.

Bissonnette, N., Wasylyk, B., and Hunting, D.J. (1997). The apoptotic and transcriptional transactivation activities of p53 can be dissociated. Biochem Cell Biol *75*, 351-358.

Boise, L.H., Gonzalez-Garcia, M., Postema, C.E., Ding, L., Lindsten, T., Turka, L.A., Mao, X., Nunez, G., and Thompson, C.B. (1993). bcl-x, a bcl-2-related gene that functions as a dominant regulator of apoptotic cell death. Cell *74*, 597-608.

Boldin, M.P., Goncharov, T.M., Goltsev, Y.V., and Wallach, D. (1996). Involvement of MACH, a novel MORT1/FADD-interacting protease, in Fas/APO-1- and TNF receptor-induced cell death. Cell *85*, 803-815.

Boldin, M.P., Mett, I.L., Varfolomeev, E.E., Chumakov, I., Shemer-Avni, Y., Camonis, J.H., and Wallach, D. (1995). Self-association of the "death domains" of the p55 tumor necrosis factor (TNF) receptor and Fas/APO1 prompts signaling for TNF and Fas/APO1 effects. J Biol Chem *270*, 387-391.

Buckbinder, L., Talbott, R., Velasco-Miguel, S., Takenaka, I., Faha, B., Seizinger, B.R., and Kley, N. (1995). Induction of the growth inhibitor IGF-binding protein 3 by p53. Nature *377*, 646-649.

Budihardjo, I., Oliver, H., Lutter, M., Luo, X., and Wang, X. (1999). Biochemical pathways of caspase activation during apoptosis. Annu Rev Cell Dev Biol *15*, 269-290.

Byler, D.M., and Susi, H. (1986). Examination of the secondary structure of proteins by deconvolved FTIR spectra. Biopolymers *25*, 469-487.

Caelles, C., Helmberg, A., and Karin, M. (1994). p53-dependent apoptosis in the absence of transcriptional activation of p53-target genes. Nature *370*, 220-223.

Chao, D.T., and Korsmeyer, S.J. (1998). BCL-2 family: regulators of cell death. Annu Rev Immunol *16*, 395-419.

Chen, X., Ko, L.J., Jayaraman, L., and Prives, C. (1996). p53 levels, functional domains, and DNA damage determine the extent of the apoptotic response of tumor cells. Genes Dev *10*, 2438-2451.

Cheng, E.H., Kirsch, D.G., Clem, R.J., Ravi, R., Kastan, M.B., Bedi, A., Ueno, K., and Hardwick, J.M. (1997). Conversion of Bcl-2 to a Bax-like death effector by caspases. Science *278*, 1966-1968.

Cheng, E.H., Levine, B., Boise, L.H., Thompson, C.B., and Hardwick, J.M. (1996). Bax-independent inhibition of apoptosis by Bcl-XL. Nature *379*, 554-556.

Chi, S.W., Lee, S.H., Kim, D.H., Ahn, M.J., Kim, J.S., Woo, J.Y., Torizawa, T., Kainosho, M., and Han, K.H. (2005). Structural details on mdm2-p53 interaction. J Biol Chem *280*, 38795-38802.

Chinnaiyan, A.M., O'Rourke, K., Tewari, M., and Dixit, V.M. (1995). FADD, a novel death domain-containing protein, interacts with the death domain of Fas and initiates apoptosis. Cell *81*, 505-512.

Chipuk, J.E., Kuwana, T., Bouchier-Hayes, L., Droin, N.M., Newmeyer, D.D., Schuler, M., and Green, D.R. (2004). Direct activation of Bax by p53 mediates mitochondrial membrane permeabilization and apoptosis. Science *303*, 1010-1014.

Chipuk, J.E., Maurer, U., Green, D.R., and Schuler, M. (2003). Pharmacologic activation of p53 elicits Bax-dependent apoptosis in the absence of transcription. Cancer Cell *4*, 371-381.

Cho, Y., Gorina, S., Jeffrey, P.D., and Pavletich, N.P. (1994). Crystal structure of a p53 tumor suppressor-DNA complex: understanding tumorigenic mutations. Science *265*, 346-355.

Cleary, M.L., and Sklar, J. (1985). Nucleotide sequence of a t(14;18) chromosomal breakpoint in follicular lymphoma and demonstration of a breakpoint-cluster region near a transcriptionally active locus on chromosome 18. Proc Natl Acad Sci U S A *82*, 7439-7443.

Clore, G.M., Ernst, J., Clubb, R., Omichinski, J.G., Kennedy, W.M., Sakaguchi, K., Appella, E., and Gronenborn, A.M. (1995). Refined solution structure of the oligomerization domain of the tumour suppressor p53. Nat Struct Biol *2*, 321-333.

Colussi, P.A., and Kumar, S. (1999). Targeted disruption of caspase genes in mice: what they tell us about the functions of individual caspases in apoptosis. Immunol Cell Biol *77*, 58-63.

Cory, S., and Adams, J.M. (2002). The Bcl2 family: regulators of the cellular life-or-death switch. Nat Rev Cancer *2*, 647-656.

Cory, S., Huang, D.C., and Adams, J.M. (2003). The Bcl-2 family: roles in cell survival and oncogenesis. Oncogene *22*, 8590-8607.

Crook, T., Marston, N.J., Sara, E.A., and Vousden, K.H. (1994). Transcriptional activation by p53 correlates with suppression of growth but not transformation. Cell *79*, 817-827.

Dawson, R., Muller, L., Dehner, A., Klein, C., Kessler, H., and Buchner, J. (2003). The N-terminal domain of p53 is natively unfolded. J Mol Biol *332*, 1131-1141.

de Rozieres, S., Maya, R., Oren, M., and Lozano, G. (2000). The loss of mdm2 induces p53-mediated apoptosis. Oncogene *19*, 1691-1697.

Debatin, K.M., and Krammer, P.H. (2004). Death receptors in chemotherapy and cancer. Oncogene *23*, 2950-2966.

Decaudin, D., Geley, S., Hirsch, T., Castedo, M., Marchetti, P., Macho, A., Kofler, R., and Kroemer, G. (1997). Bcl-2 and Bcl-XL antagonize the mitochondrial dysfunction preceding nuclear apoptosis induced by chemotherapeutic agents. Cancer Res *57*, 62-67.

Degli Esposti, M. (2004). Mitochondria in apoptosis: past, present and future. Biochem Soc Trans *32*, 493-495.

Degterev, A., Boyce, M., and Yuan, J. (2003). A decade of caspases. Oncogene *22*, 8543-8567.

DeLeo, A.B., Jay, G., Appella, E., Dubois, G.C., Law, L.W., and Old, L.J. (1979). Detection of a transformation-related antigen in chemically induced sarcomas and other transformed cells of the mouse. Proc Natl Acad Sci U S A *76*, 2420-2424.

Desagher, S., and Martinou, J.C. (2000). Mitochondria as the central control point of apoptosis. Trends Cell Biol *10*, 369-377.

Ding, H.F., Lin, Y.L., McGill, G., Juo, P., Zhu, H., Blenis, J., Yuan, J., and Fisher, D.E. (2000). Essential role for caspase-8 in transcription-independent apoptosis triggered by p53. J Biol Chem *275*, 38905-38911.

Donehower, L.A., Harvey, M., Slagle, B.L., McArthur, M.J., Montgomery, C.A., Jr., Butel, J.S., and Bradley, A. (1992). Mice deficient for p53 are developmentally normal but susceptible to spontaneous tumours. Nature *356*, 215-221.

Dramsi, S., Scheid, M.P., Maiti, A., Hojabrpour, P., Chen, X., Schubert, K., Goodlett, D.R., Aebersold, R., and Duronio, V. (2002). Identification of a novel phosphorylation site, Ser-170, as a regulator of bad pro-apoptotic activity. J Biol Chem *277*, 6399-6405.

Dumont, P., Leu, J.I., Della Pietra, A.C., 3rd, George, D.L., and Murphy, M. (2003). The codon 72 polymorphic variants of p53 have markedly different apoptotic potential. Nat Genet *33*, 357-365.

el-Deiry, W.S. (1998). Regulation of p53 downstream genes. Semin Cancer Biol *8*, 345-357.

Ellis, H.M., and Horvitz, H.R. (1986). Genetic control of programmed cell death in the nematode C. elegans. Cell *44*, 817-829.

Ellis, R.E., Yuan, J.Y., and Horvitz, H.R. (1991). Mechanisms and functions of cell death. Annu Rev Cell Biol *7*, 663-698.

Erster, S., Mihara, M., Kim, R.H., Petrenko, O., and Moll, U.M. (2004). In vivo mitochondrial p53 translocation triggers a rapid first wave of cell death in response to DNA damage that can precede p53 target gene activation. Mol Cell Biol *24*, 6728-6741.

Erster, S., and Moll, U.M. (2004). Stress-induced p53 runs a direct mitochondrial death program: its role in physiologic and pathophysiologic stress responses in vivo. Cell Cycle *3*, 1492-1495.

Erster, S., and Moll, U.M. (2005). Stress-induced p53 runs a transcription-independent death program. Biochem Biophys Res Commun *331*, 843-850.

Eskes, R., Antonsson, B., Osen-Sand, A., Montessuit, S., Richter, C., Sadoul, R., Mazzei, G., Nichols, A., and Martinou, J.C. (1998). Bax-induced cytochrome C release from mitochondria is independent of the permeability transition pore but highly dependent on Mg2+ ions. J Cell Biol *143*, 217-224.

Essmann, F., Pohlmann, S., Gillissen, B., Daniel, P.T., Schulze-Osthoff, K., and Janicke, R.U. (2005). Irradiation-induced translocation of p53 to mitochondria in the absence of apoptosis. J Biol Chem *280*, 37169-37177.

Fang, S., Jensen, J.P., Ludwig, R.L., Vousden, K.H., and Weissman, A.M. (2000). Mdm2 is a RING finger-dependent ubiquitin protein ligase for itself and p53. J Biol Chem *275*, 8945-8951.

Fields, S., and Jang, S.K. (1990). Presence of a potent transcription activating sequence in the p53 protein. Science *249*, 1046-1049.

Fuchs, S.Y., Adler, V., Buschmann, T., Yin, Z., Wu, X., Jones, S.N., and Ronai, Z. (1998). JNK targets p53 ubiquitination and degradation in nonstressed cells. Genes Dev *12*, 2658-2663.

Fumarola, C., and Guidotti, G.G. (2004). Stress-induced apoptosis: toward a symmetry with receptor-mediated cell death. Apoptosis *9*, 77-82.

Garcia-Cao, I., Garcia-Cao, M., Martin-Caballero, J., Criado, L.M., Klatt, P., Flores, J.M., Weill, J.C., Blasco, M.A., and Serrano, M. (2002). "Super p53"

mice exhibit enhanced DNA damage response, are tumor resistant and age normally. Embo J *21*, 6225-6235.

Germain, M., and Shore, G.C. (2003). Cellular distribution of Bcl-2 family proteins. Sci STKE *2003*, pe10.

Gonzalez-Garcia, M., Perez-Ballestero, R., Ding, L., Duan, L., Boise, L.H., Thompson, C.B., and Nunez, G. (1994). bcl-XL is the major bcl-x mRNA form expressed during murine development and its product localizes to mitochondria. Development *120*, 3033-3042.

Goping, I.S., Gross, A., Lavoie, J.N., Nguyen, M., Jemmerson, R., Roth, K., Korsmeyer, S.J., and Shore, G.C. (1998). Regulated targeting of BAX to mitochondria. J Cell Biol *143*, 207-215.

Gottlieb, E., Lindner, S., and Oren, M. (1996). Relationship of sequence-specific transactivation and p53-regulated apoptosis in interleukin 3-dependent hematopoietic cells. Cell Growth Differ *7*, 301-310.

Green, D.R., and Reed, J.C. (1998). Mitochondria and apoptosis. Science *281*, 1309-1312.

Gross, A., McDonnell, J.M., and Korsmeyer, S.J. (1999). BCL-2 family members and the mitochondria in apoptosis. Genes Dev *13*, 1899-1911.

Gruss, H.J., and Dower, S.K. (1995). Tumor necrosis factor ligand superfamily: involvement in the pathology of malignant lymphomas. Blood *85*, 3378-3404.

Harris, C.C. (1996). p53 tumor suppressor gene: from the basic research laboratory to the clinic--an abridged historical perspective. Carcinogenesis *17*, 1187-1198.

Haupt, Y., Barak, Y., and Oren, M. (1996). Cell type-specific inhibition of p53-mediated apoptosis by mdm2. Embo J *15*, 1596-1606.

Haupt, Y., Maya, R., Kazaz, A., and Oren, M. (1997). Mdm2 promotes the rapid degradation of p53. Nature *387*, 296-299.

Haupt, Y., Rowan, S., Shaulian, E., Vousden, K.H., and Oren, M. (1995). Induction of apoptosis in HeLa cells by trans-activation-deficient p53. Genes Dev *9*, 2170-2183.

Hawkins, C.J., and Vaux, D.L. (1997). The role of the Bcl-2 family of apoptosis regulatory proteins in the immune system. Semin Immunol *9*, 25-33.

Hay, B.A., Huh, J.R., and Guo, M. (2004). The genetics of cell death: approaches, insights and opportunities in Drosophila. Nat Rev Genet *5*, 911-922.

Hengartner, M.O. (2000). The biochemistry of apoptosis. Nature *407*, 770-776.
Hipfner, D.R., and Cohen, S.M. (2004). Connecting proliferation and apoptosis in development and disease. Nat Rev Mol Cell Biol *5*, 805-815.

Hockenbery, D., Nunez, G., Milliman, C., Schreiber, R.D., and Korsmeyer, S.J. (1990). Bcl-2 is an inner mitochondrial membrane protein that blocks programmed cell death. Nature *348*, 334-336.

Hofseth, L.J., Hussain, S.P., and Harris, C.C. (2004). p53: 25 years after its discovery. Trends Pharmacol Sci *25*, 177-181.

Hollstein, M., Sidransky, D., Vogelstein, B., and Harris, C.C. (1991). p53 mutations in human cancers. Science *253*, 49-53.

Honda, R., and Yasuda, H. (2000). Activity of MDM2, a ubiquitin ligase, toward p53 or itself is dependent on the RING finger domain of the ligase. Oncogene *19*, 1473-1476.

Horvitz, H.R. (1999). Genetic control of programmed cell death in the nematode Caenorhabditis elegans. Cancer Res *59*, 1701s-1706s.

Huang, B., Eberstadt, M., Olejniczak, E.T., Meadows, R.P., and Fesik, S.W. (1996). NMR structure and mutagenesis of the Fas (APO-1/CD95) death domain. Nature *384*, 638-641.

Huang, S.T., and Cidlowski, J.A. (2002). Phosphorylation status modulates Bcl-2 function during glucocorticoid-induced apoptosis in T lymphocytes. Faseb J *16*, 825-832.

Ishioka, C., Englert, C., Winge, P., Yan, Y.X., Engelstein, M., and Friend, S.H. (1995). Mutational analysis of the carboxy-terminal portion of p53 using both yeast and mammalian cell assays in vivo. Oncogene *10*, 1485-1492.

Israeli, D., Tessler, E., Haupt, Y., Elkeles, A., Wilder, S., Amson, R., Telerman, A., and Oren, M. (1997). A novel p53-inducible gene, PAG608, encodes a nuclear zinc finger protein whose overexpression promotes apoptosis. Embo J *16*, 4384-4392.

Jacobson, M.D., Weil, M., and Raff, M.C. (1997). Programmed cell death in animal development. Cell *88*, 347-354.

Jayaraman, L., and Prives, C. (1999). Covalent and noncovalent modifiers of the p53 protein. Cell Mol Life Sci *55*, 76-87.

Jiang, P., Du, W., Heese, K., and Wu, M. (2006). The Bad guy cooperates with good cop p53: Bad is transcriptionally up-regulated by p53 and forms a Bad/p53 complex at the mitochondria to induce apoptosis. Mol Cell Biol *26*, 9071-9082.

Johnson, B.A. (2004). Using NMRView to visualize and analyze the NMR spectra of macromolecules. Methods Mol Biol *278*, 313-352.

Jones, S.N., Roe, A.E., Donehower, L.A., and Bradley, A. (1995). Rescue of embryonic lethality in Mdm2-deficient mice by absence of p53. Nature *378*, 206-208.

Kang, C.B., Tai, J., Chia, J., and Yoon, H.S. (2005). The flexible loop of Bcl-2 is required for molecular interaction with immunosuppressant FK-506 binding protein 38 (FKBP38). FEBS Lett *579*, 1469-1476.

Kang, C.B., Ye, H., Vivekanandan, S., Simon, B., Sattler, M., and Yoon, H.S. (2006). Backbone 1H, 13C, and 15N resonance assignments of the N-terminal domain of FKBP38 (FKBP38NTD). J Biomol NMR *36 Suppl 1*, 37.

Karpova, T.S., Baumann, C.T., He, L., Wu, X., Grammer, A., Lipsky, P., Hager, G.L., and McNally, J.G. (2003). Fluorescence resonance energy transfer from cyan to yellow fluorescent protein detected by acceptor photobleaching using confocal microscopy and a single laser. J Microsc *209*, 56-70.

Kasibhatla, S., and Tseng, B. (2003). Why target apoptosis in cancer treatment? Mol Cancer Ther *2*, 573-580.

Kastan, M.B., Onyekwere, O., Sidransky, D., Vogelstein, B., and Craig, R.W. (1991). Participation of p53 protein in the cellular response to DNA damage. Cancer Res *51*, 6304-6311.

Kelekar, A., Chang, B.S., Harlan, J.E., Fesik, S.W., and Thompson, C.B. (1997). Bad is a BH3 domain-containing protein that forms an inactivating dimer with Bcl-XL. Mol Cell Biol *17*, 7040-7046.

Kenworthy, A.K. (2001). Imaging protein-protein interactions using fluorescence resonance energy transfer microscopy. Methods *24*, 289-296.

Kerr, J.F., Wyllie, A.H., and Currie, A.R. (1972). Apoptosis: a basic biological phenomenon with wide-ranging implications in tissue kinetics. Br J Cancer *26*, 239-257.

Kim, S., Cullis, D.N., Feig, L.A., and Baleja, J.D. (2001). Solution structure of the Reps1 EH domain and characterization of its binding to NPF target sequences. Biochemistry *40*, 6776-6785.

Kokontis, J.M., Wagner, A.J., O'Leary, M., Liao, S., and Hay, N. (2001). A transcriptional activation function of p53 is dispensable for and inhibitory of its apoptotic function. Oncogene *20*, 659-668.

Kress, M., May, E., Cassingena, R., and May, P. (1979). Simian virus 40-transformed cells express new species of proteins precipitable by anti-simian virus 40 tumor serum. J Virol *31*, 472-483.

Kubbutat, M.H., Jones, S.N., and Vousden, K.H. (1997). Regulation of p53 stability by Mdm2. Nature *387*, 299-303.

Kubbutat, M.H., and Vousden, K.H. (1997). Proteolytic cleavage of human p53 by calpain: a potential regulator of protein stability. Mol Cell Biol *17*, 460-468.

Kussie, P.H., Gorina, S., Marechal, V., Elenbaas, B., Moreau, J., Levine, A.J., and Pavletich, N.P. (1996). Structure of the MDM2 oncoprotein bound to the p53 tumor suppressor transactivation domain. Science *274*, 948-953.

Kuwana, T., and Newmeyer, D.D. (2003). Bcl-2-family proteins and the role of mitochondria in apoptosis. Curr Opin Cell Biol *15*, 691-699.

Lane, D.P. (1992). Cancer. p53, guardian of the genome. Nature *358*, 15-16.

Lane, D.P., and Crawford, L.V. (1979). T antigen is bound to a host protein in SV40-transformed cells. Nature *278*, 261-263.

Lavigueur, A., Maltby, V., Mock, D., Rossant, J., Pawson, T., and Bernstein, A. (1989). High incidence of lung, bone, and lymphoid tumors in transgenic mice overexpressing mutant alleles of the p53 oncogene. Mol Cell Biol *9*, 3982-3991.

Lee, H., Mok, K.H., Muhandiram, R., Park, K.H., Suk, J.E., Kim, D.H., Chang, J., Sung, Y.C., Choi, K.Y., and Han, K.H. (2000). Local structural elements in the mostly unstructured transcriptional activation domain of human p53. J Biol Chem *275*, 29426-29432.

Lee, W., Harvey, T.S., Yin, Y., Yau, P., Litchfield, D., and Arrowsmith, C.H. (1994). Solution structure of the tetrameric minimum transforming domain of p53. Nat Struct Biol *1*, 877-890.

Leu, J.I., Dumont, P., Hafey, M., Murphy, M.E., and George, D.L. (2004). Mitochondrial p53 activates Bak and causes disruption of a Bak-Mcl1 complex. Nat Cell Biol *6*, 443-450.

Levine, A.J. (1997). p53, the cellular gatekeeper for growth and division. Cell *88*, 323-331.

Levine, A.J., Momand, J., and Finlay, C.A. (1991). The p53 tumour suppressor gene. Nature *351*, 453-456.

Linzer, D.I., and Levine, A.J. (1979). Characterization of a 54K dalton cellular SV40 tumor antigen present in SV40-transformed cells and uninfected embryonal carcinoma cells. Cell *17*, 43-52.

Liu, Q.A., and Hengartner, M.O. (1999). The molecular mechanism of programmed cell death in C. elegans. Ann N Y Acad Sci *887*, 92-104.

Lohrum, M.A., and Vousden, K.H. (1999). Regulation and activation of p53 and its family members. Cell Death Differ *6*, 1162-1168.

Losonczi, J.A., Olejniczak, E.T., Betz, S.F., Harlan, J.E., Mack, J., and Fesik, S.W. (2000). NMR studies of the anti-apoptotic protein Bcl-xL in micelles. Biochemistry *39*, 11024-11033.

MacFarlane, M., and Williams, A.C. (2004). Apoptosis and disease: a life or death decision. EMBO Rep *5*, 674-678.

Maki, C.G., Huibregtse, J.M., and Howley, P.M. (1996). In vivo ubiquitination and proteasome-mediated degradation of p53(1). Cancer Res *56*, 2649-2654.

Maltzman, W., and Czyzyk, L. (1984). UV irradiation stimulates levels of p53 cellular tumor antigen in nontransformed mouse cells. Mol Cell Biol *4*, 1689-1694.

Marchenko, N.D., Zaika, A., and Moll, U.M. (2000). Death signal-induced localization of p53 protein to mitochondria. A potential role in apoptotic signaling. J Biol Chem *275*, 16202-16212.

Marston, N.J., Crook, T., and Vousden, K.H. (1994). Interaction of p53 with MDM2 is independent of E6 and does not mediate wild type transformation suppressor function. Oncogene *9*, 2707-2716.

Martinou, J.C., and Green, D.R. (2001). Breaking the mitochondrial barrier. Nat Rev Mol Cell Biol *2*, 63-67.

McDonnell, T.J., Deane, N., Platt, F.M., Nunez, G., Jaeger, U., McKearn, J.P., and Korsmeyer, S.J. (1989). bcl-2-immunoglobulin transgenic mice demonstrate extended B cell survival and follicular lymphoproliferation. Cell *57*, 79-88.

McDonnell, T.J., Nunez, G., Platt, F.M., Hockenberry, D., London, L., McKearn, J.P., and Korsmeyer, S.J. (1990). Deregulated Bcl-2-immunoglobulin transgene expands a resting but responsive immunoglobulin M and D-expressing B-cell population. Mol Cell Biol *10*, 1901-1907.

Meek, D.W. (1998). Multisite phosphorylation and the integration of stress signals at p53. Cell Signal *10*, 159-166.

Meier, P., Finch, A., and Evan, G. (2000). Apoptosis in development. Nature *407*, 796-801.

Michael, D., and Oren, M. (2003). The p53-Mdm2 module and the ubiquitin system. Semin Cancer Biol *13*, 49-58.

Midgley, C.A., and Lane, D.P. (1997). p53 protein stability in tumour cells is not determined by mutation but is dependent on Mdm2 binding. Oncogene *15*, 1179-1189.

Mihara, M., Erster, S., Zaika, A., Petrenko, O., Chittenden, T., Pancoska, P., and Moll, U.M. (2003). p53 has a direct apoptogenic role at the mitochondria. Mol Cell *11*, 577-590.

Minn, A.J., Velez, P., Schendel, S.L., Liang, H., Muchmore, S.W., Fesik, S.W., Fill, M., and Thompson, C.B. (1997). Bcl-x(L) forms an ion channel in synthetic lipid membranes. Nature *385*, 353-357.

Miyashita, T., and Reed, J.C. (1995). Tumor suppressor p53 is a direct transcriptional activator of the human bax gene. Cell *80*, 293-299.

Momand, J., Zambetti, G.P., Olson, D.C., George, D., and Levine, A.J. (1992). The mdm-2 oncogene product forms a complex with the p53 protein and inhibits p53-mediated transactivation. Cell *69*, 1237-1245.

Montes de Oca Luna, R., Wagner, D.S., and Lozano, G. (1995). Rescue of early embryonic lethality in mdm2-deficient mice by deletion of p53. Nature *378*, 203-206.

Motoyama, N., Wang, F., Roth, K.A., Sawa, H., Nakayama, K., Nakayama, K., Negishi, I., Senju, S., Zhang, Q., Fujii, S., *et al.* (1995). Massive cell death of immature hematopoietic cells and neurons in Bcl-x-deficient mice. Science *267*, 1506-1510.

Muchmore, S.W., Sattler, M., Liang, H., Meadows, R.P., Harlan, J.E., Yoon, H.S., Nettesheim, D., Chang, B.S., Thompson, C.B., Wong, S.L., *et al.* (1996). X-ray and NMR structure of human Bcl-xL, an inhibitor of programmed cell death. Nature *381*, 335-341.

Muqit, M.M., and Feany, M.B. (2002). Modelling neurodegenerative diseases in Drosophila: a fruitful approach? Nat Rev Neurosci *3*, 237-243.

Muzio, M., Stockwell, B.R., Stennicke, H.R., Salvesen, G.S., and Dixit, V.M. (1998). An induced proximity model for caspase-8 activation. J Biol Chem *273*, 2926-2930.

Nagata, S. (1997). Apoptosis by death factor. Cell *88*, 355-365.

Nakano, K., and Vousden, K.H. (2001). PUMA, a novel proapoptotic gene, is induced by p53. Mol Cell *7*, 683-694.

Nemajerova, A., Erster, S., and Moll, U.M. (2005). The post-translational phosphorylation and acetylation modification profile is not the determining factor in targeting endogenous stress-induced p53 to mitochondria. Cell Death Differ *12*, 197-200.

Nguyen, M., Millar, D.G., Yong, V.W., Korsmeyer, S.J., and Shore, G.C. (1993). Targeting of Bcl-2 to the mitochondrial outer membrane by a COOH-terminal signal anchor sequence. J Biol Chem *268*, 25265-25268.

Oda, E., Ohki, R., Murasawa, H., Nemoto, J., Shibue, T., Yamashita, T., Tokino, T., Taniguchi, T., and Tanaka, N. (2000). Noxa, a BH3-only member of the Bcl-2 family and candidate mediator of p53-induced apoptosis. Science *288*, 1053-1058.

Offer, H., Wolkowicz, R., Matas, D., Blumenstein, S., Livneh, Z., and Rotter, V. (1999). Direct involvement of p53 in the base excision repair pathway of the DNA repair machinery. FEBS Lett *450*, 197-204.

Ojala, P.M., Yamamoto, K., Castanos-Velez, E., Biberfeld, P., Korsmeyer, S.J., and Makela, T.P. (2000). The apoptotic v-cyclin-CDK6 complex phosphorylates and inactivates Bcl-2. Nat Cell Biol *2*, 819-825.

Oliner, J.D., Pietenpol, J.A., Thiagalingam, S., Gyuris, J., Kinzler, K.W., and Vogelstein, B. (1993). Oncoprotein MDM2 conceals the activation domain of tumour suppressor p53. Nature *362*, 857-860.

Oltvai, Z.N., Milliman, C.L., and Korsmeyer, S.J. (1993). Bcl-2 heterodimerizes in vivo with a conserved homolog, Bax, that accelerates programmed cell death. Cell *74*, 609-619.

Ottilie, S., Diaz, J.L., Horne, W., Chang, J., Wang, Y., Wilson, G., Chang, S., Weeks, S., Fritz, L.C., and Oltersdorf, T. (1997). Dimerization properties of human BAD. Identification of a BH-3 domain and analysis of its binding to mutant BCL-2 and BCL-XL proteins. J Biol Chem *272*, 30866-30872.

Owen-Schaub, L.B., Zhang, W., Cusack, J.C., Angelo, L.S., Santee, S.M., Fujiwara, T., Roth, J.A., Deisseroth, A.B., Zhang, W.W., Kruzel, E., *et al.*

(1995). Wild-type human p53 and a temperature-sensitive mutant induce Fas/APO-1 expression. Mol Cell Biol *15*, 3032-3040.

Page, R., Peti, W., Wilson, I.A., Stevens, R.C., and Wuthrich, K. (2005). NMR screening and crystal quality of bacterially expressed prokaryotic and eukaryotic proteins in a structural genomics pipeline. Proc Natl Acad Sci U S A *102*, 1901-1905.

Pariat, M., Carillo, S., Molinari, M., Salvat, C., Debussche, L., Bracco, L., Milner, J., and Piechaczyk, M. (1997). Proteolysis by calpains: a possible contribution to degradation of p53. Mol Cell Biol *17*, 2806-2815.

Pastorino, J.G., Chen, S.T., Tafani, M., Snyder, J.W., and Farber, J.L. (1998). The overexpression of Bax produces cell death upon induction of the mitochondrial permeability transition. J Biol Chem *273*, 7770-7775.

Petros, A.M., Gunasekera, A., Xu, N., Olejniczak, E.T., and Fesik, S.W. (2004). Defining the p53 DNA-binding domain/Bcl-x(L)-binding interface using NMR. FEBS Lett *559*, 171-174.

Petros, A.M., Medek, A., Nettesheim, D.G., Kim, D.H., Yoon, H.S., Swift, K., Matayoshi, E.D., Oltersdorf, T., and Fesik, S.W. (2001). Solution structure of the antiapoptotic protein bcl-2. Proc Natl Acad Sci U S A *98*, 3012-3017.

Petros, A.M., Nettesheim, D.G., Wang, Y., Olejniczak, E.T., Meadows, R.P., Mack, J., Swift, K., Matayoshi, E.D., Zhang, H., Thompson, C.B., *et al.* (2000). Rationale for Bcl-xL/Bad peptide complex formation from structure, mutagenesis, and biophysical studies. Protein Sci *9*, 2528-2534.

Pietenpol, J.A., Tokino, T., Thiagalingam, S., el-Deiry, W.S., Kinzler, K.W., and Vogelstein, B. (1994). Sequence-specific transcriptional activation is essential for growth suppression by p53. Proc Natl Acad Sci U S A *91*, 1998-2002.

Polyak, K., Xia, Y., Zweier, J.L., Kinzler, K.W., and Vogelstein, B. (1997). A model for p53-induced apoptosis. Nature *389*, 300-305.

Ptashne, M., and Gann, A. (1997). Transcriptional activation by recruitment. Nature *386*, 569-577.

Raman, V., Martensen, S.A., Reisman, D., Evron, E., Odenwald, W.F., Jaffee, E., Marks, J., and Sukumar, S. (2000). Compromised HOXA5 function can limit p53 expression in human breast tumours. Nature *405*, 974-978.

Ranger, A.M., Malynn, B.A., and Korsmeyer, S.J. (2001). Mouse models of cell death. Nat Genet *28*, 113-118.

Reed, J.C. (1998). Bcl-2 family proteins. Oncogene *17*, 3225-3236.

Reinke, V., and Lozano, G. (1997). The p53 targets mdm2 and Fas are not required as mediators of apoptosis in vivo. Oncogene *15*, 1527-1534.

Rosse, T., Olivier, R., Monney, L., Rager, M., Conus, S., Fellay, I., Jansen, B., and Borner, C. (1998). Bcl-2 prolongs cell survival after Bax-induced release of cytochrome c. Nature *391*, 496-499.

Rowan, S., Ludwig, R.L., Haupt, Y., Bates, S., Lu, X., Oren, M., and Vousden, K.H. (1996). Specific loss of apoptotic but not cell-cycle arrest function in a human tumor derived p53 mutant. Embo J *15*, 827-838.

Sakaguchi, K., Saito, S., Higashimoto, Y., Roy, S., Anderson, C.W., and Appella, E. (2000). Damage-mediated phosphorylation of human p53 threonine 18 through a cascade mediated by a casein 1-like kinase. Effect on Mdm2 binding. J Biol Chem *275*, 9278-9283.

Sansome, C., Zaika, A., Marchenko, N.D., and Moll, U.M. (2001). Hypoxia death stimulus induces translocation of p53 protein to mitochondria. Detection by immunofluorescence on whole cells. FEBS Lett *488*, 110-115.

Sattler, M., Liang, H., Nettesheim, D., Meadows, R.P., Harlan, J.E., Eberstadt, M., Yoon, H.S., Shuker, S.B., Chang, B.S., Minn, A.J., *et al.* (1997). Structure of Bcl-xL-Bak peptide complex: recognition between regulators of apoptosis. Science *275*, 983-986.

Sax, J.K., Fei, P., Murphy, M.E., Bernhard, E., Korsmeyer, S.J., and El-Deiry, W.S. (2002). BID regulation by p53 contributes to chemosensitivity. Nat Cell Biol *4*, 842-849.

Sayan, B.S., Sayan, A.E., Knight, R.A., Melino, G., and Cohen, G.M. (2006). p53 is cleaved by caspases generating fragments localizing to mitochondria. J Biol Chem *281*, 13566-13573.

Scheffner, M., Huibregtse, J.M., Vierstra, R.D., and Howley, P.M. (1993). The HPV-16 E6 and E6-AP complex functions as a ubiquitin-protein ligase in the ubiquitination of p53. Cell *75*, 495-505.

Schendel, S.L., Montal, M., and Reed, J.C. (1998). Bcl-2 family proteins as ion-channels. Cell Death Differ *5*, 372-380.

Schendel, S.L., Xie, Z., Montal, M.O., Matsuyama, S., Montal, M., and Reed, J.C. (1997). Channel formation by antiapoptotic protein Bcl-2. Proc Natl Acad Sci U S A *94*, 5113-5118.

Schlesinger, P.H., Gross, A., Yin, X.M., Yamamoto, K., Saito, M., Waksman, G., and Korsmeyer, S.J. (1997). Comparison of the ion channel characteristics of proapoptotic BAX and antiapoptotic BCL-2. Proc Natl Acad Sci U S A *94*, 11357-11362.

Schon, O., Friedler, A., Bycroft, M., Freund, S.M., and Fersht, A.R. (2002). Molecular mechanism of the interaction between MDM2 and p53. J Mol Biol *323*, 491-501.

Schuler, M., Bossy-Wetzel, E., Goldstein, J.C., Fitzgerald, P., and Green, D.R. (2000). p53 induces apoptosis by caspase activation through mitochondrial cytochrome c release. J Biol Chem *275*, 7337-7342.

Schuler, M., and Green, D.R. (2001). Mechanisms of p53-dependent apoptosis. Biochem Soc Trans *29*, 684-688.

Shindler, K.S., Latham, C.B., and Roth, K.A. (1997). Bax deficiency prevents the increased cell death of immature neurons in bcl-x-deficient mice. J Neurosci *17*, 3112-3119.

Sionov, R.V., and Haupt, Y. (1999). The cellular response to p53: the decision between life and death. Oncogene *18*, 6145-6157.

Smet, C., Duckert, J.F., Wieruszeski, J.M., Landrieu, I., Buee, L., Lippens, G., and Deprez, B. (2005). Control of protein-protein interactions: structure-based discovery of low molecular weight inhibitors of the interactions between Pin1 WW domain and phosphopeptides. J Med Chem *48*, 4815-4823.

Sot, B., Freund, S.M., and Fersht, A.R. (2007). Comparative biophysical characterization of p53 with the pro-apoptotic BAK and the anti-apoptotic BCL-xL. J Biol Chem *282*, 29193-29200.

Symonds, H., Krall, L., Remington, L., Saenz-Robles, M., Lowe, S., Jacks, T., and Van Dyke, T. (1994). p53-dependent apoptosis suppresses tumor growth and progression in vivo. Cell *78*, 703-711.

Thompson, C.B. (1995). Apoptosis in the pathogenesis and treatment of disease. Science *267*, 1456-1462.

Thornberry, N.A., and Lazebnik, Y. (1998). Caspases: enemies within. Science *281*, 1312-1316.

Triezenberg, S.J. (1995). Structure and function of transcriptional activation domains. Curr Opin Genet Dev *5*, 190-196.

Tsujimoto, Y. (1989). Stress-resistance conferred by high level of bcl-2 alpha protein in human B lymphoblastoid cell. Oncogene *4*, 1331-1336.

Tsujimoto, Y., Cossman, J., Jaffe, E., and Croce, C.M. (1985). Involvement of the bcl-2 gene in human follicular lymphoma. Science *228*, 1440-1443.

Tsujimoto, Y., and Croce, C.M. (1986). Analysis of the structure, transcripts, and protein products of bcl-2, the gene involved in human follicular lymphoma. Proc Natl Acad Sci U S A *83*, 5214-5218.

Tsujimoto, Y., Finger, L.R., Yunis, J., Nowell, P.C., and Croce, C.M. (1984). Cloning of the chromosome breakpoint of neoplastic B cells with the t(14;18) chromosome translocation. Science *226*, 1097-1099.

Tyner, S.D., Venkatachalam, S., Choi, J., Jones, S., Ghebranious, N., Igelmann, H., Lu, X., Soron, G., Cooper, B., Brayton, C., *et al.* (2002). p53 mutant mice that display early ageing-associated phenotypes. Nature *415*, 45-53.

Vander Heiden, M.G., Chandel, N.S., Williamson, E.K., Schumacker, P.T., and Thompson, C.B. (1997). Bcl-xL regulates the membrane potential and volume homeostasis of mitochondria. Cell *91*, 627-637.

Vaux, D.L., Cory, S., and Adams, J.M. (1988). Bcl-2 gene promotes haemopoietic cell survival and cooperates with c-myc to immortalize pre-B cells. Nature *335*, 440-442.

Vaux, D.L., and Strasser, A. (1996). The molecular biology of apoptosis. Proc Natl Acad Sci U S A *93*, 2239-2244.

Wajant, H. (2002). The Fas signaling pathway: more than a paradigm. Science *296*, 1635-1636.

Wang, X. (2001). The expanding role of mitochondria in apoptosis. Genes Dev *15*, 2922-2933.

Webster, G.A., and Perkins, N.D. (1999). Transcriptional cross talk between NF-kappaB and p53. Mol Cell Biol *19*, 3485-3495.

Wei, C.L., Wu, Q., Vega, V.B., Chiu, K.P., Ng, P., Zhang, T., Shahab, A., Yong, H.C., Fu, Y., Weng, Z., *et al.* (2006). A global map of p53 transcription-factor binding sites in the human genome. Cell *124*, 207-219.

Wu, G.S., Burns, T.F., McDonald, E.R., 3rd, Jiang, W., Meng, R., Krantz, I.D., Kao, G., Gan, D.D., Zhou, J.Y., Muschel, R., *et al.* (1997). KILLER/DR5 is a DNA damage-inducible p53-regulated death receptor gene. Nat Genet *17*, 141-143.

Wu, X., Bayle, J.H., Olson, D., and Levine, A.J. (1993). The p53-mdm-2 autoregulatory feedback loop. Genes Dev *7*, 1126-1132.

Wyllie, A.H., Kerr, J.F., and Currie, A.R. (1980). Cell death: the significance of apoptosis. Int Rev Cytol *68*, 251-306.

Yan, Y., Shay, J.W., Wright, W.E., and Mumby, M.C. (1997). Inhibition of protein phosphatase activity induces p53-dependent apoptosis in the absence of p53 transactivation. J Biol Chem *272*, 15220-15226.

Yin, Y., Terauchi, Y., Solomon, G.G., Aizawa, S., Rangarajan, P.N., Yazaki, Y., Kadowaki, T., and Barrett, J.C. (1998). Involvement of p85 in p53-dependent apoptotic response to oxidative stress. Nature *391*, 707-710.

Yue, T.L., Ohlstein, E.H., and Ruffolo, R.R., Jr. (1999). Apoptosis: a potential target for discovering novel therapies for cardiovascular diseases. Curr Opin Chem Biol *3*, 474-480.

Zamzami, N., Marchetti, P., Castedo, M., Decaudin, D., Macho, A., Hirsch, T., Susin, S.A., Petit, P.X., Mignotte, B., and Kroemer, G. (1995). Sequential reduction of mitochondrial transmembrane potential and generation of reactive oxygen species in early programmed cell death. J Exp Med *182*, 367-377.

Zamzami, N., Susin, S.A., Marchetti, P., Hirsch, T., Gomez-Monterrey, I., Castedo, M., and Kroemer, G. (1996). Mitochondrial control of nuclear apoptosis. J Exp Med *183*, 1533-1544.

Zhang, K.Z., Westberg, J.A., Holtta, E., and Andersson, L.C. (1996). BCL2 regulates neural differentiation. Proc Natl Acad Sci U S A *93*, 4504-4508.

Zhang, W., Lu, Q., Xie, Z.J., and Mellgren, R.L. (1997). Inhibition of the growth of WI-38 fibroblasts by benzyloxycarbonyl-Leu-Leu-Tyr diazomethyl ketone: evidence that cleavage of p53 by a calpain-like protease is necessary for G1 to S-phase transition. Oncogene *14*, 255-263.

Zhao, Y., Chaiswing, L., Velez, J.M., Batinic-Haberle, I., Colburn, N.H., Oberley, T.D., and St Clair, D.K. (2005). p53 translocation to mitochondria precedes its nuclear translocation and targets mitochondrial oxidative defense protein-manganese superoxide dismutase. Cancer Res *65*, 3745-3750.

Zhou, J., Ahn, J., Wilson, S.H., and Prives, C. (2001). A role for p53 in base excision repair. Embo J *20*, 914-923.

Zimmermann, K.C., Bonzon, C., and Green, D.R. (2001). The machinery of programmed cell death. Pharmacol Ther *92*, 57-70.

Zuiderweg, E.R. (2002). Mapping protein-protein interactions in solution by NMR spectroscopy. Biochemistry *41*, 1-7.